Advanced k-space instrumentation: Photoemission and resonant scattering

SOLEIL SYNCHROTRON

N. Jaouen
Synchrotron SOLEIL, France

Outline

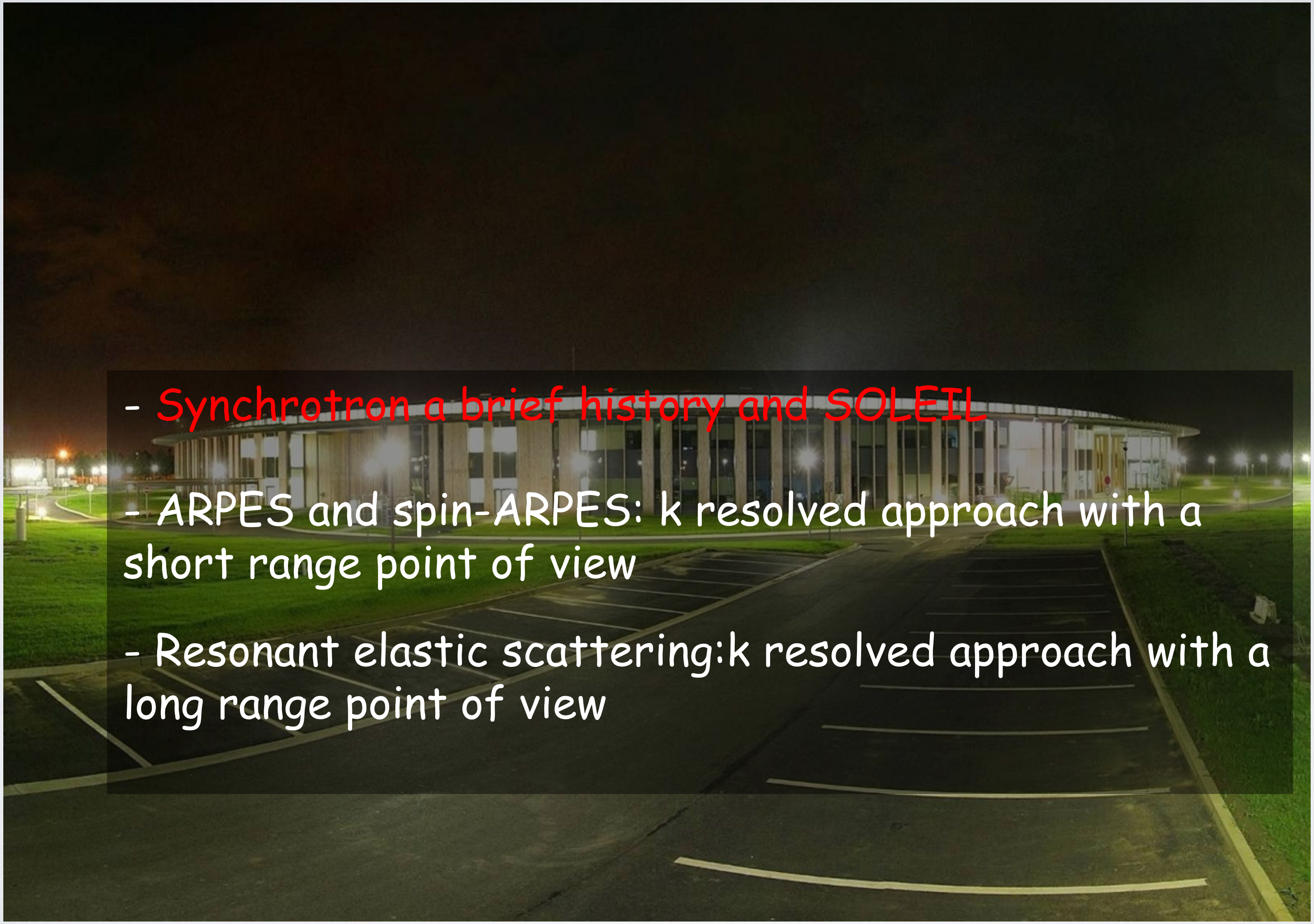

- Synchrotron a brief history and SOLEIL

- ARPES and spin-ARPES: k resolved approach with a short range point of view

- Resonant elastic scattering:k resolved approach with a long range point of view

Synchrotron: a brief history

Brief history

- Before synchrotron: X-ray tubes.
- Synchrotron evolution: the race for higher brilliance.
  - ➢ 1st generation: Accelerators and storage rings parasitically used as light sources.
  - ➢ 2nd generation: Dedicated rings designed and optimised as light sources.
  - ➢ 3rd generation: Dedicated rings built to maximise brilliance by reducing the beam emittance and by the extensive use of undulators as light sources.
  - ➢ 4th generation: Diffraction-limited sources
  - ➢ Free electron laser: Ultimate source: fully coherent and 100fs pulse

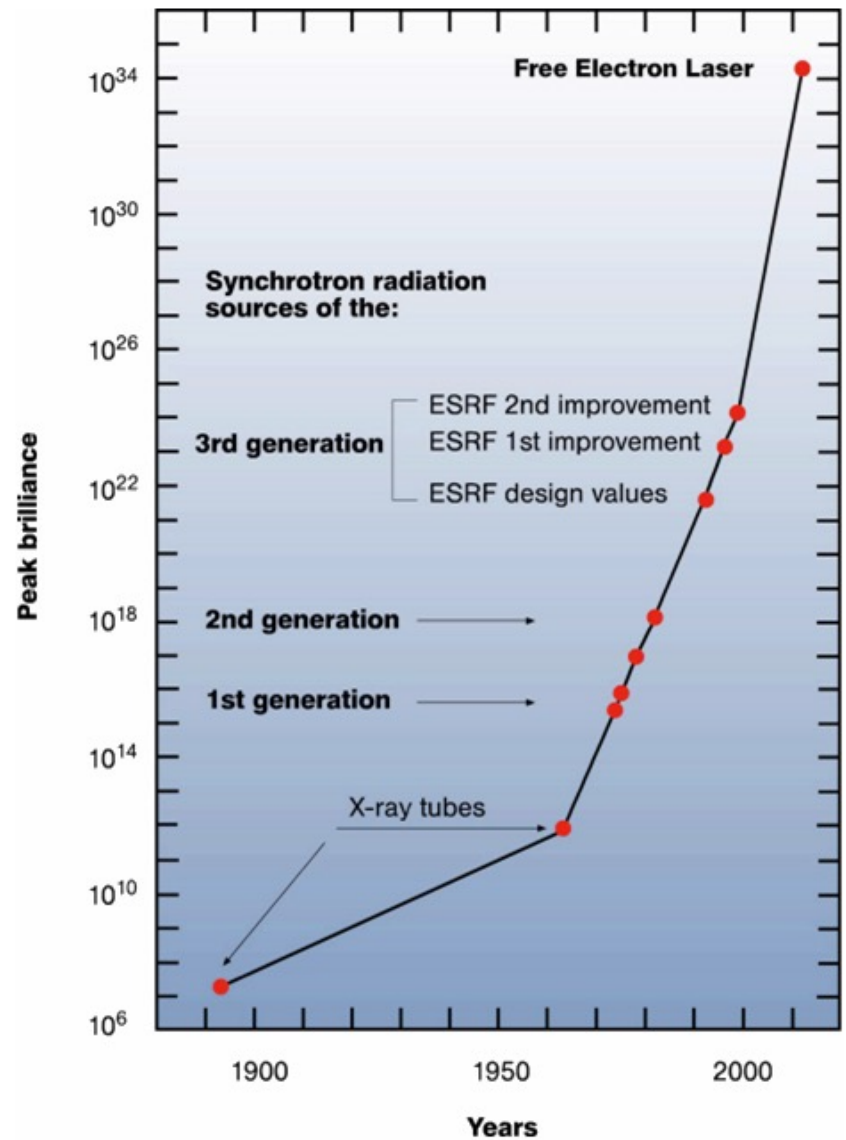

Synchrotron: a brief history

From the X-ray spectroscopy point of view

- Increase of brilliance ≡ increase of photon flux density on the sample. With fragile samples one has to be careful with beam damage.
- But synchrotron radiation has also brought:
  - ➢ Wider energy range: access to edges from low energy (soft x-rays) to very hard x-rays.
  - ➢ Fully tuneable polarisation by the use of undulators.
  - ➢ Time-resolved experiment if the fs time-scale: 4th generation free electron laser and bunch slicing on the 3rd generation sources.
  - ➢ Coherence

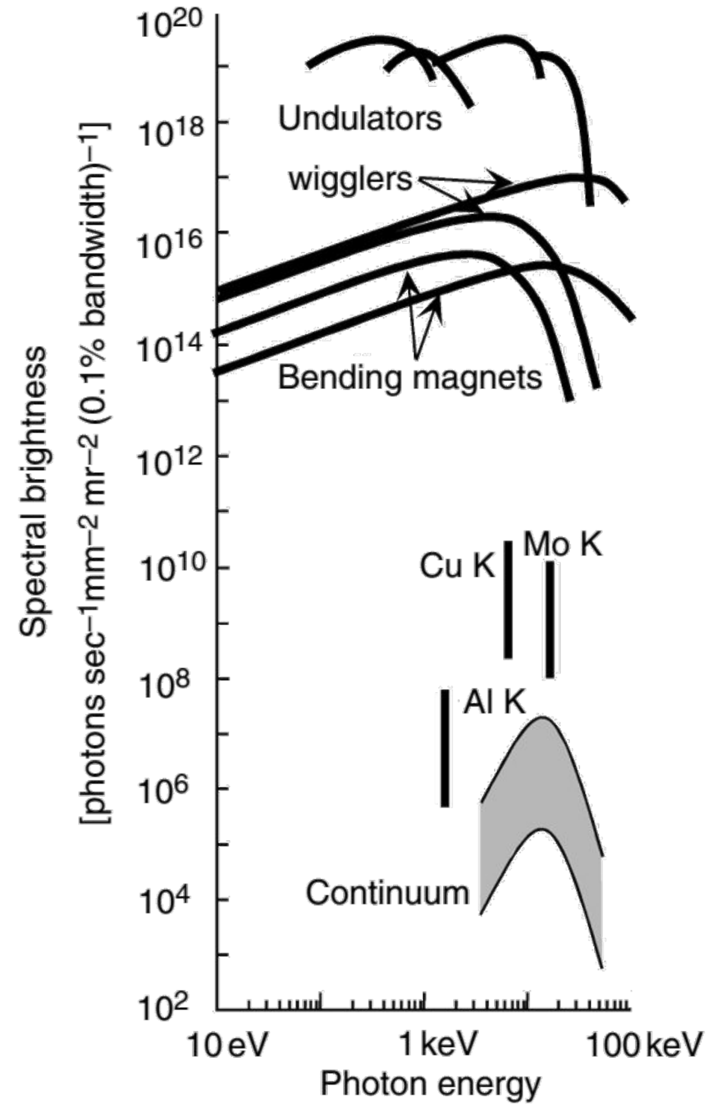

Introduction to SOLEIL facility

Covered spectral range at SOLEIL

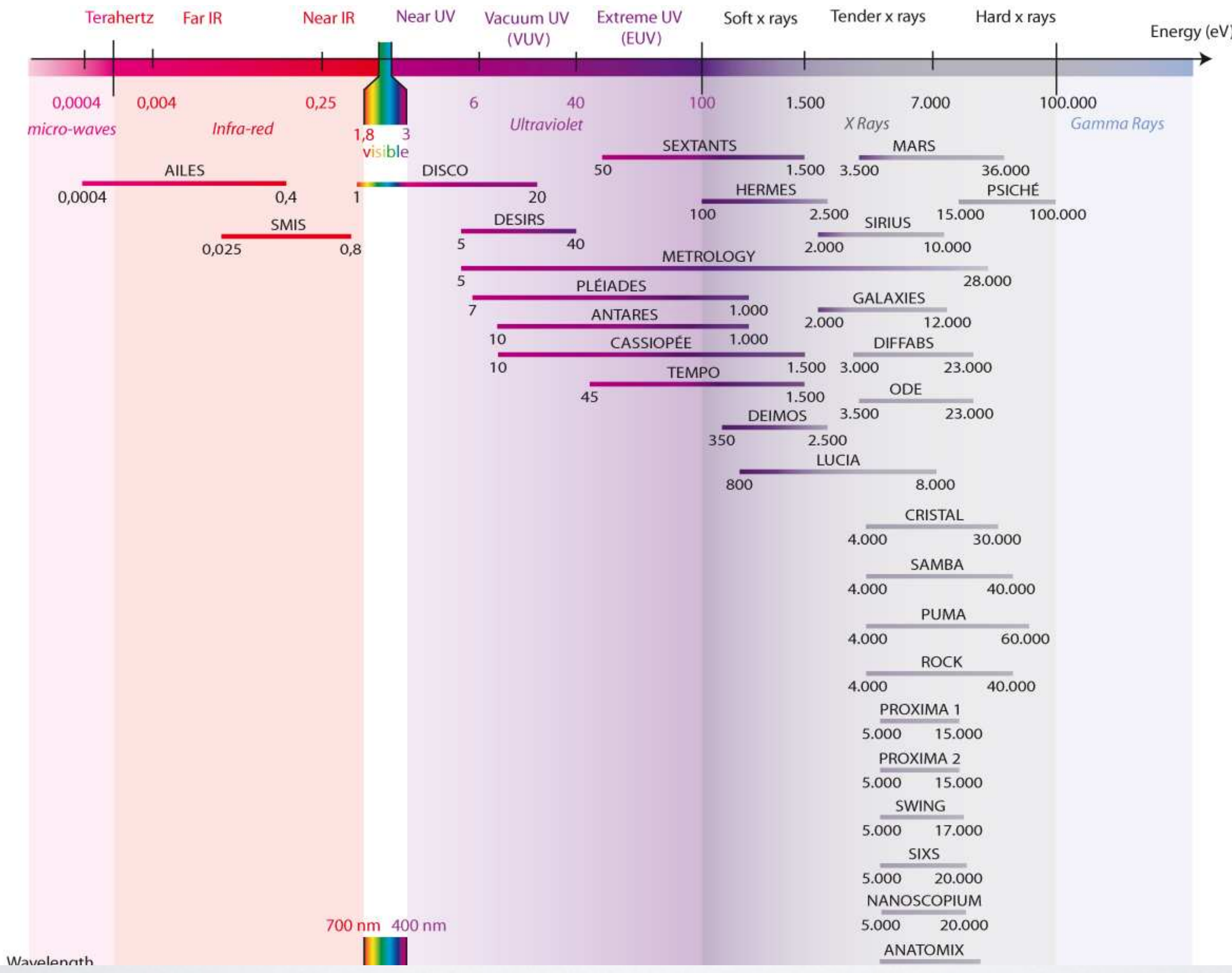

Introduction to SOLEIL facility

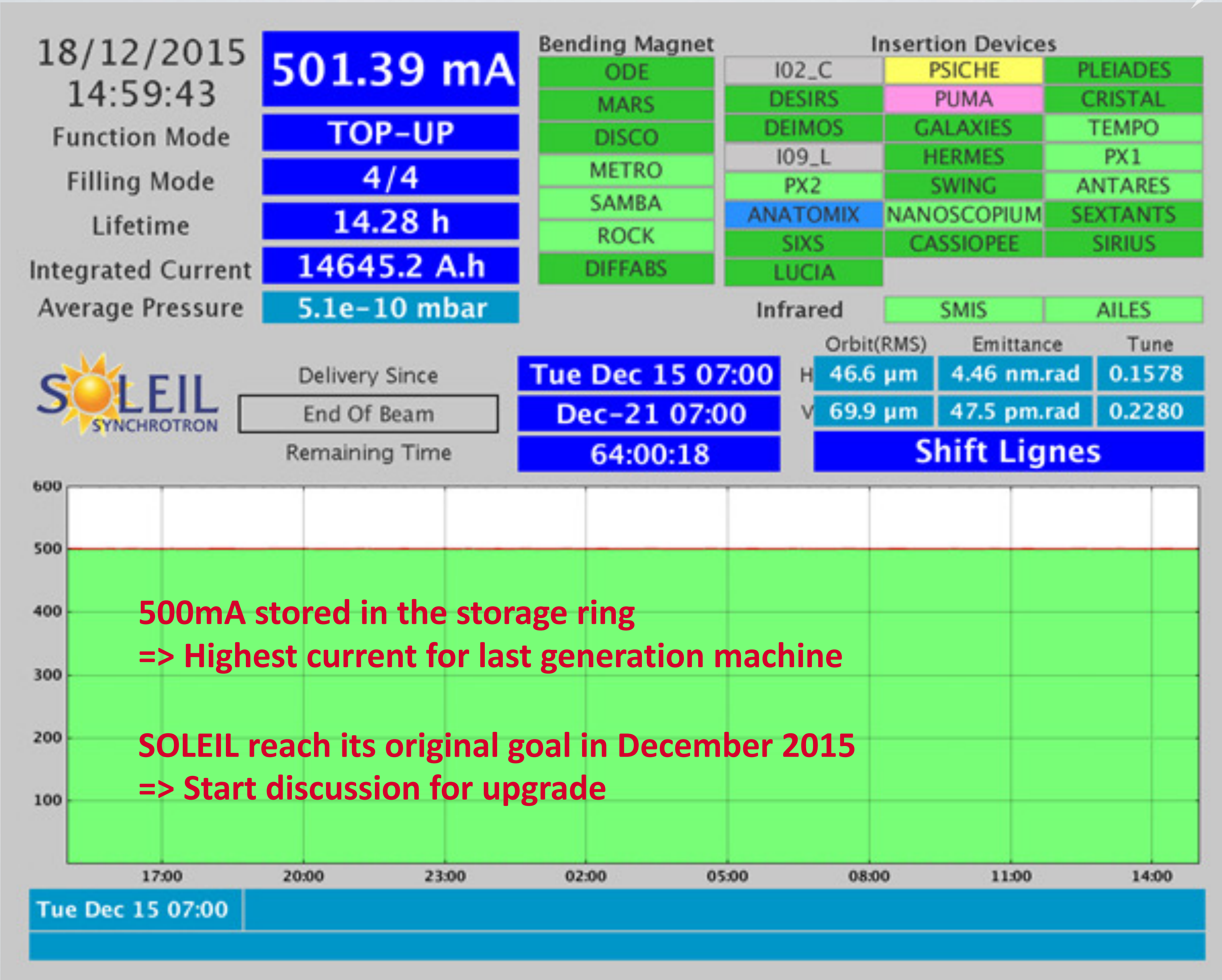

Outline

sextants

Soft x-ray EXperimenT resonANT Scattering

- Synchrotron a brief history and SOLEIL

- ARPES and spin-ARPES: k resolved approach with a short range point of view

- Resonant elastic scattering: k resolved approach with a long range point of view

Summary

1. Introduction : spintronics and electronic structure

   Rashba systems, half-metals, topological insulators...

2. Photoemission and Angle-Resolved photoemission

   Photoelectric effect, a photoemission experiment, ARPES, surface sensitivity

3. Spin-resolved ARPES

   Spin detectors, actual developments

4. ARPES and Spin-Resolved ARPES for Spintronics

   α-Sn, half-metal Heusler alloys, BiSb

Great thanks to P Lefevre !!!!!
CASSIOPEE beamline

Photoemission and

Angle-Resolved Photoemission

The photoelectric effect

...The photon energy is used to eject a photoelectron.

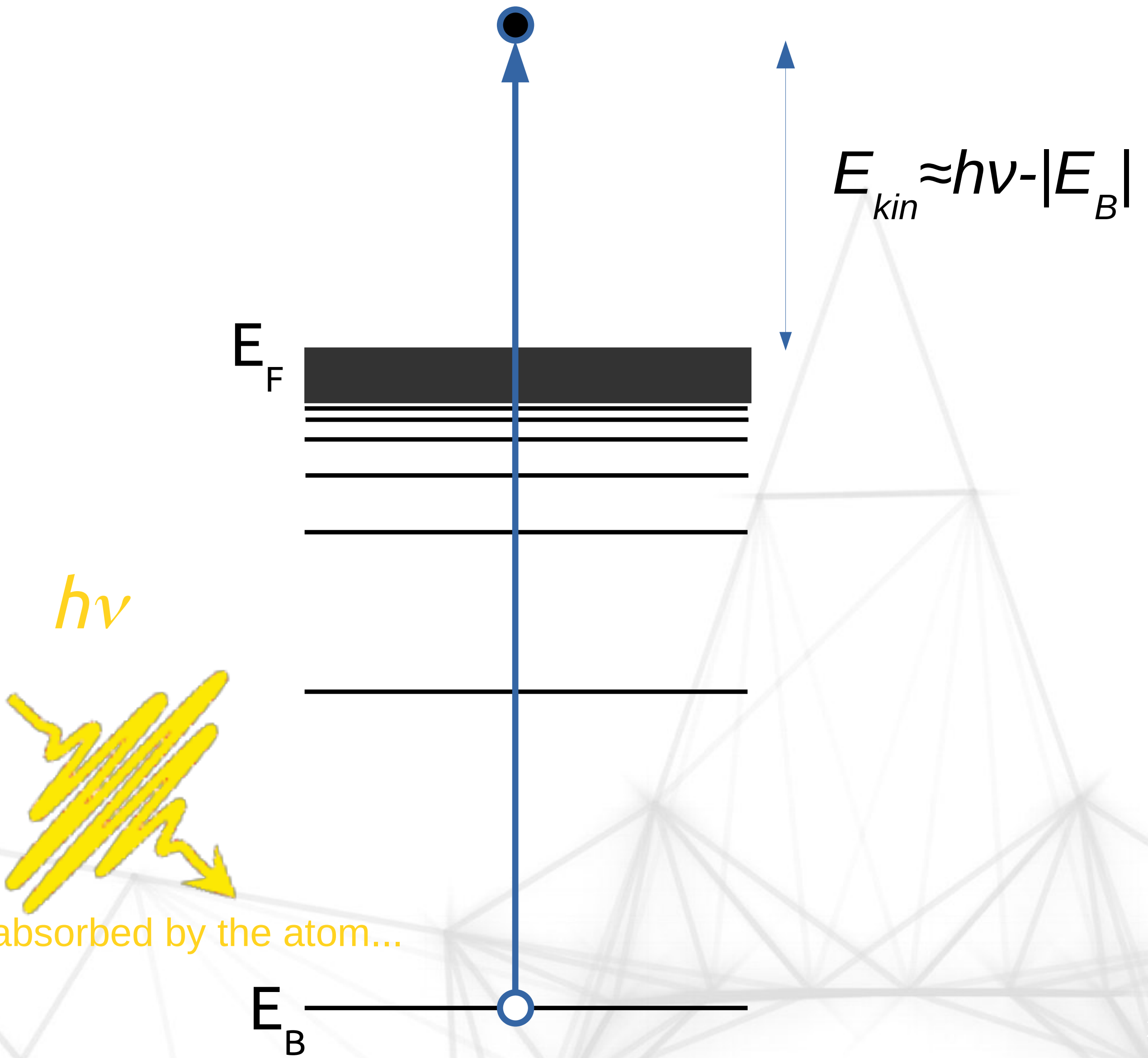

A photon is absorbed by the atom...

The photoelectric effect

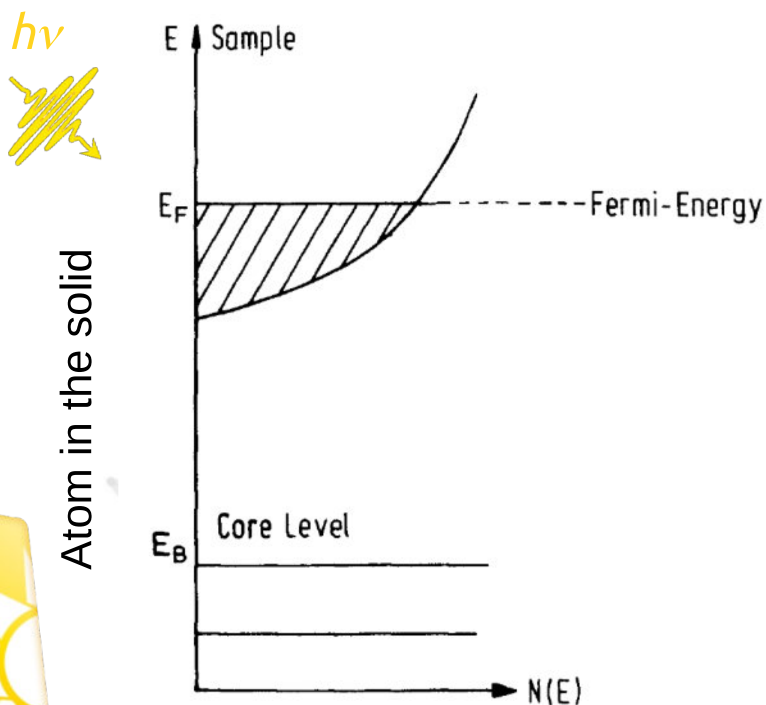

S. Hüfner, Photoelectron Spectroscopy (Springer)

The photoelectric effect

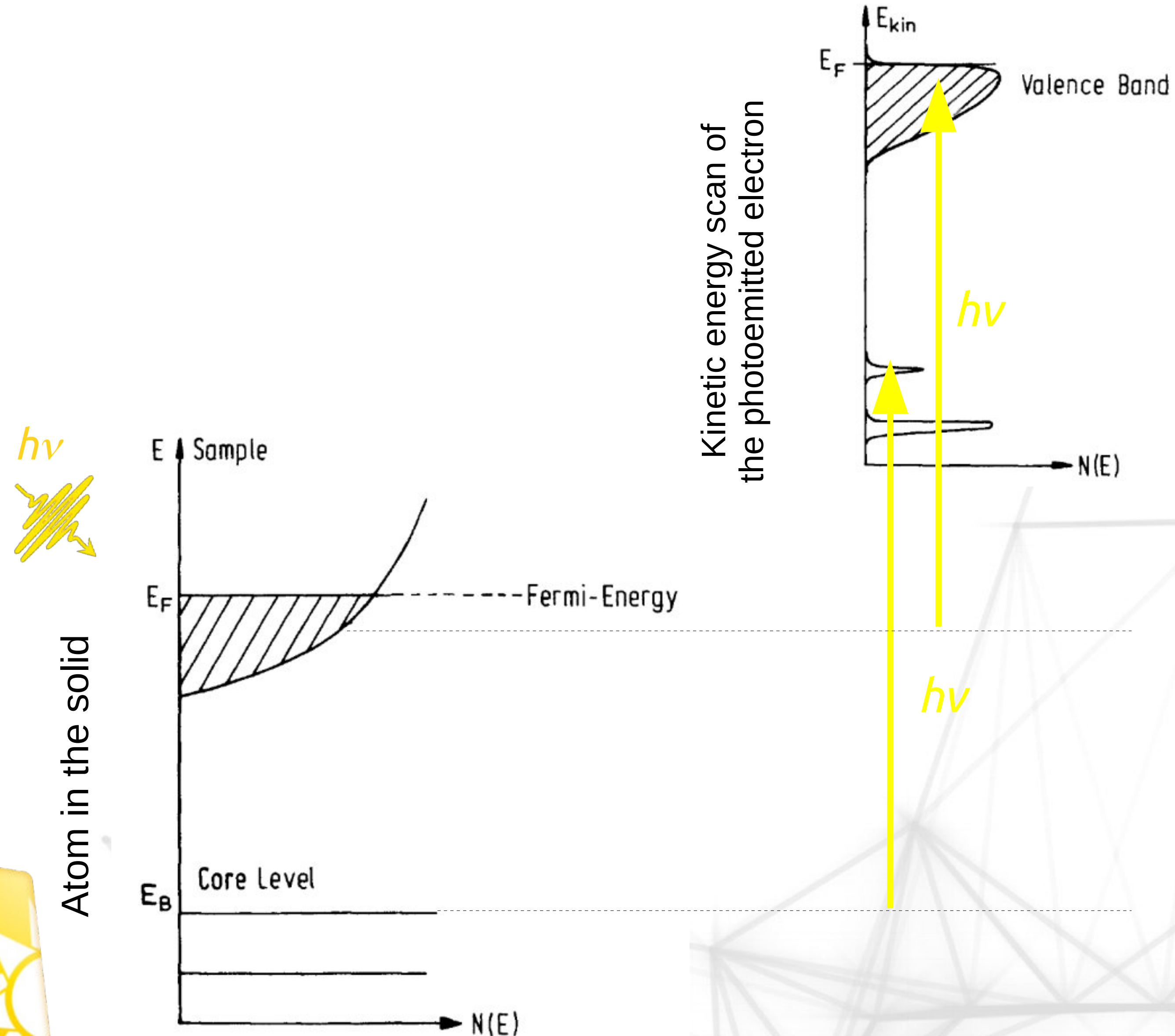

S. Hüfner, Photoelectron Spectroscopy (Springer)

A photoemission experiment

Laser

UV-lamps :
He-Lamp (21.2eV)

X-ray tubes :
Al-Kα (1486eV)
Mg-Kα (1253.6eV)

SR:
From 10 to 10000eV

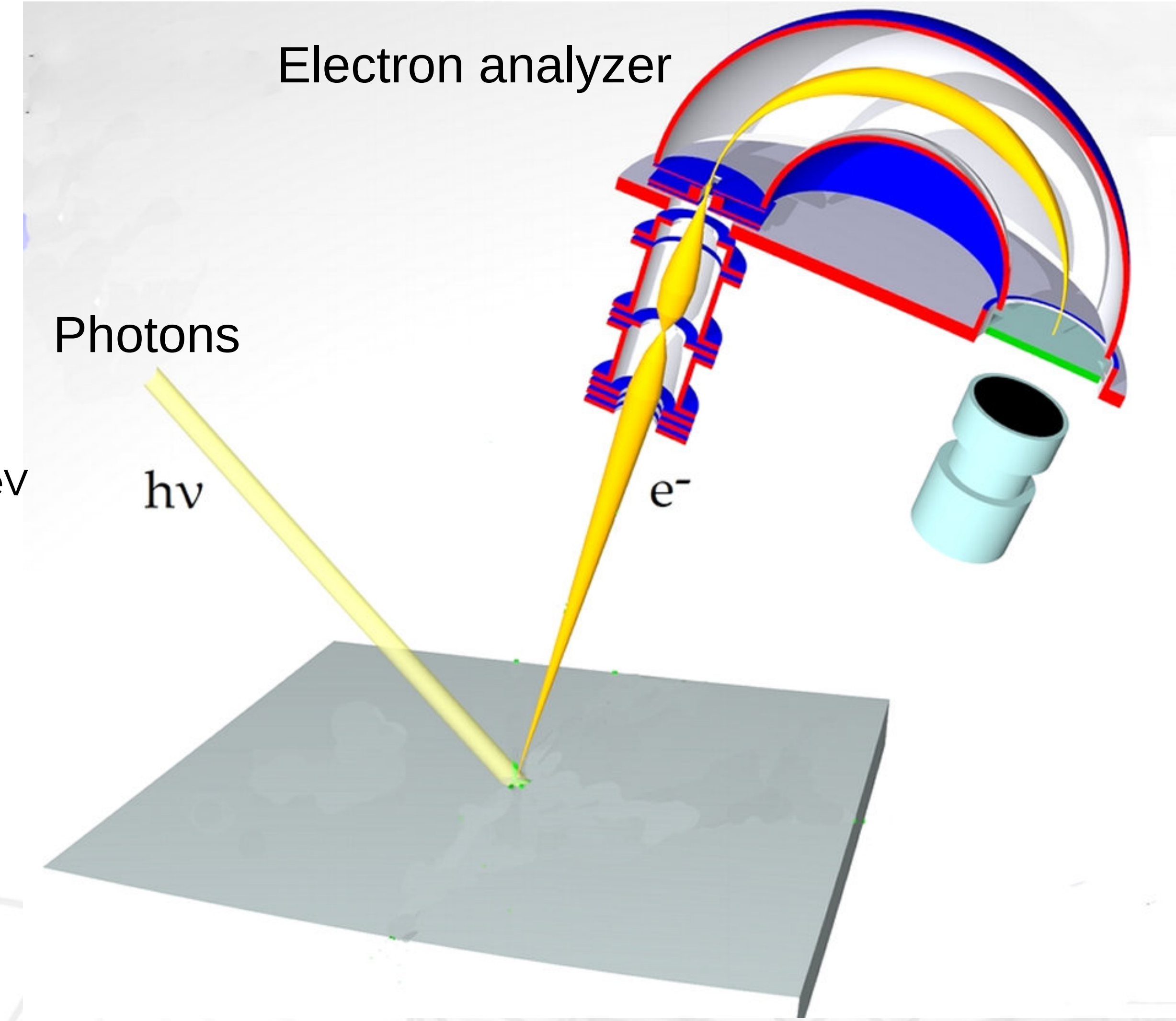

http://en.wikipedia.org/wiki/Photoemission_spectroscopy

A photoemission experiment

$[Bi_2Ba_2O_4][CoO_2]$

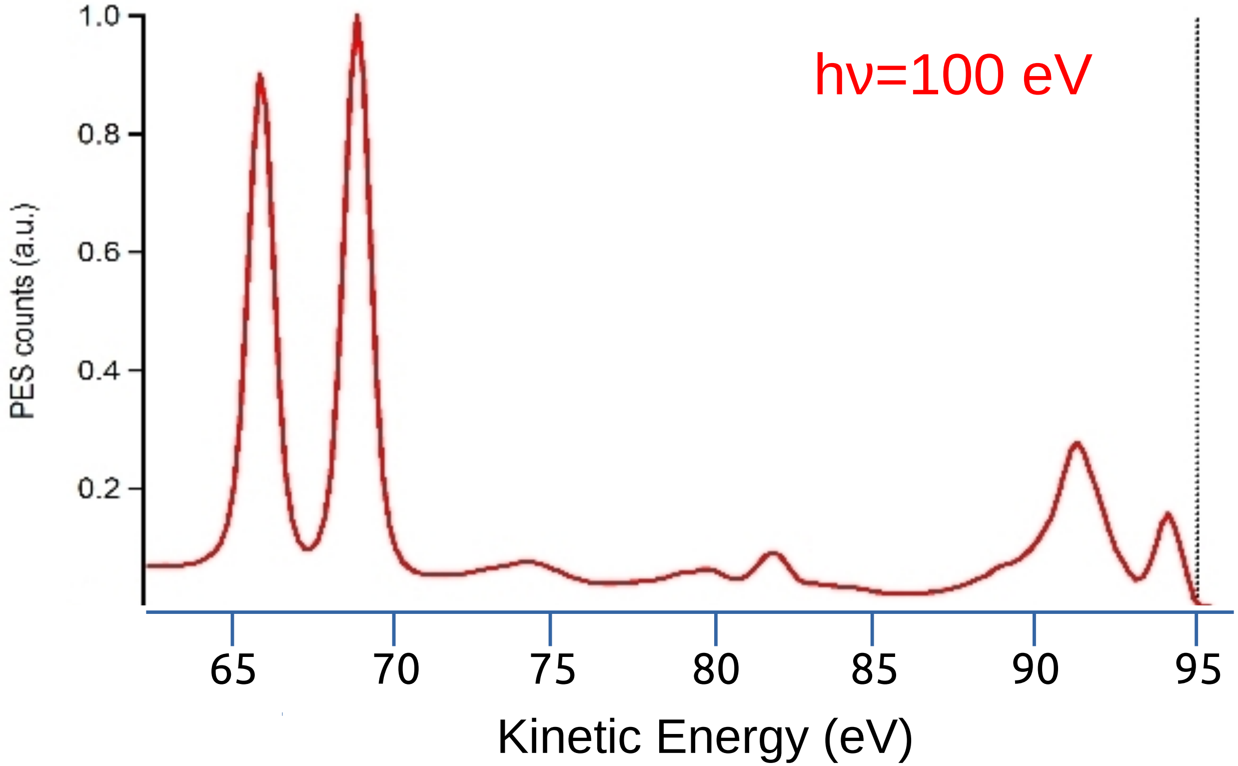

A. Nicolaou et al.

A photoemission experiment

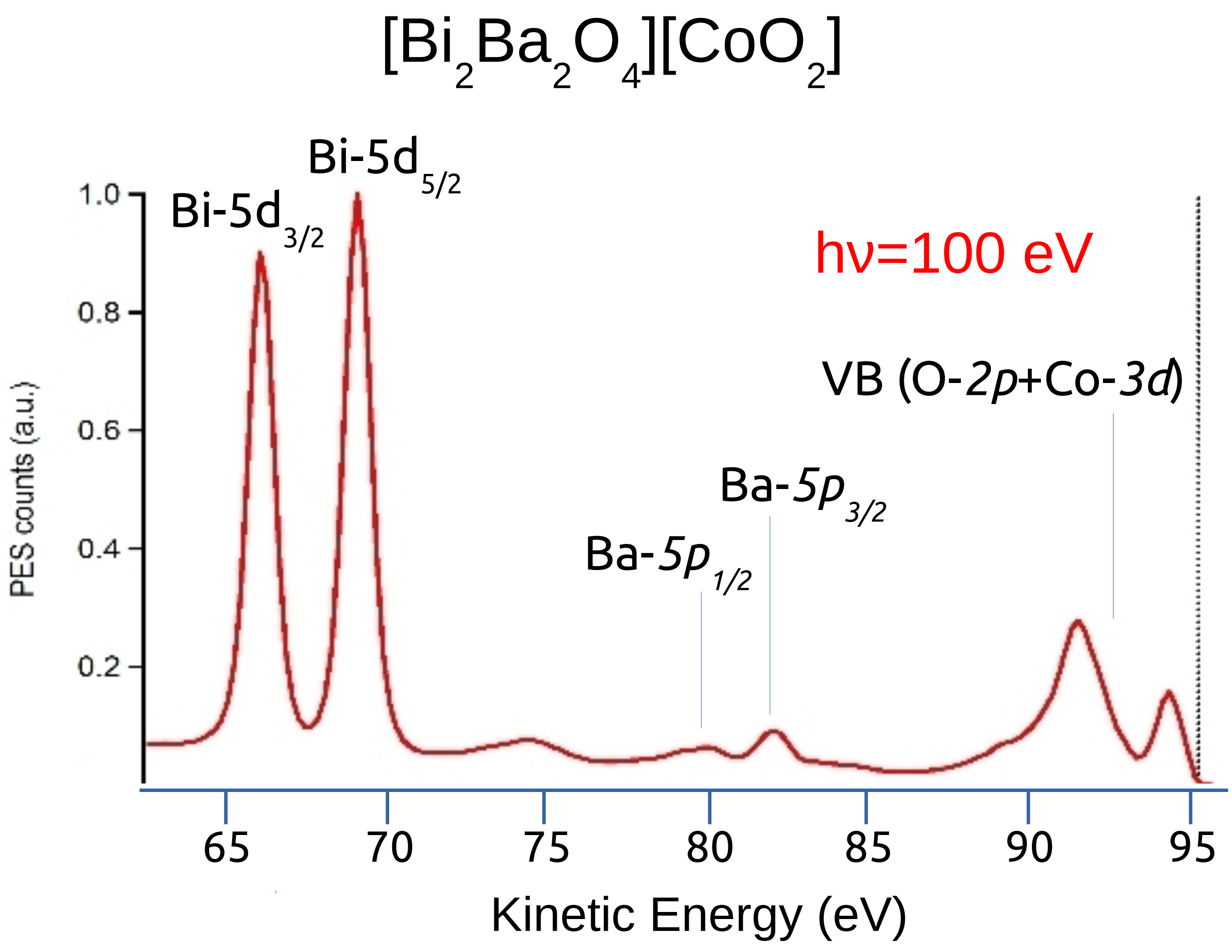

$$E_{kin} \approx h\nu - |E_B|$$

A. Nicolaou et al.

A photoemission experiment

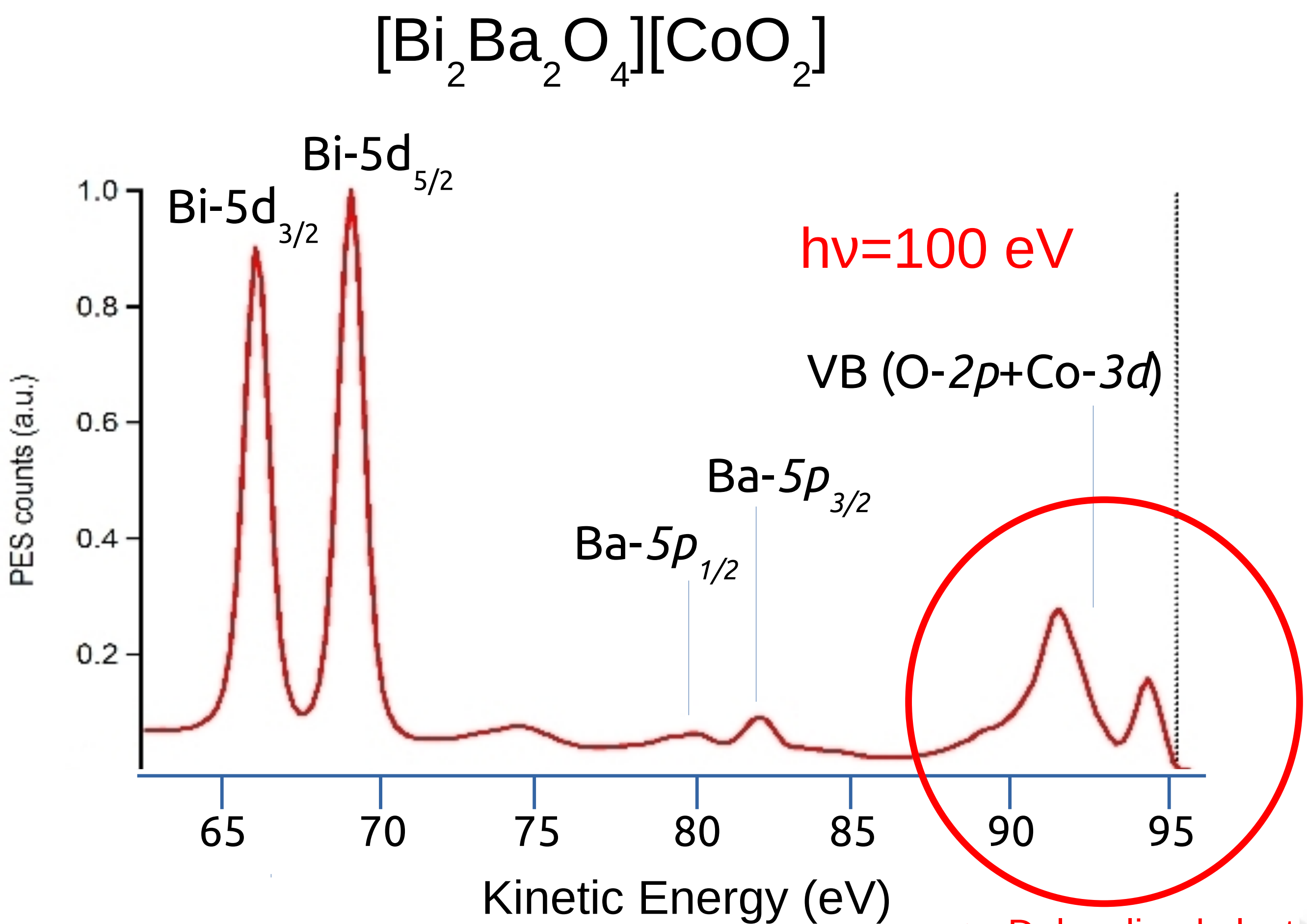

- ► Delocalized electrons
- ► Described by E_B and k
- ► E_B(k) forms the band structure

A. Nicolaou et al.

An ARPES experiment

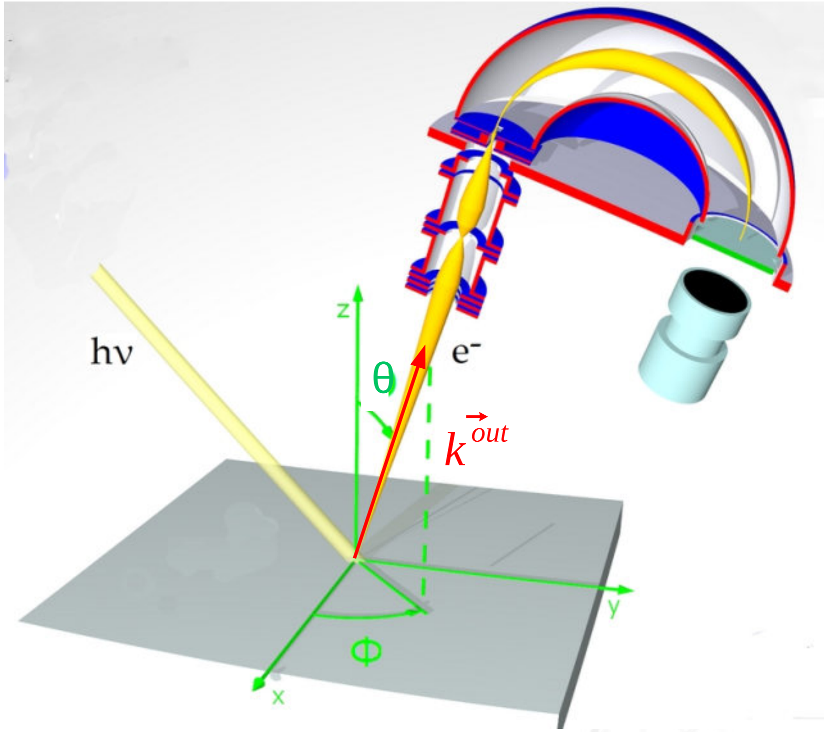

let's now assume that, in addition to its **kinetic energy**, one also measures **θ** the angle between the photoelectron emission direction (direction of the photoelectron wave vector) and the surface normal.

ARPES
Angle **R**esolved **P**hotoelectron **S**pectroscopy

Could we measure the band structure E(k) ?

ARPES : Measured quantities

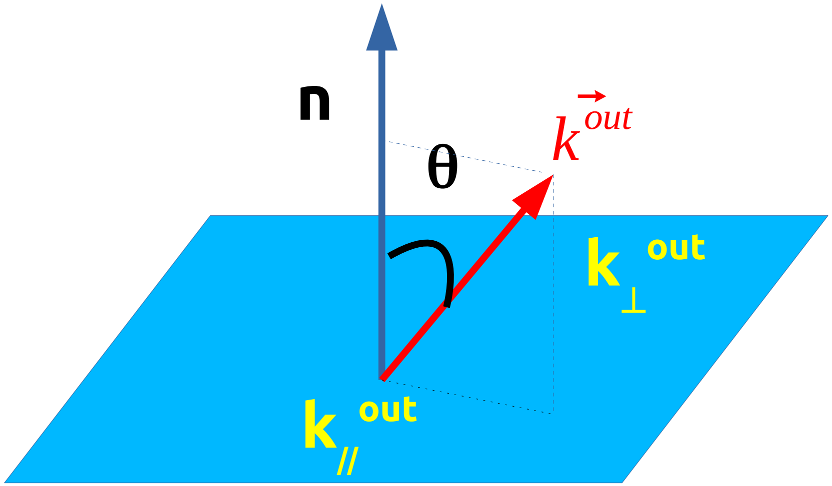

$$E_K = \frac{\hbar^2 k^2}{2m} \Rightarrow |k| = \frac{\sqrt{2mE_K}}{\hbar}$$

$$\vec{k}^{out} \begin{pmatrix} k_{\perp}^{out} = \dfrac{\sqrt{2mE_K}}{\hbar} \cos\theta \\ k_{//}^{out} = \dfrac{\sqrt{2mE_K}}{\hbar} \sin\theta \end{pmatrix}$$

It is easy to claculate the coordinates of the *k* outside the solid $\vec{k}^{out}$ ...

ARPES : Measured quantities

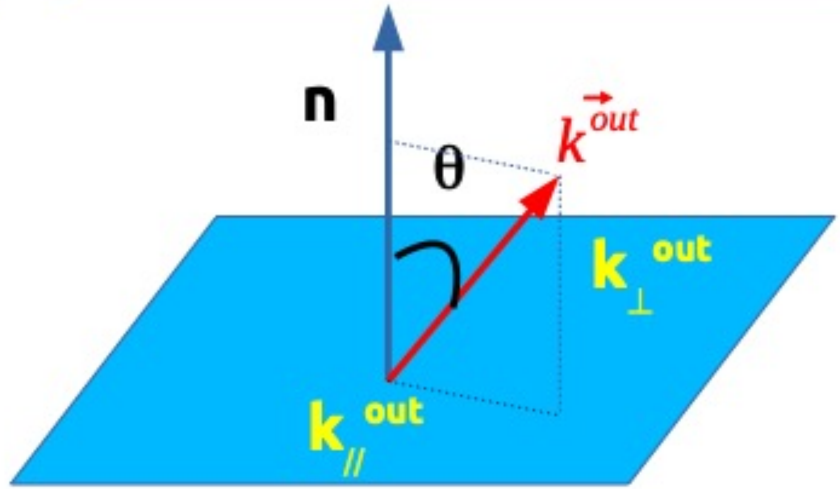

$$\vec{k}^{out} \begin{pmatrix} k_{\perp}^{out} = \dfrac{\sqrt{2mE_K}}{\hbar}\cos\theta \\ k_{//}^{out} = \dfrac{\sqrt{2mE_K}}{\hbar}\sin\theta \end{pmatrix}$$

It is easy to claculate the coordinates of the k outside the solid $\vec{k}^{out}$ ...

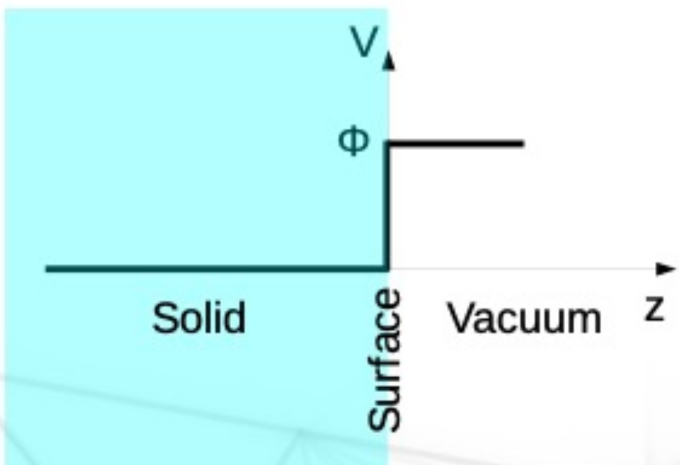

But there is a potential at the surface…

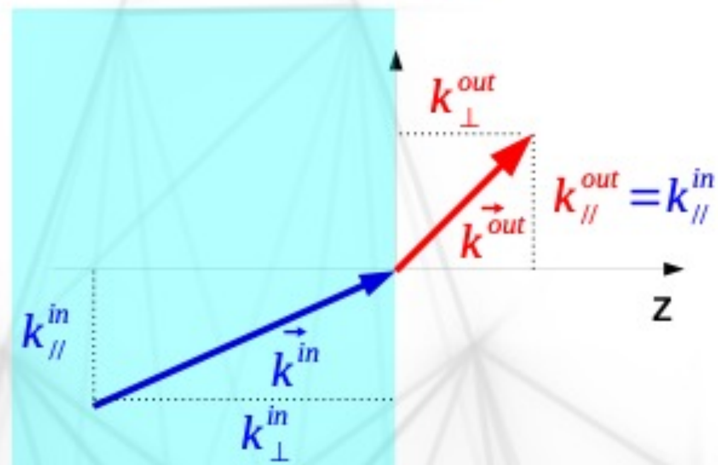

… which refracts the electron !

Potential discontinuity in the z direction

$\rightarrow k_{//}$ is conserved but not $k_{\perp}$

ARPES : Excitation inside the solid

So, let's start from the beginning...

An electron of the band structure of initial state (**E_B**,**k**) is excited into an empty state...

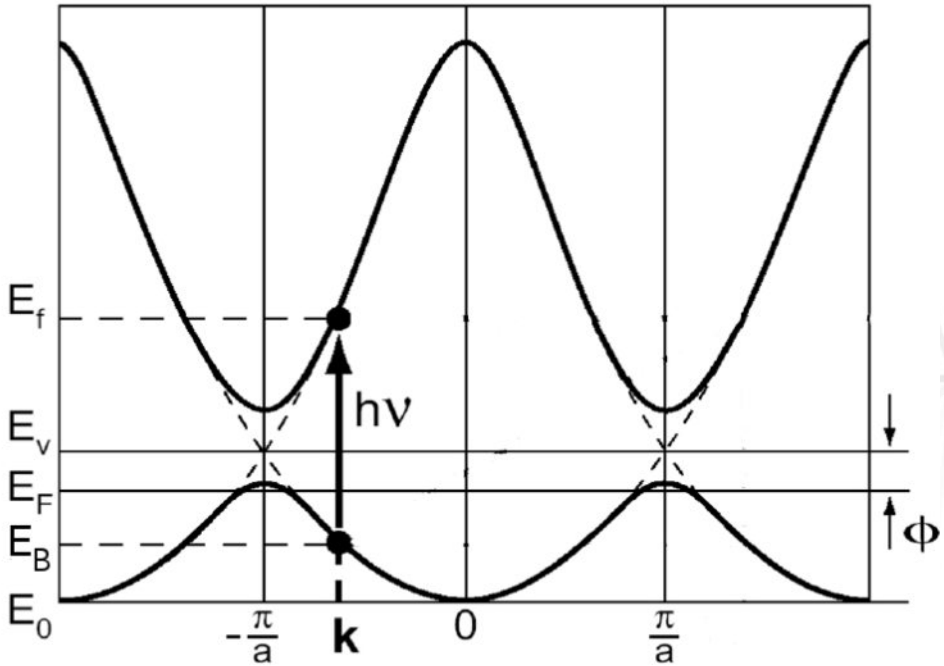

$$k_f = k + k_{Photon} \simeq k$$

$$\frac{k_{Electron}}{k_{Photon}} = \frac{\sqrt{2mE_{Electron}}}{E_{Photon}/c} \sim 10^3$$

$$(E_{Electron} = E_{Photon} = 1\mathrm{eV})$$

The initial wave vector is conserved during the excitation process.

ARPES : Excitation inside the solid

So, let’s start from the beginning...

An electron of the band structure of initial state (**E_B**,**k**) is excited into an empty state...

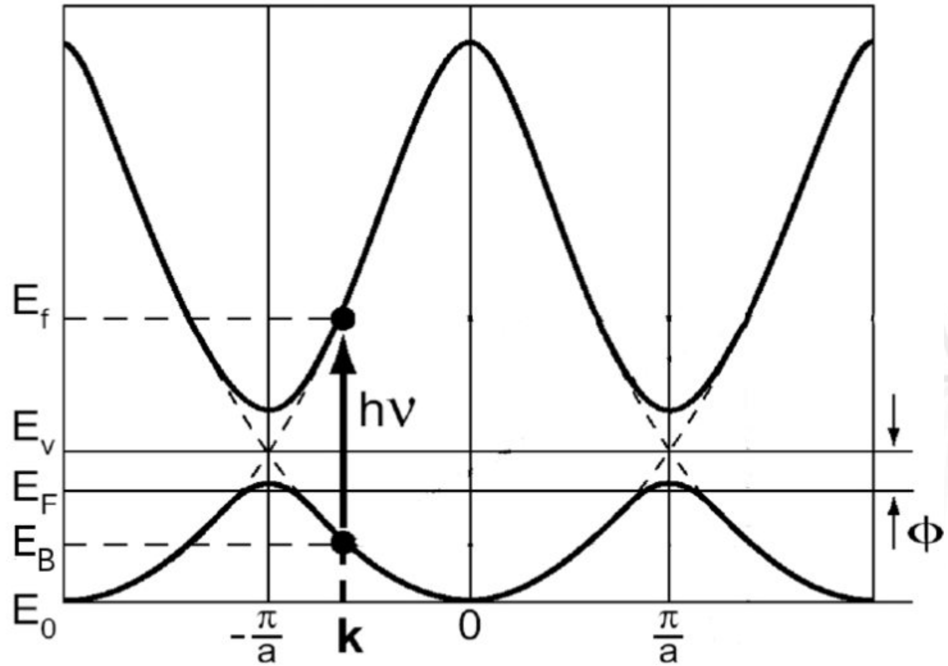

$$\vec{k} = \vec{k}^{in}$$

$$E_f = h\nu - |E_B|$$

ARPES : Calculation of E_B and $k_{//}$

We can now calculate $\boldsymbol{k_{//}}$ as a function of the measured quantities $\boldsymbol{E_K}$ and $\boldsymbol{\theta}$:

- $E_K = E_f - |\phi|$ (To take into account the crossing of the surface barrier)
  $E_f = h\nu - |E_B|$

$$\boxed{E_B = h\nu - E_K - |\phi|}$$

- $$k_{//} = k_{//}^{in} = k_{//}^{out} = \frac{\sqrt{2mE_K}}{\hbar}\sin\theta$$

$$\boxed{k_{//} = \frac{\sqrt{2mE_K}}{\hbar}\sin\theta}$$

It is a little more complicated for $k_{\perp}$… (but still easy)

The ARPES formulas

$$\begin{cases} E_B = h\nu - E_K - \phi \\ k_\perp = \dfrac{\sqrt{2m}}{\hbar}\left(E_K cos^2\theta + V_0\right)^{1/2} \\ k_{//} = \dfrac{\sqrt{2m}}{\hbar} E_K{}^{1/2}\ sin\theta \end{cases}$$

The ARPES formulas

$$\begin{cases} E_B = h\nu - E_K - \phi \\ k_\perp = \dfrac{\sqrt{2m}}{\hbar}\left(E_K \cos^2\theta + V_0\right)^{1/2} \\ k_{//} = \dfrac{\sqrt{2m}}{\hbar} E_K^{\ 1/2} \sin\theta \end{cases}$$

► ARPES determines E_B and k

With these 3 formulas, we are able to (almost) completely describe the electron initial state from the measured quantities E_K and θ.

The ARPES formulas

$$\begin{cases} E_B = h\nu - E_K - \phi \\ k_\perp = \dfrac{\sqrt{2m}}{\hbar}\left(E_K \cos^2\theta + V_0\right)^{1/2} \\ k_{//} = \dfrac{\sqrt{2m}}{\hbar} E_K^{1/2} \sin\theta \end{cases}$$

- ARPES determines E_B and k
- One can travel in the reciprocal space by changing either hν or θ

Ex : hν=20 eV, θ varies from 0° to 10°
$k_{//}$ varies from 0 to 0.40 $Å^{-1}$
$k_\perp$ varies from 2.8 to 2.78 $Å^{-1}$ (V_0=10 eV)

$$\frac{\sqrt{2m}}{\hbar} = 0.512$$

(with energy in eV and *k* in $Å^{-1}$)

θ=0°, hν varies from 20 to 100 eV
$k_{//}$ is always 0 $Å^{-1}$
$k_\perp$ varies from 2.8 to 5.4 $Å^{-1}$

Changing hν = changing only $k_\perp$ (@ θ=0°)
Changing θ ~ changing only $k_{//}$

The ARPES formulas

$$
\begin{cases}
E_B = h\nu - E_K - \phi \\
k_\perp = \dfrac{\sqrt{2m}}{\hbar}\left(E_K \cos^2\theta + V_0\right)^{1/2} \\
k_{//} = \dfrac{\sqrt{2m}}{\hbar} E_K^{\ 1/2} \ \sin\theta
\end{cases}
$$

- ARPES determines E_B and k
- One can travel in the reciprocal space by changing either hν or θ

  Changing hν = changing only $k_\perp$ (@ θ=0°)

  Changing θ ~ changing only $k_{//}$

- Another exemple :

  hν=20 eV, θ varies from 0° to 10°

  $k_{//}$ varies from 0 to 0.40 $Å^{-1}$

  hν=100 eV, θ varies from 0° to 10°

  $k_{//}$ varies from 0 to 0.89 $Å^{-1}$!

The ARPES formulas

$$\begin{cases} E_B = h\nu - E_K - \phi \\ k_\perp = \dfrac{\sqrt{2m}}{\hbar}\left(E_K \cos^2\theta + V_0\right)^{1/2} \\ k_{//} = \dfrac{\sqrt{2m}}{\hbar} E_K^{\;1/2} \sin\theta \end{cases}$$

- ARPES determines E_B and k
- One can travel in the reciprocal space by changing either hν or θ

  Changing hν = changing only $k_\perp$ (@ θ=0°)

  Changing θ ~ changing only $k_{//}$

- By increasing hν, one shrinks the explored reciprocal space into a smaller θ range

Let's see now how to do these measurements...

Analyzers for ARPES : single channel energy detection

The hemispherical analyzer

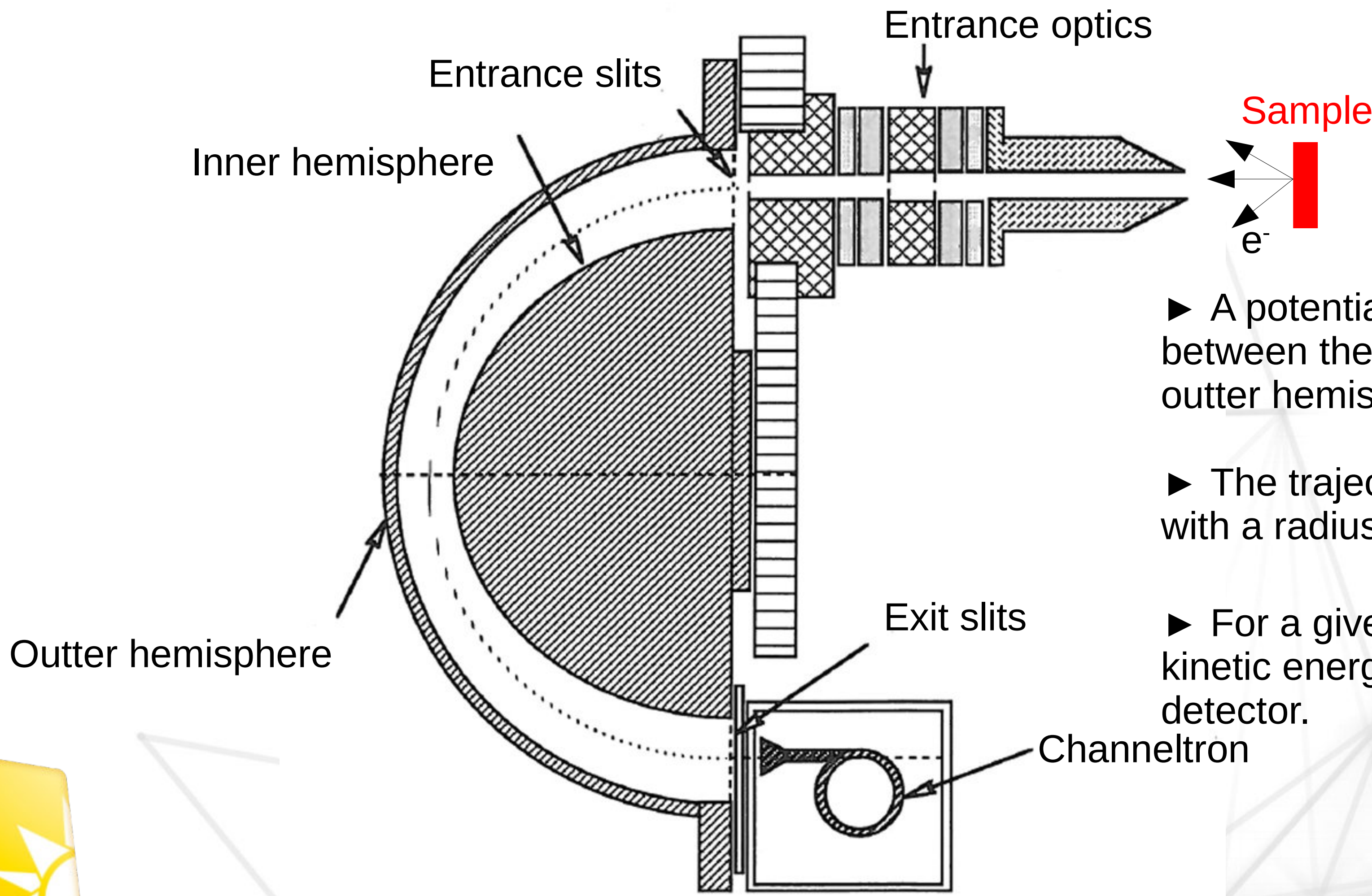

► A potential V is applied between the inner and the outter hemisphere.

► The trajectory is circular with a radius=f(V,E_K)

► For a given V, only one kinetic energy can reach the detector.

Analyzers for ARPES : multichannel energy detection

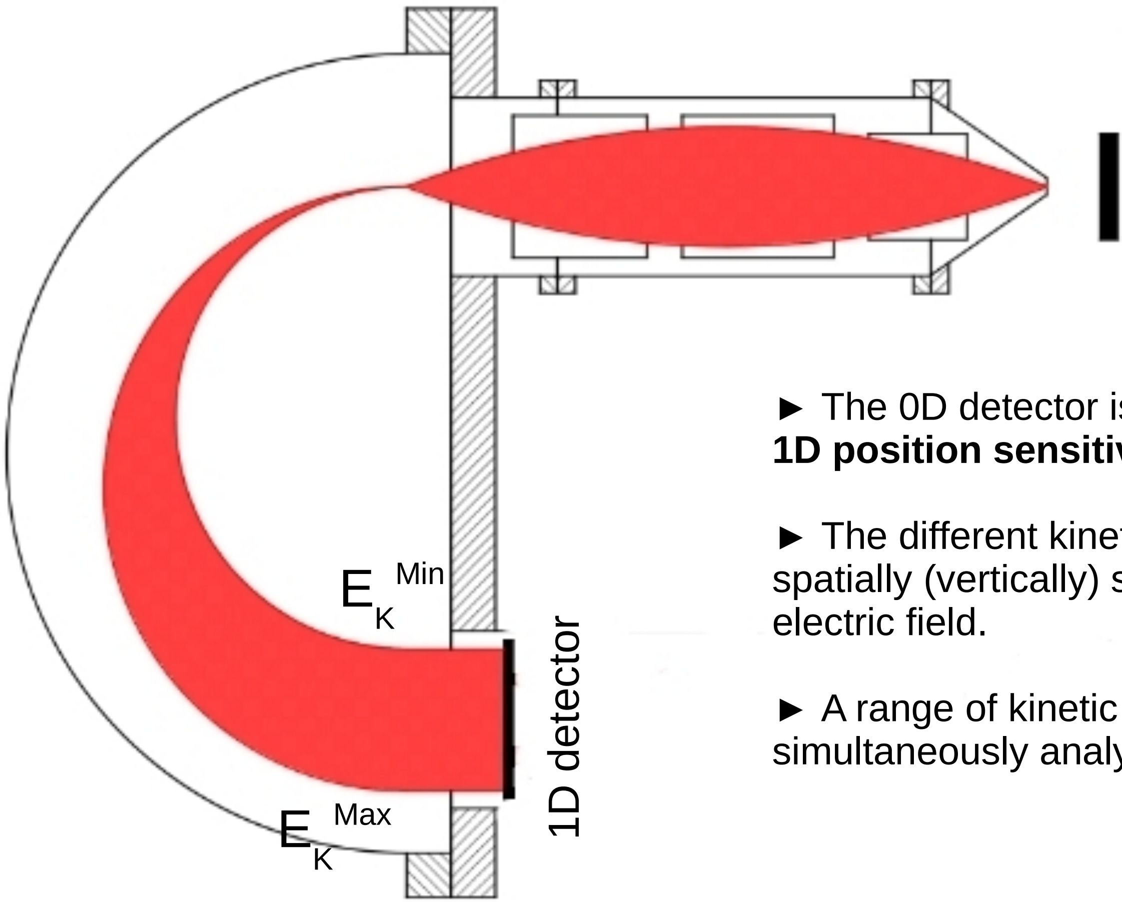

► The 0D detector is replaced by a **1D position sensitive detector**.

► The different kinetic energies are spatially (vertically) sorted by the electric field.

► A range of kinetic energies are simultaneously analyzed.

Analyzers for ARPES : 2D detector

« Scienta-type » analyzer

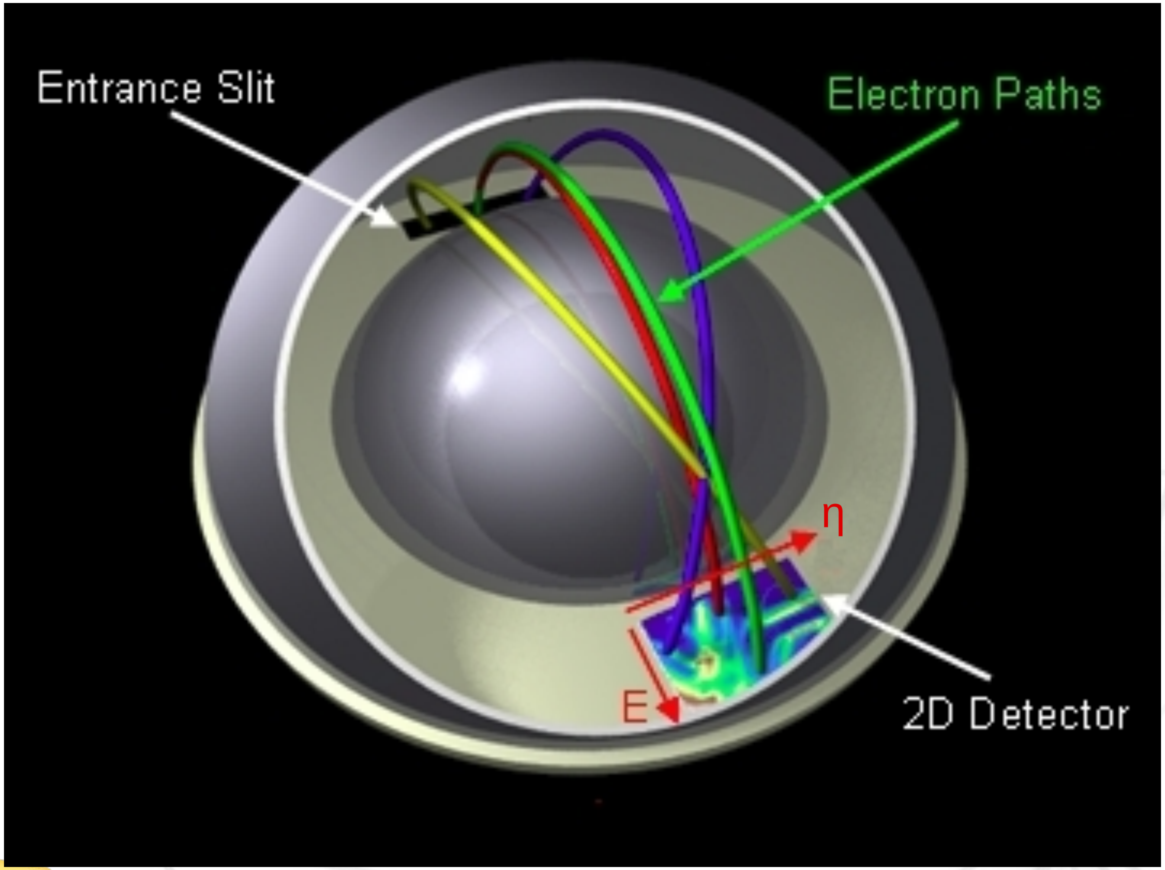

http://arpes.stanford.edu/facilities_ssrl.html

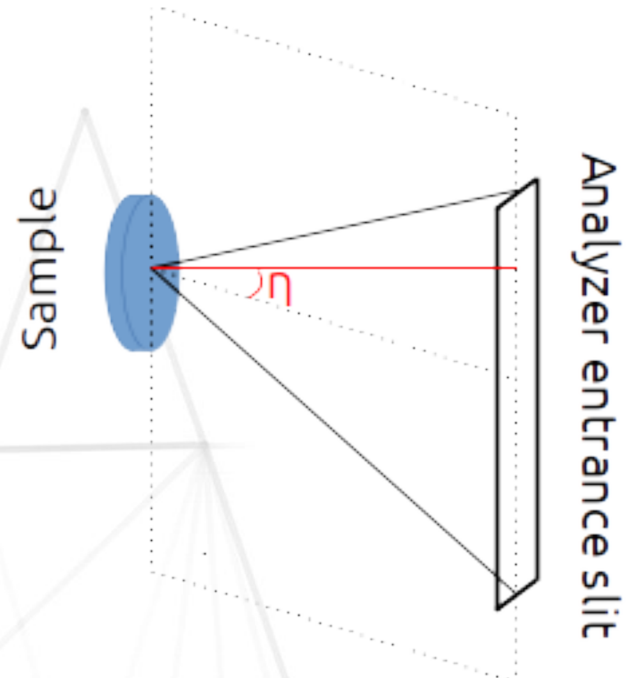

► Along the entrance slit, the emission angle η is conserved.

► Finally, the result of a measurement is an image (E_K,η).

Analyzers for ARPES : 2D detector

TiO_2-rutile(110)

From a KE vs η image… … To a BE vs $k_{//}$ image…

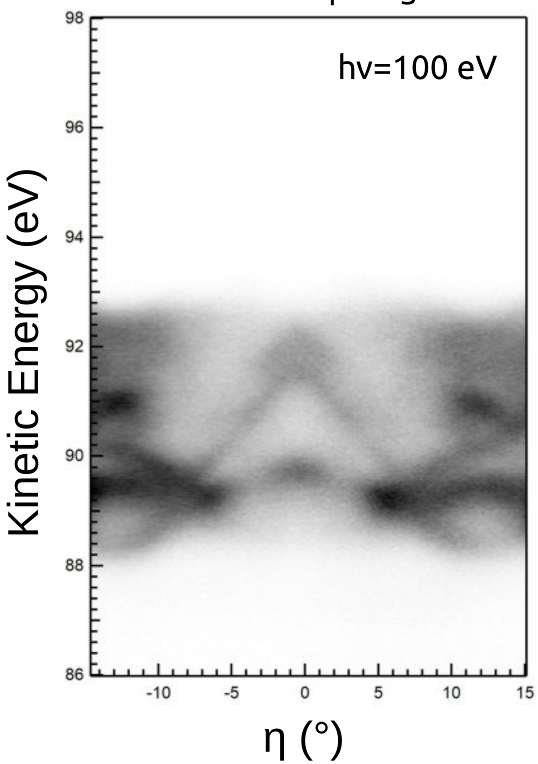

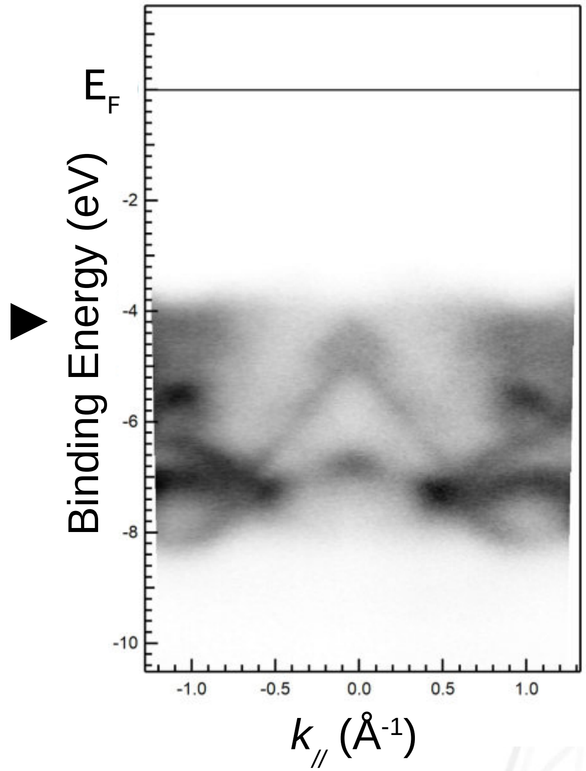

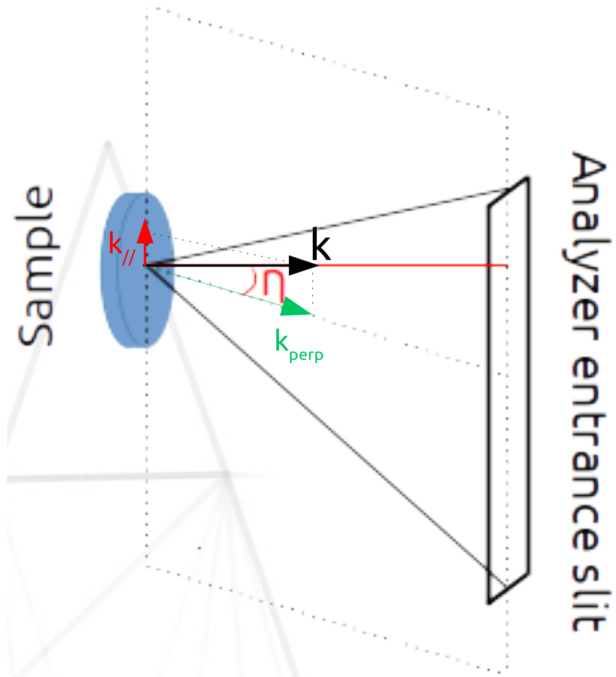

$$E_B \approx h\nu - E_{kin}$$

$$k_{//} = \frac{\sqrt{2mE_{kin}}}{\hbar}\sin(\eta)$$

► Direct measurement of the dispersion along the entrance slit direction

ARPES : scanning the reciprocal space with a 2D detector

Real space

Reciprocal space

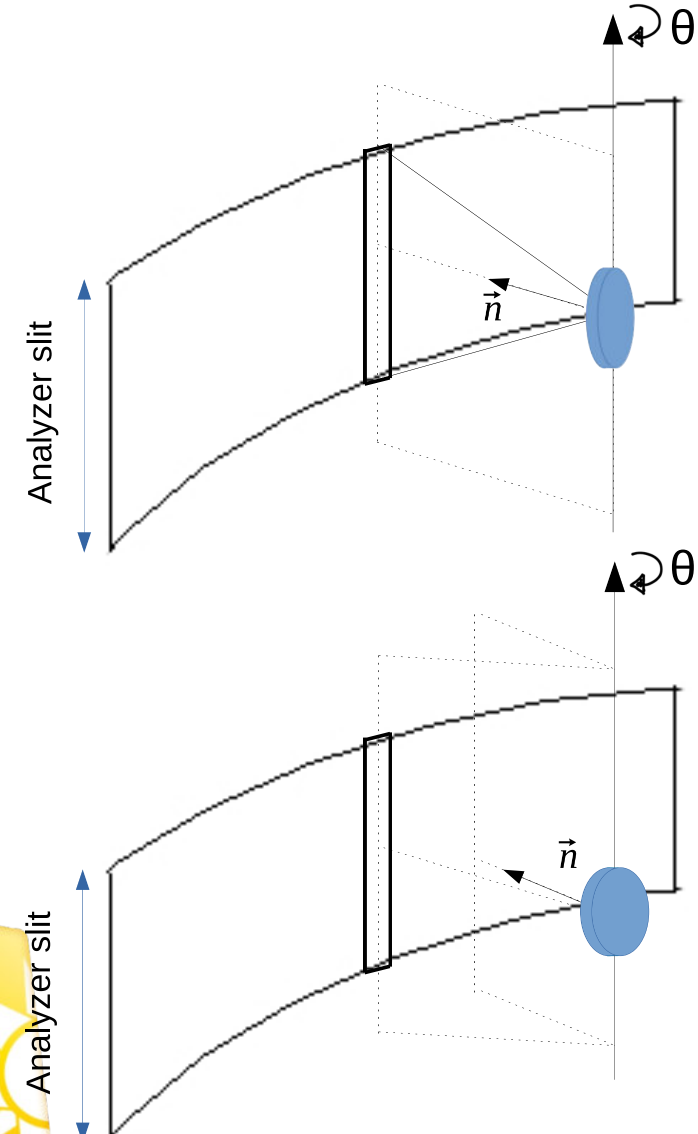

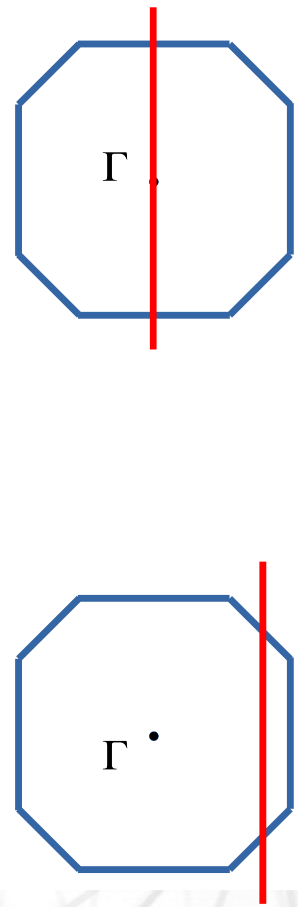

ARPES : scanning the reciprocal space with a 2D detector

Cu(111) surface state

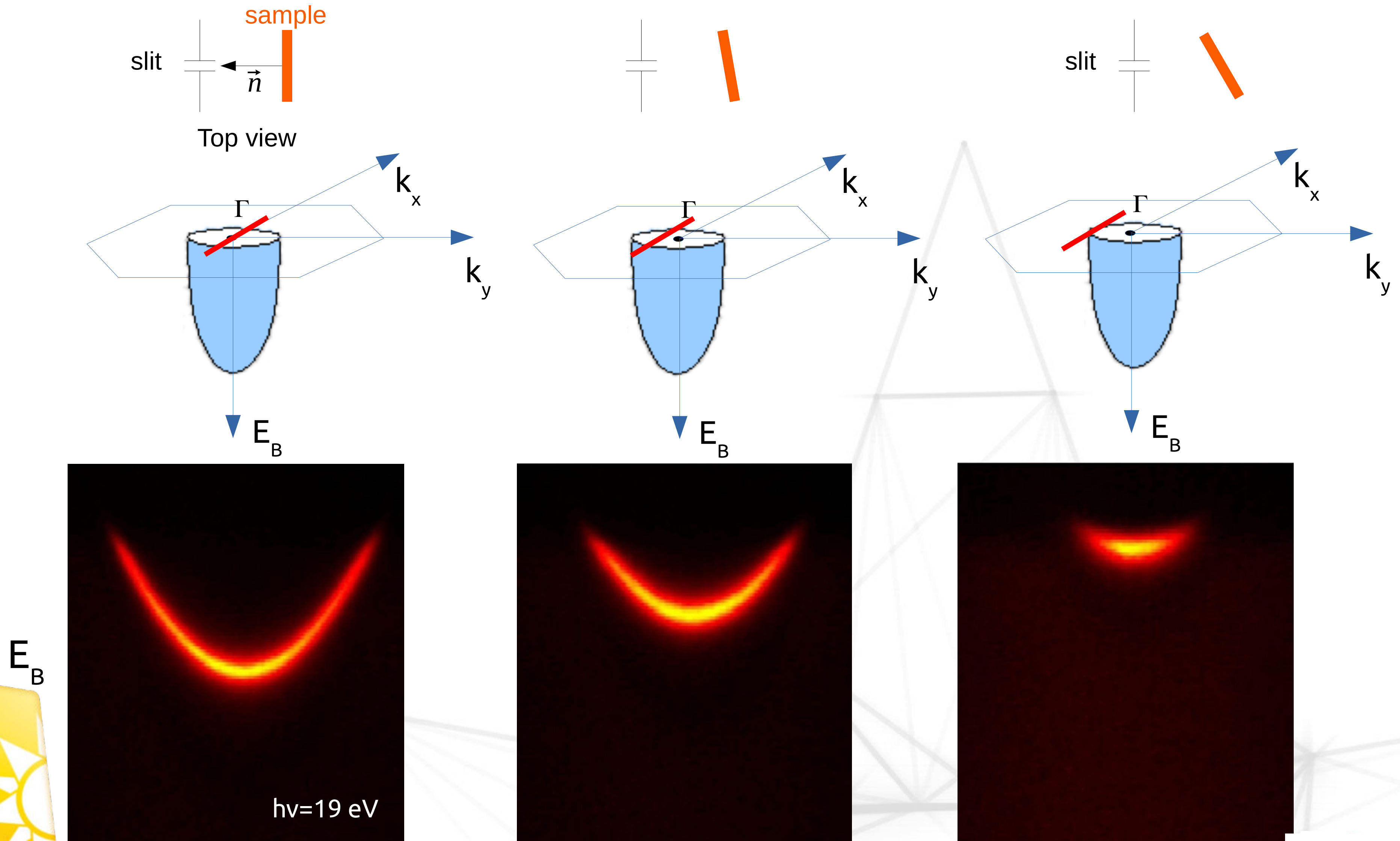

Measurements by Y. Ohtsubo

ARPES : scanning the reciprocal space with a 2D detector

Cu(111) surface state

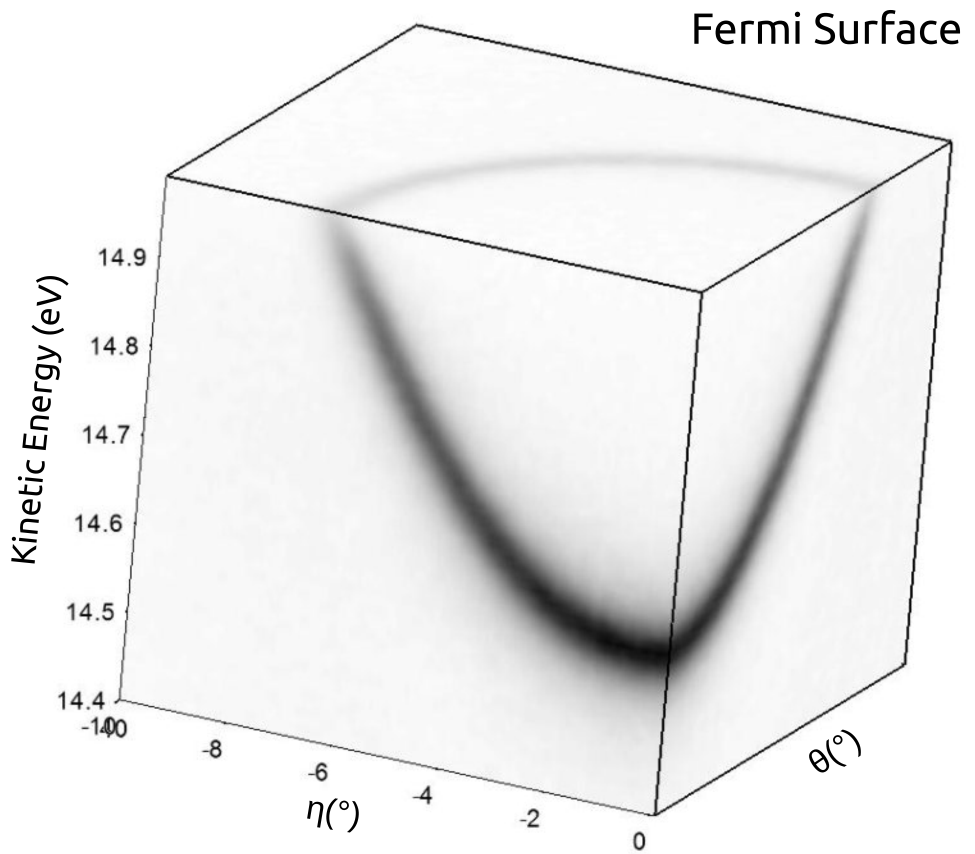

Measurements by Y. Ohtsubo

ARPES : surface sensitivity

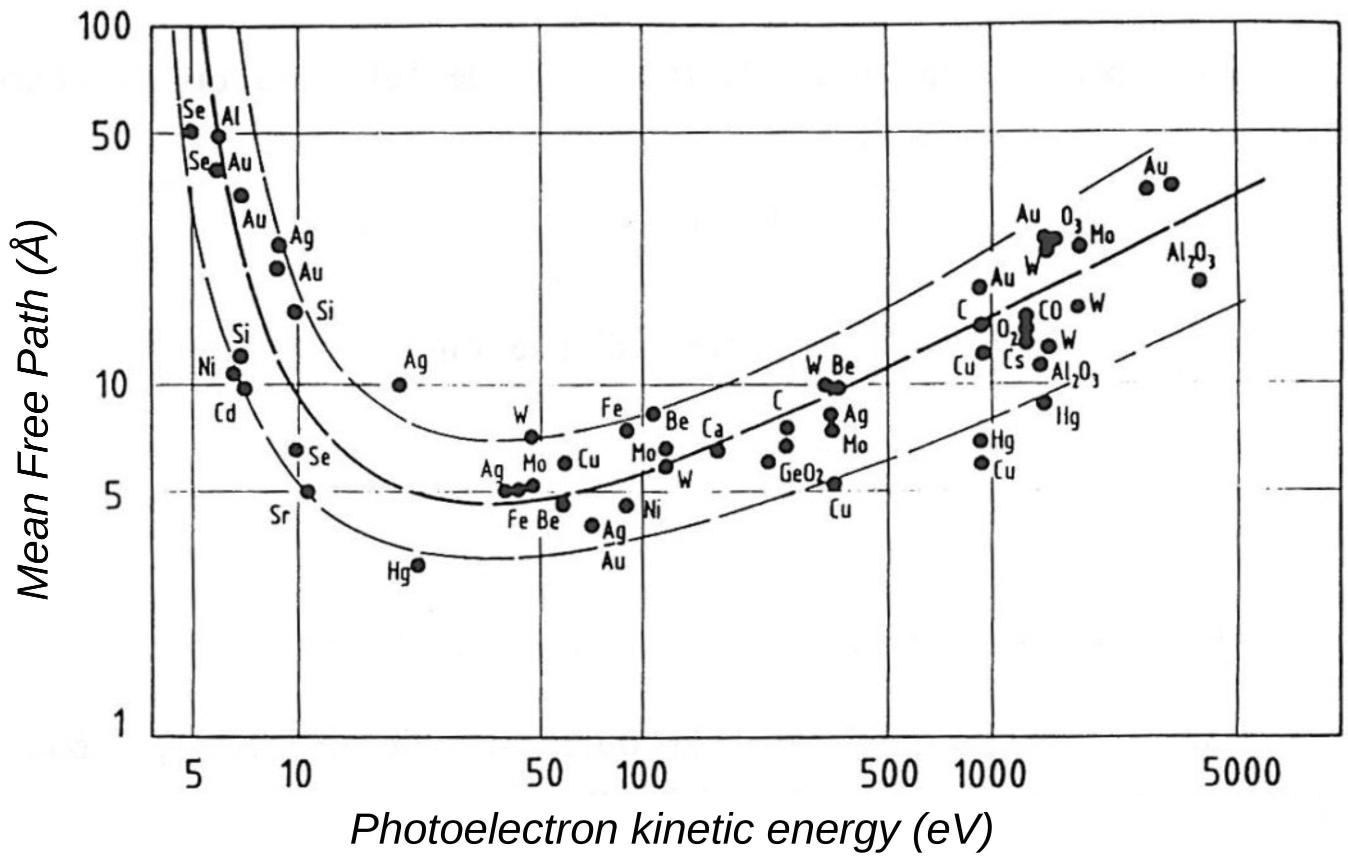

Electron cannot travel far in matter :

Photoemission is therefore a surface sensitive technique, probing the first atomic planes of the sample.

Spin-resolved Photoemission

Spin-resolved ARPES : spin detection

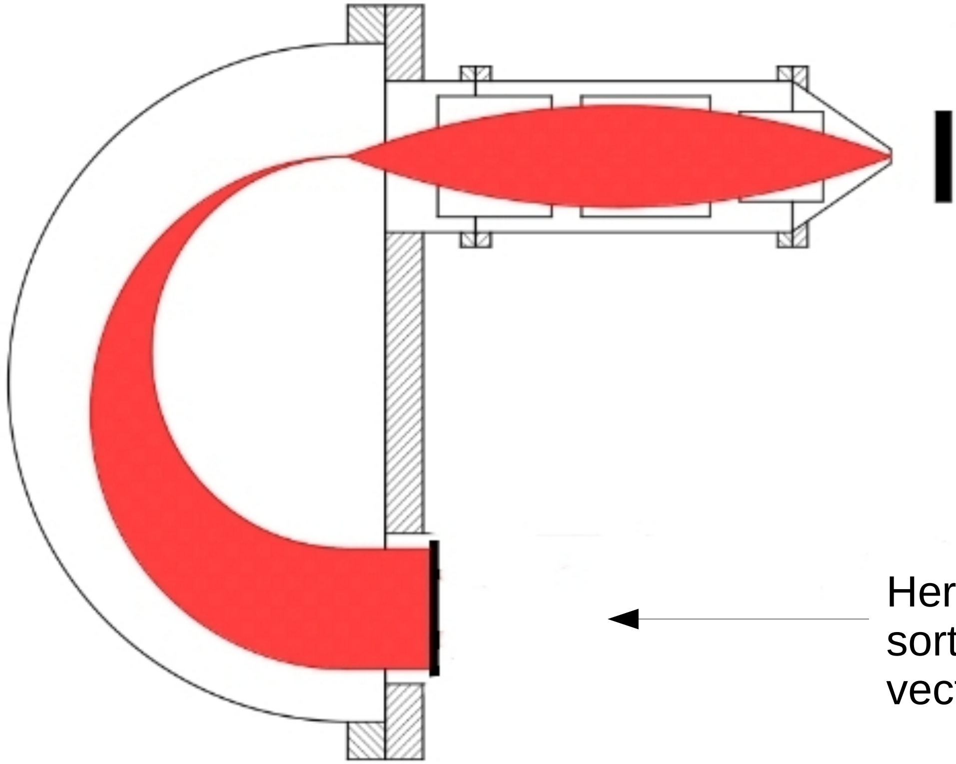

Here, the photoelectrons are sorted in energy and wave vector...

Spin-resolved ARPES : spin detection

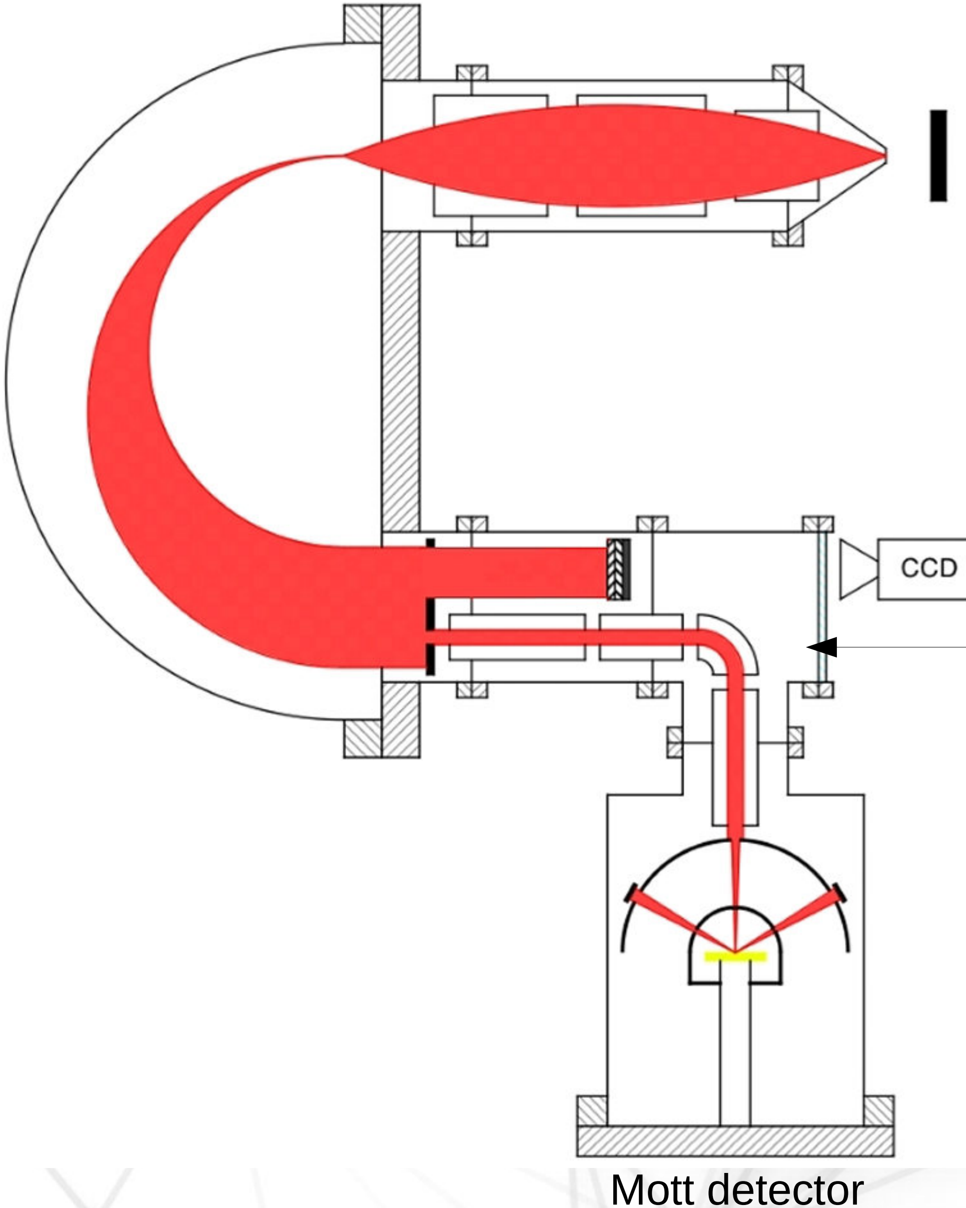

… We can select a « precise » (E_K,k) electron...

...and do a spin analysis (Spin-ARPES)

F. Bertran, CASSIOPEE beamline

Spin-ARPES : the Mott detector

Selected photoelectrons

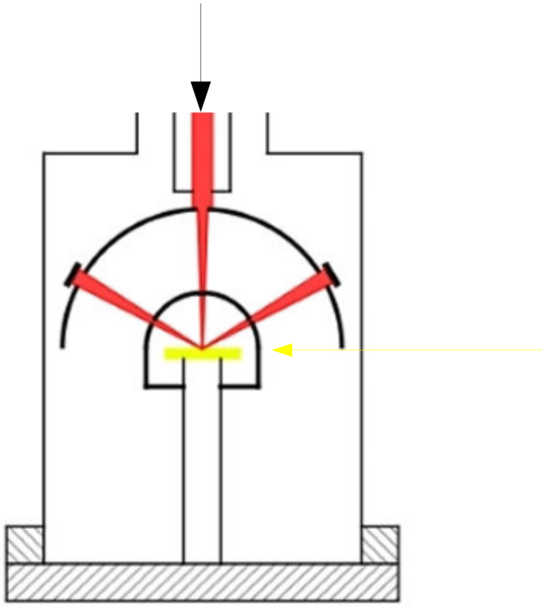

Gold target (@25 kV)

Mott detector

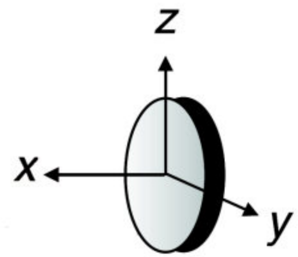

Spin-ARPES : the Mott detector

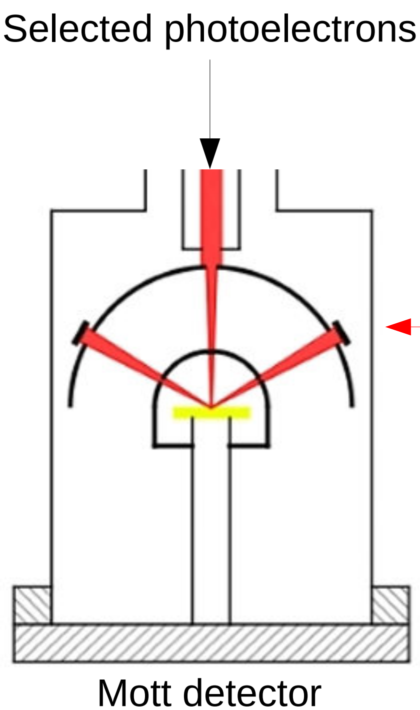

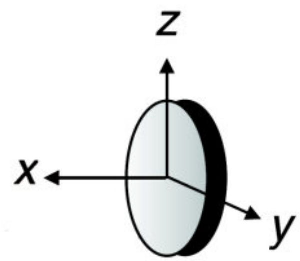

Spin-dependent scattering...

A Au-nucleus is seen as a moving charge by the electron

- ► The electron experiences a magnetic field
- ► Interaction between the electron spin and this magnetic field
- ► This interaction depends on the spin

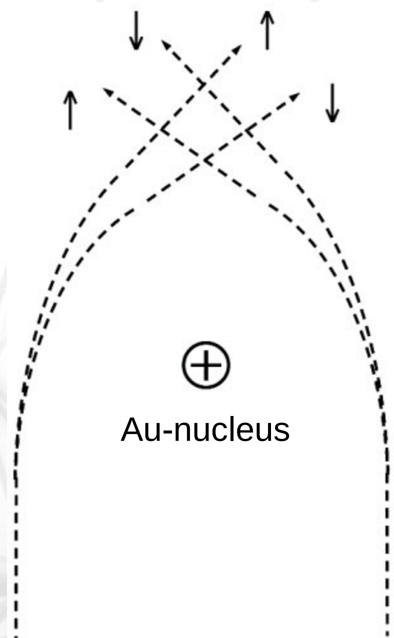

In two symmetrical directions, we should measure a spin-asymetric signal...

Spin-ARPES : the Mott detector

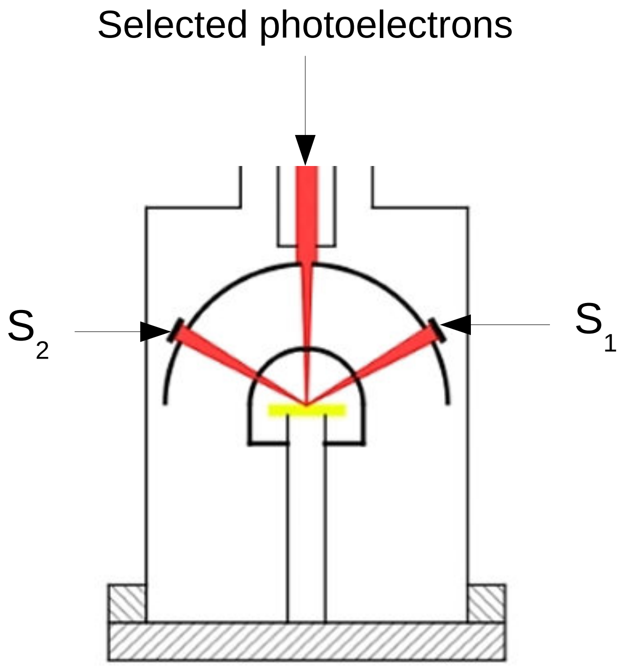

Mott detector

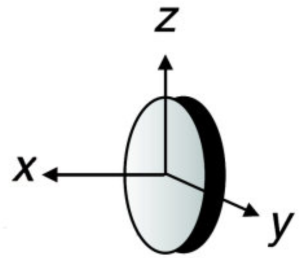

► Asymmetry ***A*** between the 2 measured signals S_1 and S_2

$$A = \frac{S_1 - S_2}{S_1 + S_2}$$

$$A = P_y . S$$

P_i : Spin polarization along i

S : Sherman function (between 0.1 and 0.2 for a Mott detector)

► Another pair of detectors measures P_x.

$$DOS(\uparrow) = \frac{1}{2}(S_1 + S_2)(1 + P)$$

$$DOS(\downarrow) = \frac{1}{2}(S_1 + S_2)(1 - P)$$

ARPES and Spin-ARPES for spintronics :

Some examples

α-Sn and topological insulators

Topological insulator :
Insulating bulk and a conductive surface

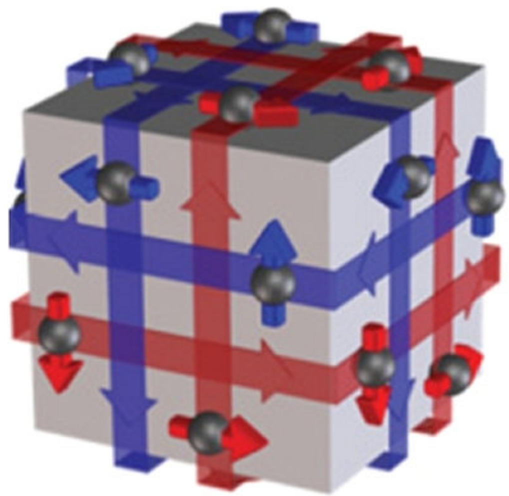

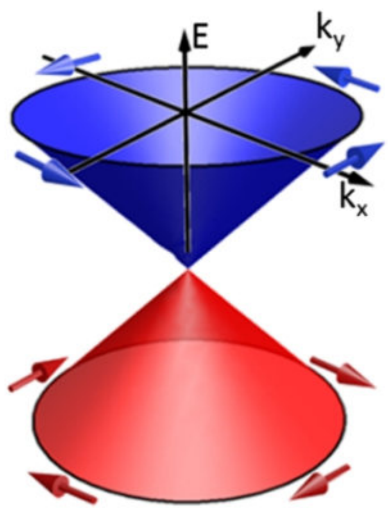

$\Rightarrow$ Spin$\perp\vec{k}$

$\Rightarrow$ Spin texture

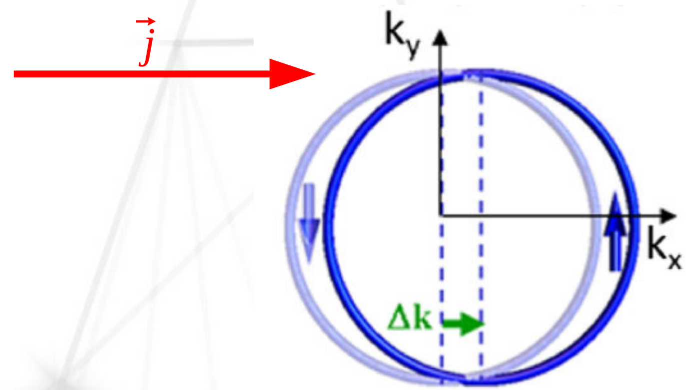

Surface state dispersion

Edelstein effect :
Charge current along ⇒Spin accumulation along y

Topological insulators could be very interesting materials for spin/charge conversion

α-Sn and topological insulators

First discovered 3D topological insulators were :

$Bi_{1-x}Sb_x$ alloys

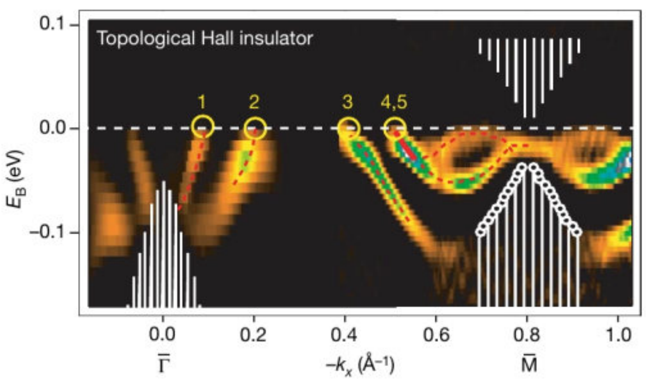

*Hsieh et al., Nature **452**, 970 (2008)*

Bi_2Se_3 and Bi_2Te_3

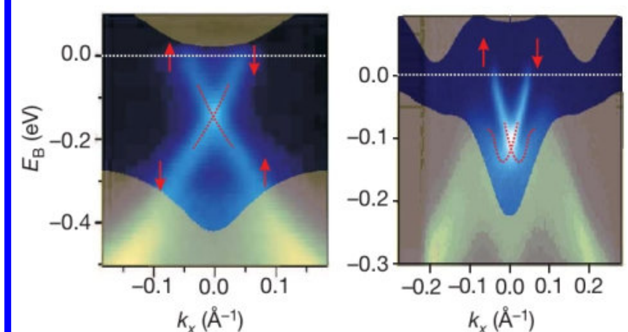

*Hsieh et al., Nature **460**, 1101 (2009)*

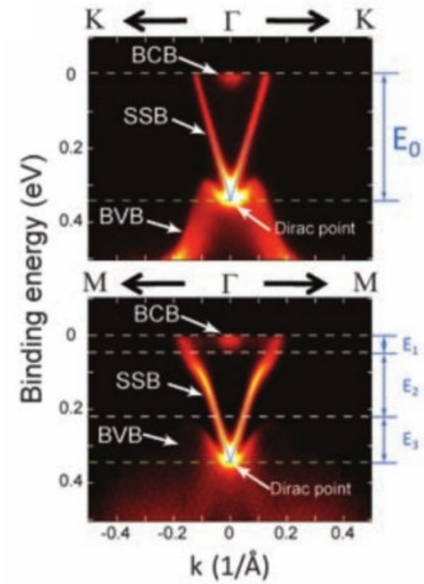

*Chen et al., Science **325**, 178 (2009)*

Surface topological state (in 3D materials) first observed by ARPES :

- ► Surface sensitivity is an advantage !
- ► 2D electronic states : very easy to study by ARPES
- ► Spin resolution to evidence the spin texture

α-Sn and topological insulators

Sn was predicted to be a topological insulator, but in its α-phase which is not stable at room temperature…

… but can be stabilzed in thin films deposited on InSb(001)

Structure of Sn

Room temperature

Below 13°C (286 K)

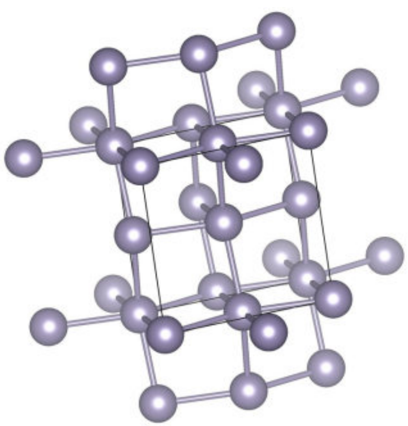

β-Sn – BCT structure

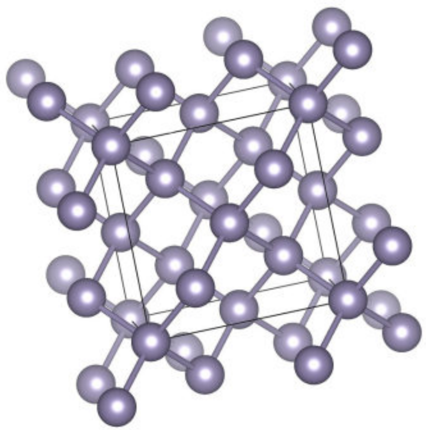

α-Sn – Diamond structure

Topological SS in α-Sn/InSb(001)

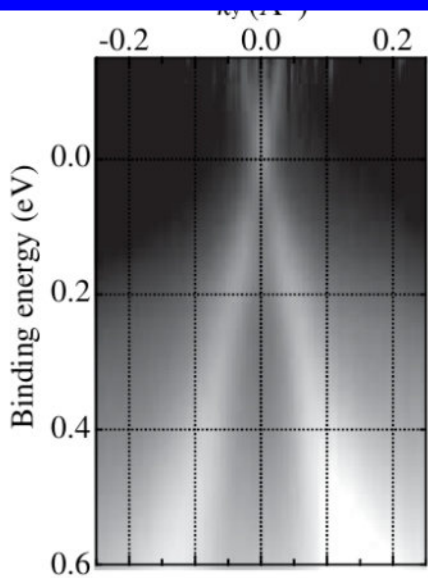

Ohtsubo et al.,
PRL ***111****, 216401 (2013)*

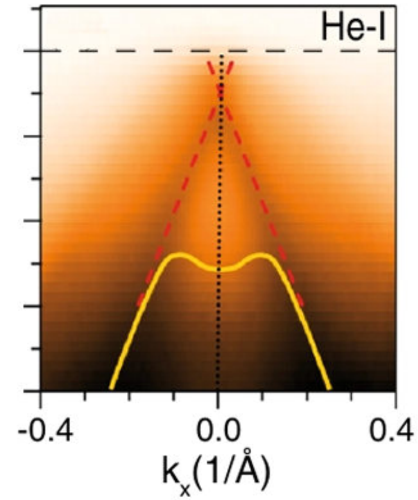

Barfuss et al.,
PRL ***111****, 157205 (2013)*

Can we use this material for spintronics ?

α-Sn for spin/charge conversion

To use α-Sn in a spintronic device, it has to be associated with a magnetic material...

SS behaviour upon capping

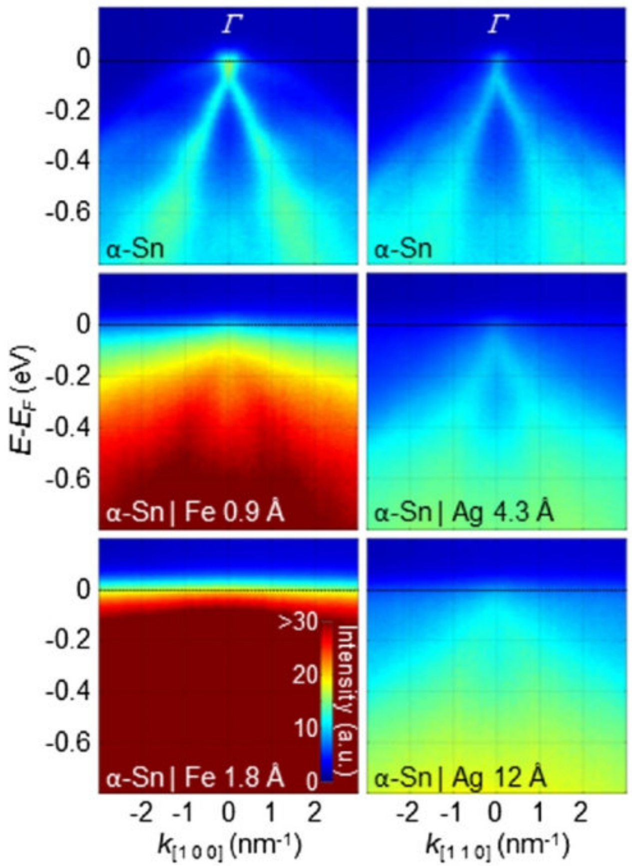

Surface state services if capped with Ag !
(but not if capped with Fe)

Inverse Edelstein effect in α-Sn

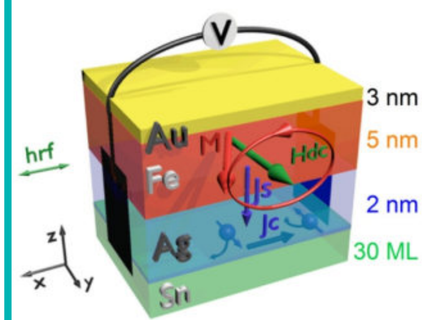

Device built with a Ag-layer in between the TI and the Fe-layer

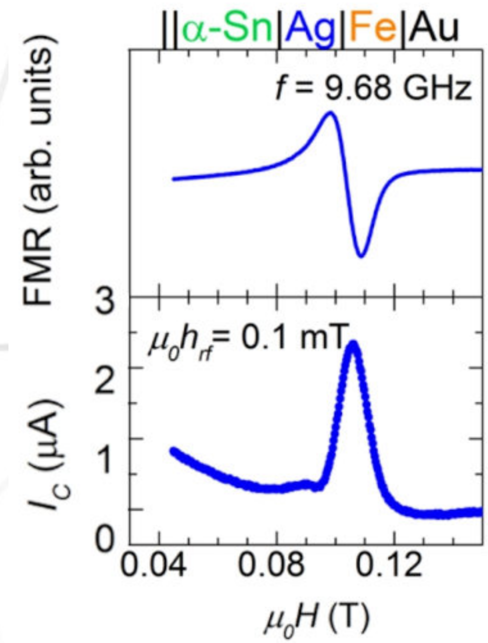

Rojas-Sanchez et al., Phys.Rev. Lett. ***116****, 096602 (2016)*

See also Barbedienne et al., Phys. Rev. B ***98****, 195445 (2018)*

Spin-resolved photoemission in half-metal Heusler alloys

Half-metals

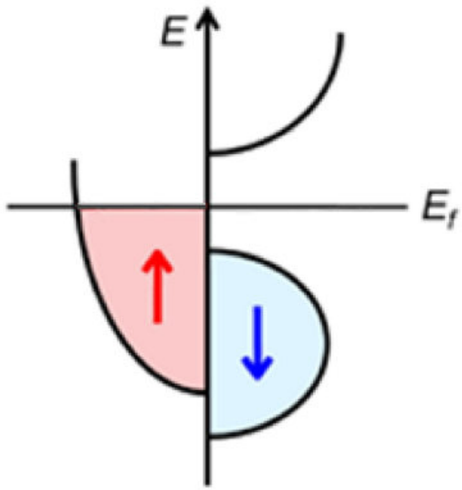

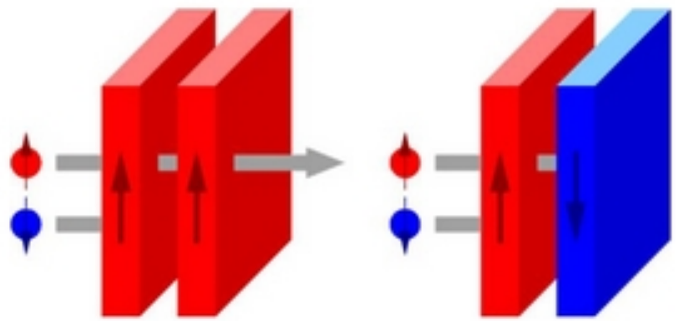

Only one spin-population at E_F :
- ► Could be very interesting for Magnetic Tunnel Junctions
- ► Or to generate spin-polarized currents
- ► Low damping materials : easy precession of the magnetization

Half-metals : $Co_2MnGe/MgO(001)$

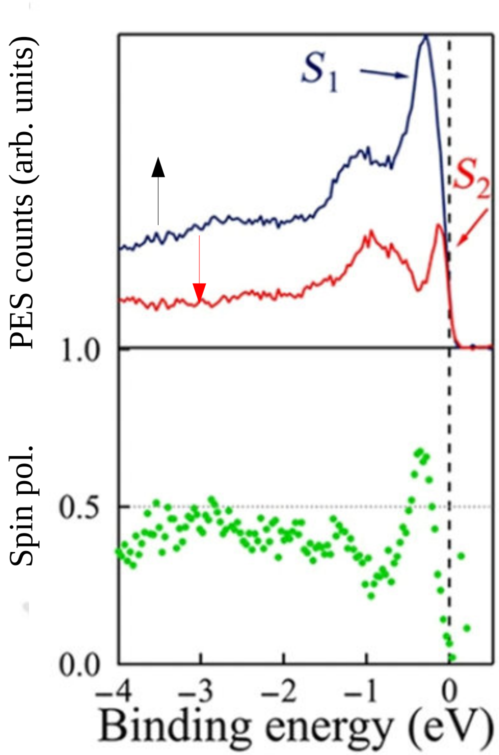

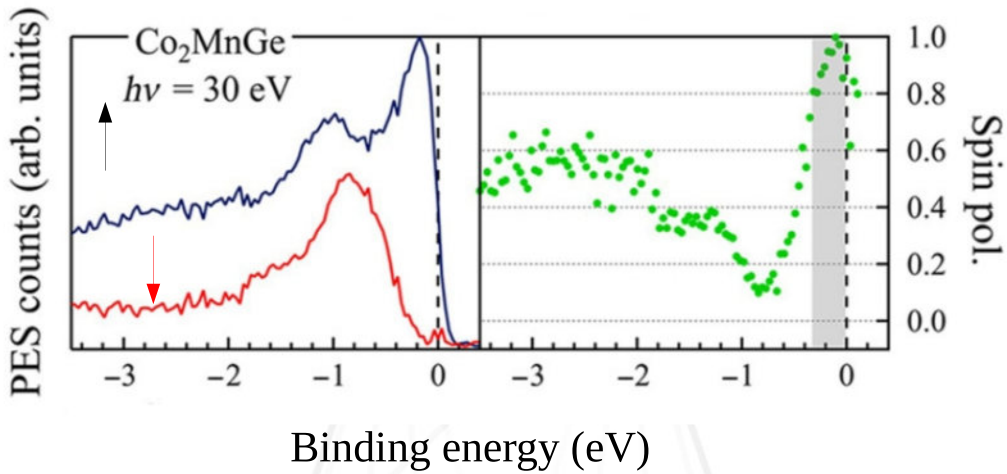

… But one can get rid of them by changing the light polarization !

Nicely illustrates strength and drawbacks of photoemission...

The measurements is perturbed by the presence of surface states...

Guillemard et al., Phys.Rev. Appl. ***11****, 064009 (2019)*
See also : Andrieu et al., Phys.Rev. B ***93****, 094417 (2016)*

ARPES : advantages and drawbacks

The surface sensitivity of photoemission and the easy determination of $k_{//}$ makes ARPES very efficient for :

► Surface electronic structure
Surface states, Rashba splitting, topological edge states...

► 2D systems
Lamellar systems, cuprates and other 2D superconductors, graphene, TMDCs...

On the other hand :

► If you are interested in the bulk electronic structure, it is hard to be sure that you are actually probing it…

► The $k_{\perp}$ problem (in addition to the V_0 determination...) :

$$\Delta x . \Delta p \simeq \frac{\hbar}{2}$$

$$\Delta z . \Delta \hbar k_{\perp} \simeq \frac{\hbar}{2}$$

$$\Delta z . \Delta k_{\perp} \simeq \frac{1}{2}$$

Since Δz is small, $\Delta k_{\perp}$ is large… For 3D materials, it is better to use soft x-rays to increase the probed depth.

Outline

SOLEIL SYNCHROTRON

sextants
Soft x-ray EXperimenT resonANT Scattering

- Synchrotron a brief history and SOLEIL

- ARPES and spin-ARPES: k resolved approach with a short range point of view

- Resonant elastic scattering:k resolved approach with a long range point of view

Outline

SOLEIL SYNCHROTRON

sextants
Soft x-ray EXperimenT resonANT Scattering

- Introduction to Resonant Elastic X-ray Scattering (REXS)
- Magnetic Chirality in thin films by REXS
  + Co/Pt multilayers
  + BiFeO3

- if time :Use of Coherence probed by REXS
  + Holography

REXS: basics

SOLEIL SYNCHROTRON

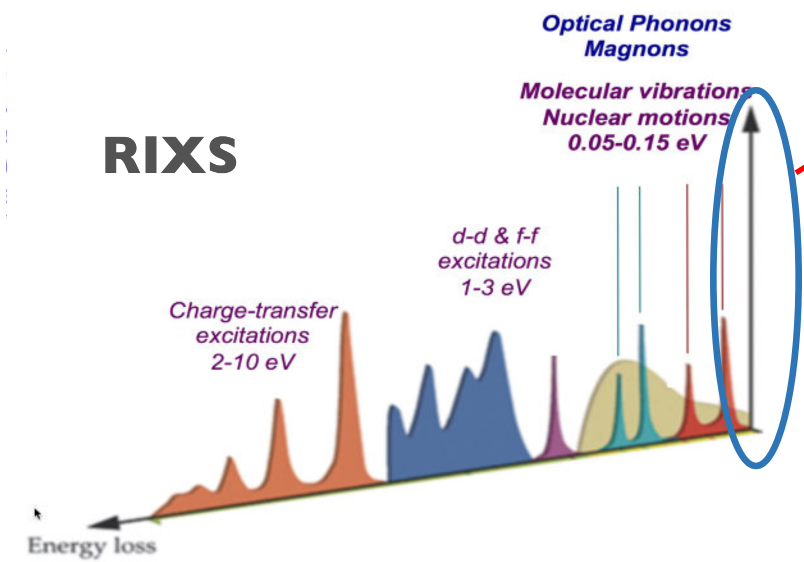

Resonant Elastic X-ray Scattering (REXS)

$$\frac{d\sigma}{d\Omega} = r_0^2 \left| \sum_n e^{i\mathbf{Q}\cdot\mathbf{R}_n} f_n(\mathbf{k}, \mathbf{k}', \hat{\epsilon}, \hat{\epsilon}', \hbar\omega_k) \right|^2$$

Structure factor   Atomic form factor

Atomic form factor give the matter tensor and its angular dependence for a single site

Structure factor gives interferences effects

Resonant x-ray scattering amplitude

$$f^{RXS} \approx -\frac{1}{m} \sum_c \frac{E_g - E_c}{\hbar\omega_k} \cdot \frac{\langle g | \sum_j e^{-i\mathbf{k}'\cdot\mathbf{r}_j} \hat{\boldsymbol{\epsilon}}'^* \cdot \mathbf{p}_j | c \rangle \langle c | \sum_j e^{i\mathbf{k}\cdot\mathbf{r}_j} \hat{\boldsymbol{\epsilon}} \cdot \mathbf{p}_j | g \rangle}{E_g - E_c + \hbar\omega_k - i\Gamma_c/2}$$

Series expansion of the transition operator

$$e^{i\mathbf{k}\cdot\mathbf{r}_j} \approx 1 + i\mathbf{k}\cdot\mathbf{r}_j - (\mathbf{k}\cdot\mathbf{r}_j)^2/2 + \ldots$$

× (ε·p)   E1   E2   E3   M1 ≈ 0 for X-rays

Δℓ=±1   Δℓ=0, ±2   Δℓ=±1, ±3

REXS: basics

Zoo of electric and magnetic multipoles in matter

Multipole	x	T, I
Charge (q)	0	+, +
Electric dipole (μ)	1	+, −
Magnetic dipole (m)	1	−, +
Polar toroidal dipole (Ω) = anapole	1	−, −
Axial toroidal dipole	1	+, +
Electric quadrupole (Q_{ij})	2	+, +
Magnetic quadrupole (M_{ij})	2	−, −
Polar toroidal quadrupole	2	−, +
Axial toroidal quadrupole (Ω_{ij})	2	+, −

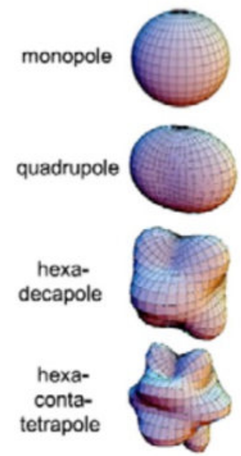

Under Time reversal (T), Spatial inversion (I)

Electric (magnetic) terms are time-even(odd).

Electric monopoles for pure E1 and E2 measure the charge density (q) and quadrupole moment (Q).

E1-E2 (parity odd) require mixed valence (e.g. p-d hybridization). It measure:

- * electric moment μ (times-odd dipole)
- * Toroidal moment (anapole)….

x		E1-E1 T, I		E1-E2 (elec.) T, I		E1-E2 (magn.) T, I		E2-E2 T, I		E1-M1[($)] T, I
0	Monopole	+, +	q					+, +	q	
1	Dipole	−, +	m	+, −	μ	−, −	Ω	−, +	m	Sugar
2	Quadrupole	+, +	Q	+, −	Ω_{ij}	−, −	M_{ij}	+, +	Q	
3	Octupole			+, −		−, −		−, +		

S. Di Matteo et al., J. Phys. D: Appl. Phys. 45, 163001 (2012)

REXS: particular case of magnetic dipole

Hannon equation :

dipolar transition (E1. E1)

Hannon et al., Phys. Rev. Lett. 61, 1241 (1988)

$$I = \sum_x f_x \left[\mathbf{e}'^*, \mathbf{e}\right]^{(x)} \cdot \mathbf{M}^{(x)} = f_0(\mathbf{e}'^* \cdot \mathbf{e}) + f_1(\mathbf{e}'^* \times \mathbf{e}) \cdot \mathbf{M} + f_2(\mathbf{e}'^* \cdot \mathbf{M})(\mathbf{e} \cdot \mathbf{M})$$

e and e'* :Polarization states of incident/diffracted beams

M magnetic moment

f_0 Thomson + resonant charge scattering

f_1 1[st] order magnetic scattering α XMCD

F_2 2[nd] order magnetic scattering α XMLD

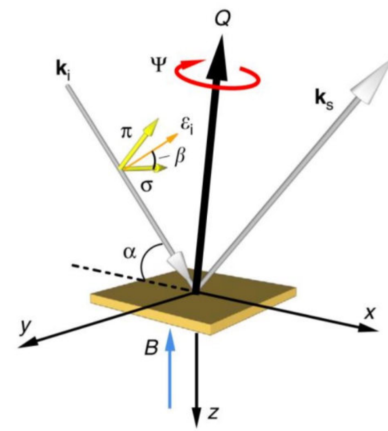

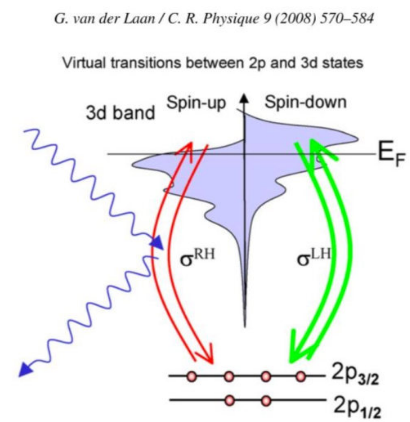

Table 1
Extensions to X-ray scattering possible with synchrotron radiation

Extensions to X-ray scattering	Allows one to probe
Tunable X-rays at resonance	Element, site and valence specificity
Polarized X-rays	Magnetic orbital and spin profile
Soft X-rays	Nanoscale sensitivity (down to 1 nm)
Coherent radiation	Local configuration
Pulsed radiation	Dynamics

G.Van der Laan, C.R. Physique 9 570 (2008)

REXS: selected examples I

√ Charge (Electric monopole)

MIT transition can be explain by charge ordering in NdNiO3 thin film (Commensurate with the lattice)

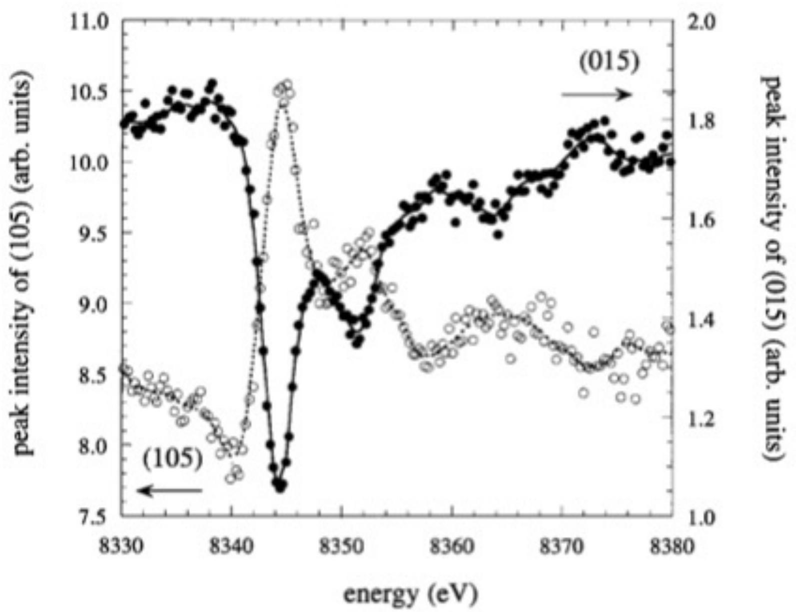

FIG. 2. Energy-dependent x-ray intensity of the (015) and (105) reflections taken at 20 K with σ-σ polarization. The lines are guides to the eye.

Two different $Ni^{3+\delta}$ site with $Ni^{3-\delta'}$ with $\delta+\delta' \approx 0.45$

U. Staub et al., Phys. Rev. Lett. 88, 126402 (2002)

REXS: selected examples 2

✓ Charge (Electric monopole)

Competition between CDW and superconductivity in cuprate by REXS
(Incommensurate with the lattice)

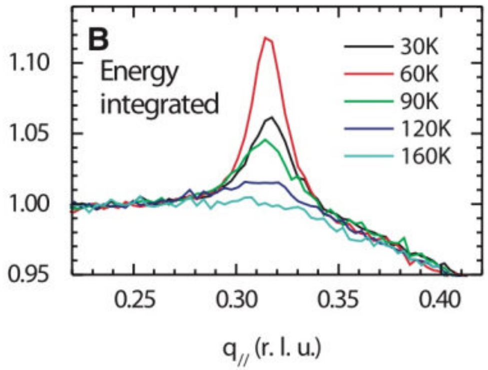

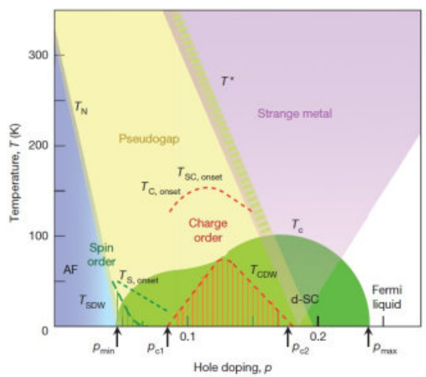

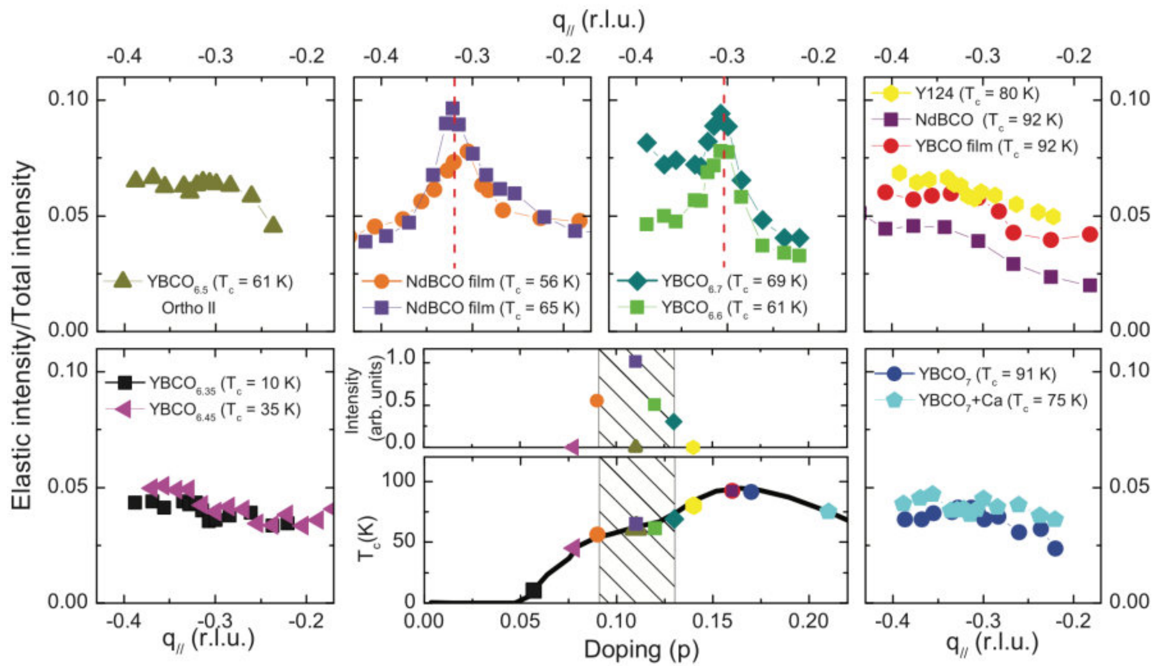

G. Ghiringhelli et al., Science 337, 821 (2012)

REXS: selected examples 3

✓ Charge (Electric monopole)

✓ Orbital

First direct observation of Orbital Order by soft x-ray resonant diffraction. Manganites case.

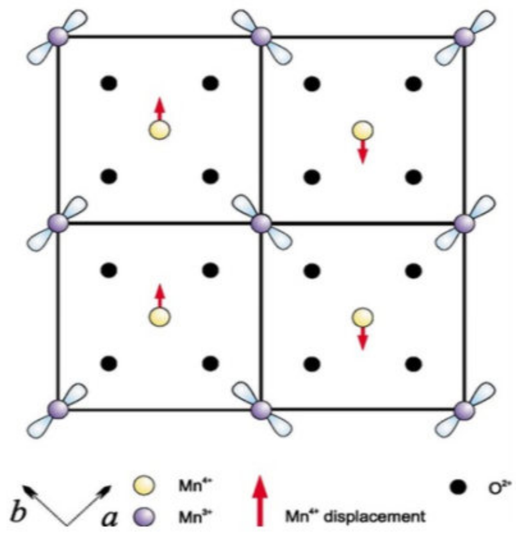

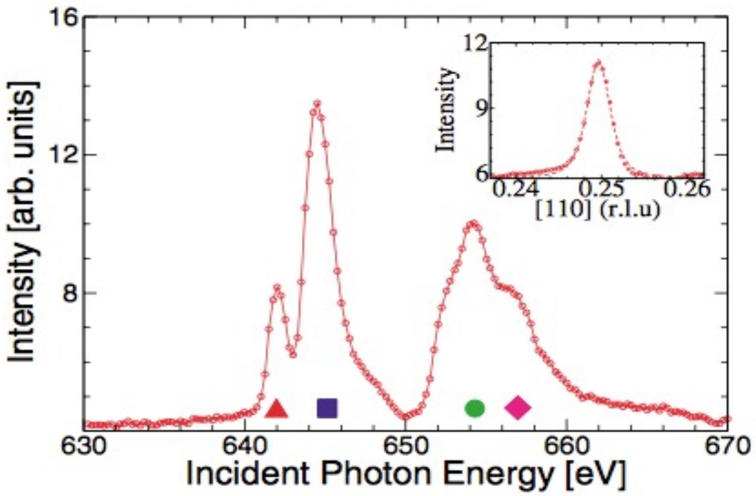

S. Wilkins et al., Phys Rev. Lett 91, 167205 (2003)

REXS: selected exemples 4

√ Charge (Electric monopole)

√ Orbital

√ Spin (Magnetic dipole)

Magnetic profilometry by x-ray resonant magnetic reflectivity

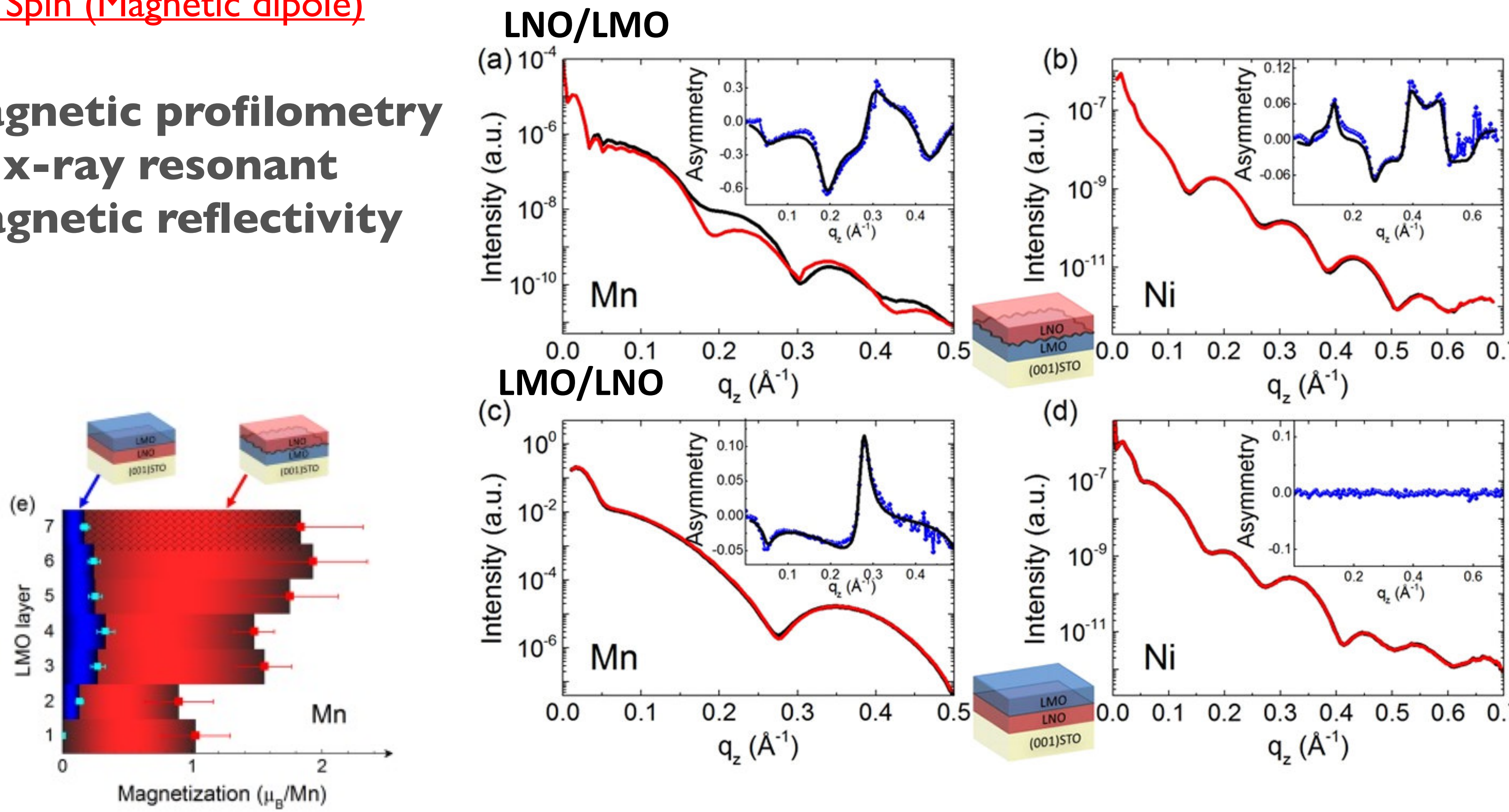

M. Gibert, .., NJ, .. et al., Nat. Comm. 7,11227 (2016)

REXS: selected examples 5

✓ Charge (Electric monopole)
✓ Orbital
✓ Spin (Magnetic dipole)
✓ Electric dipole

Electric chirality in $PbTiO_3/SrTiO_3$ titanate superlattices probed by circular dichroism in REXS

⇒ Indirect* access to Chiral Ferroelectric order

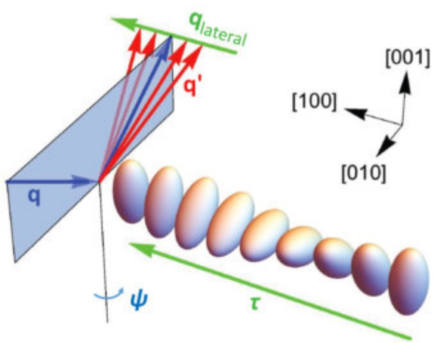

*Lovesey and Van der Laan, Phys. Rev. B 98, 155410 (2018)

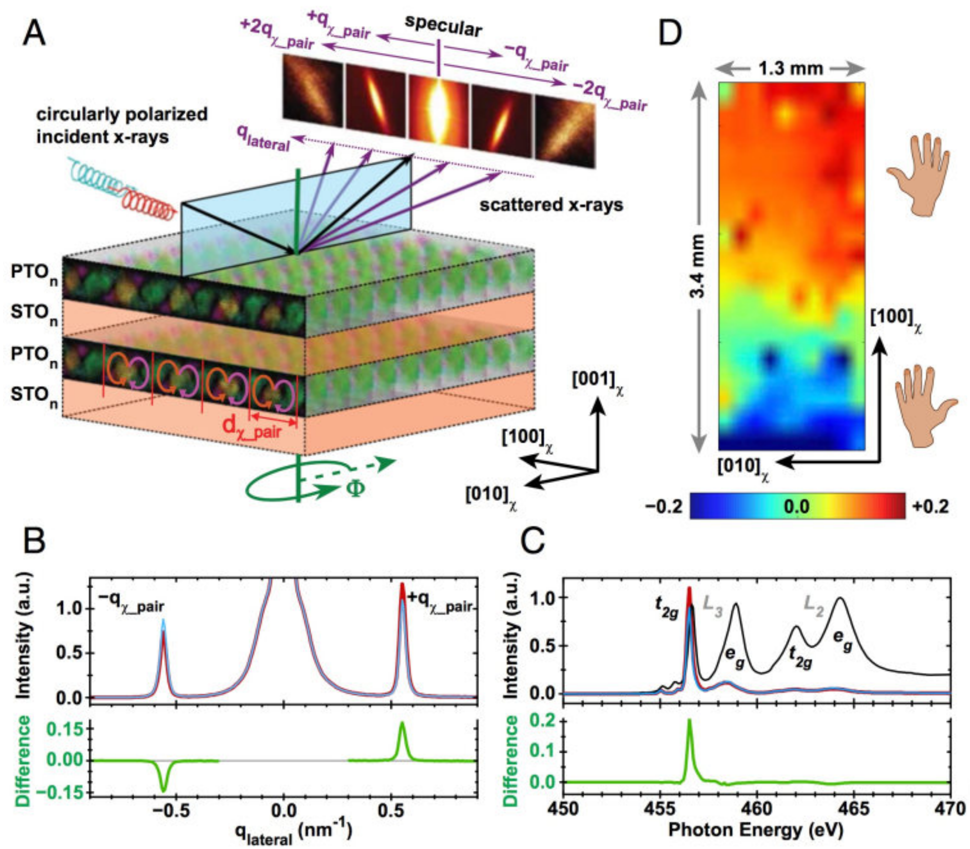

P. Shaffer et al., PNAS 115, 915 (2018)

REXS: selected examples 6

<u>✓ Charge (Electric monopole)</u>
<u>✓ Orbital</u>
<u>✓ Spin (Magnetic dipole)</u>
<u>✓ Electric dipole</u>

Electric and magnetic Chirality in $BiFeO_3$ thin films

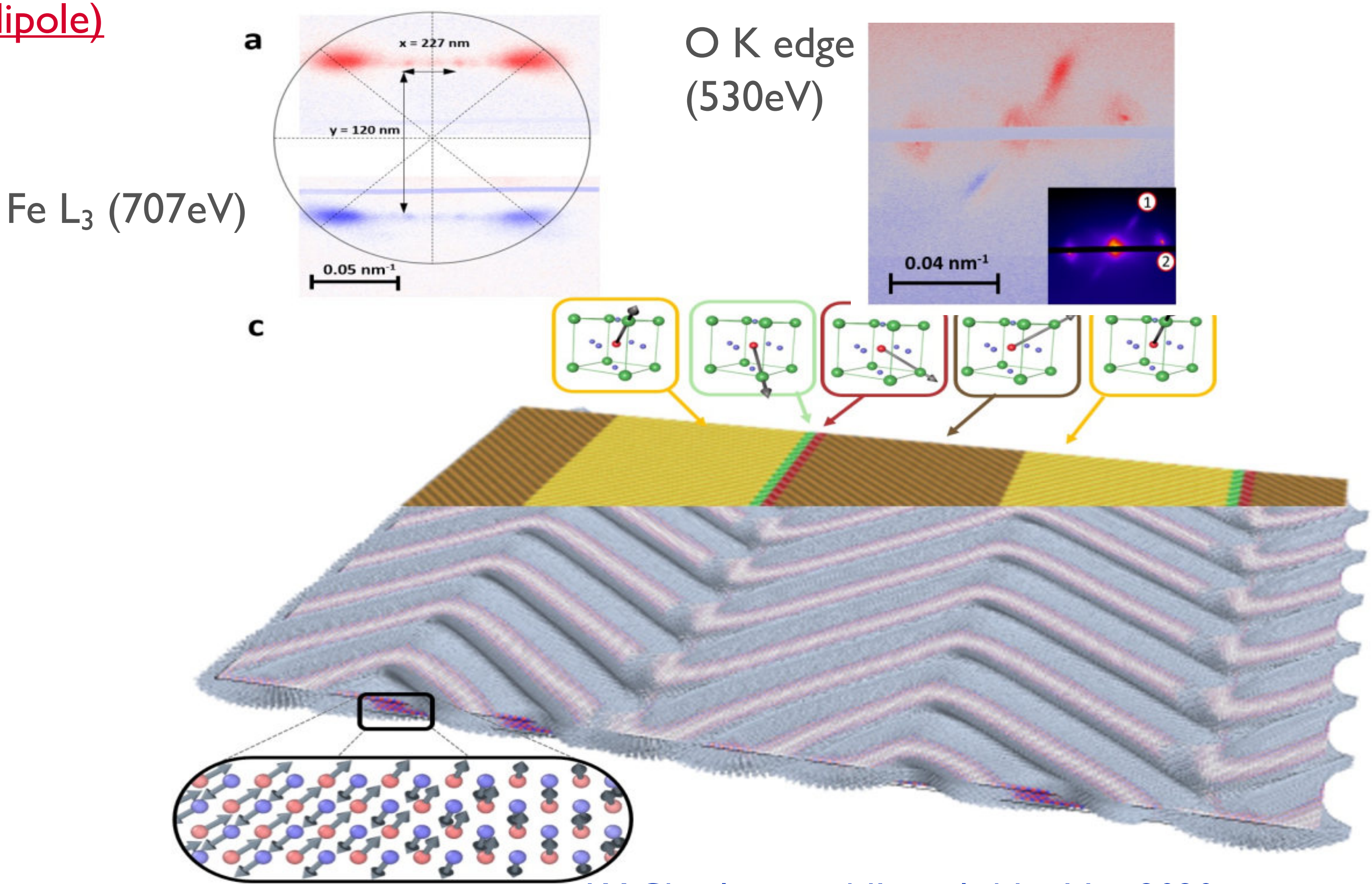

J.Y. Chauleau, …,NJ, et al., Nat Mat. 2020

Outline

sextants

Soft x-ray EXperimenT resonANT Scattering

- Introduction to Resonant Elastic X-ray Scattering (REXS)
- Magnetic Chirality in thin films by REXS
  + Co/Pt multilayers
  + BiFeO3
- if time :Use of Coherence probed by REXS
  + Holography

X-ray resonant scattering : revealing chirality in thin films

2 magnetic systems

Pt/Co multilayers :

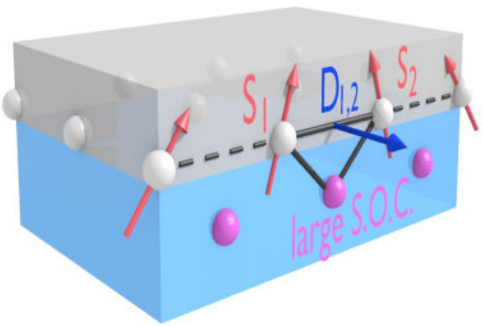

From A. Fert *et al*, *Nature Nanotechnol.* **8**, 152 (2013)

Multiferroic $BiFeO_3$:

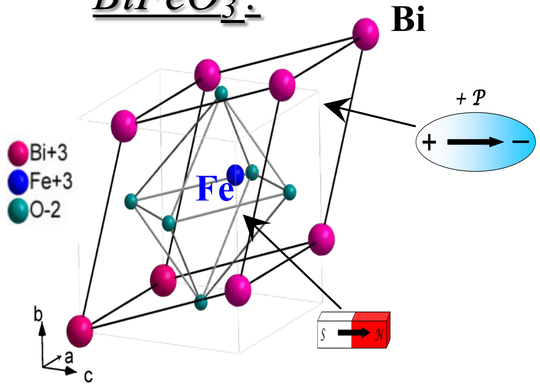

From Kubel *et al*, Acta Cryst. B. **46**, 698 (1990)

Introduction

Magnetic chirality, important aspect of modern magnetism

Skyrmions

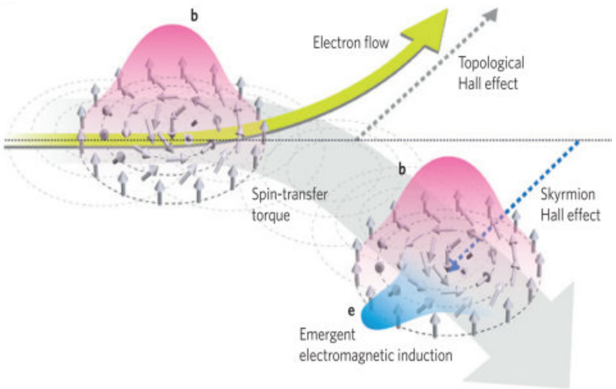

From Nagaosa et al. *Nat. Materials* (2013)

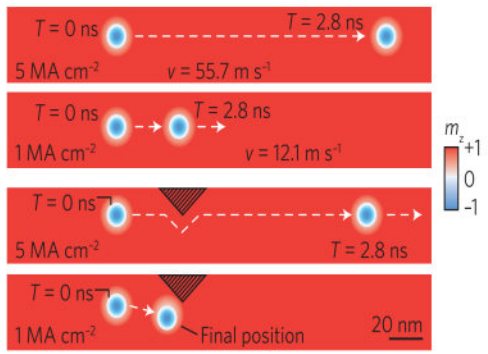

Sampaio et al. Nature Nano. **8**, 839 (2013)

Spin Orbit Torque and Chiral domain walls

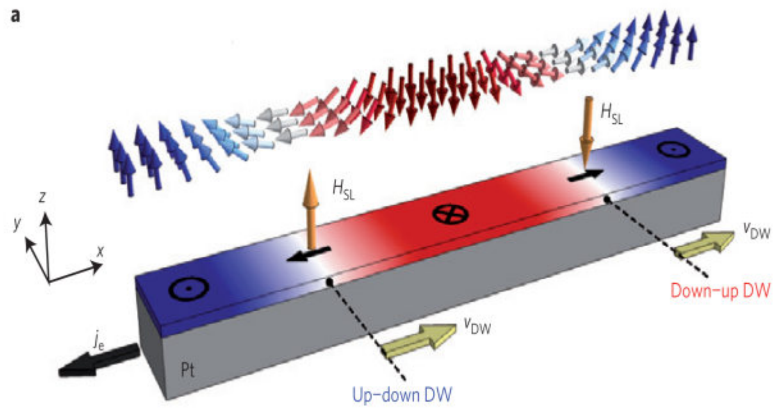

Emori et al. Nat. Materials (2013)

Need to access the full magnetization distribution

Introduction

Neutron scattering

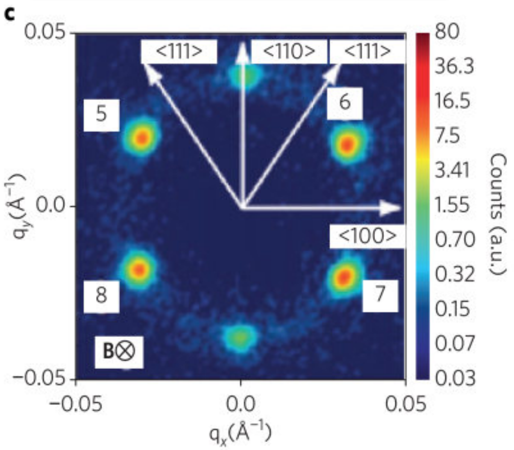

Mülhbauer et al. *Science* **323** 915 (2009)

Electron microscopy

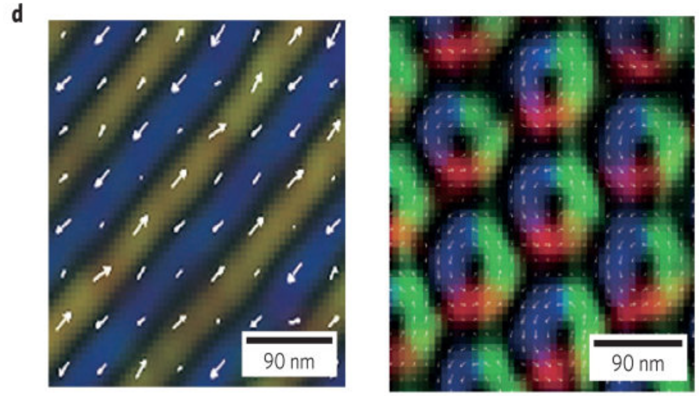

Yu et al. *Nature* **465** 901 (2010)

N.V. magnetometry

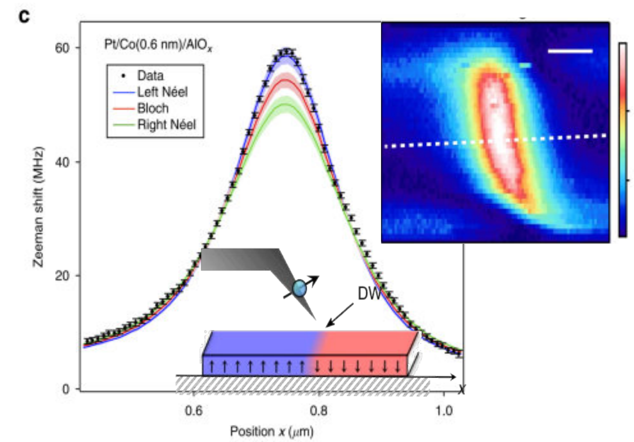

Tetienne et al. *Nat. Comm.* (2015)

SP-STM

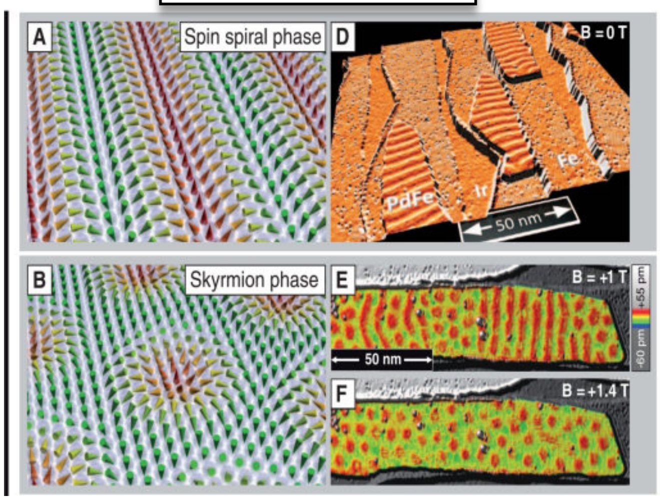

Romming et al. *Science* ***341*** 636 (2013)

MFM

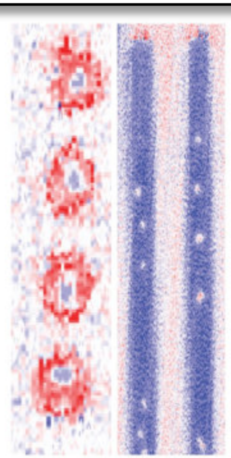

Moreau-Luchaire et al. *Nat. Nano.* **11** 444 (2016)

STXM

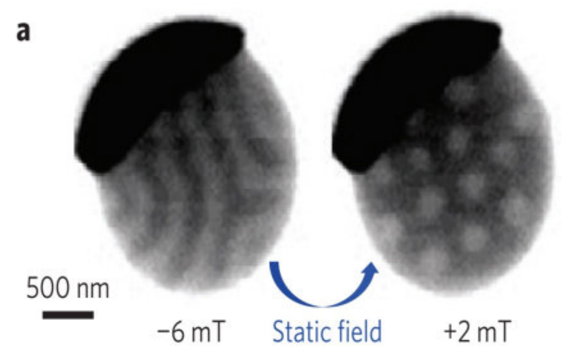

Woo et al. *Nat. Materials* **15** 501 (2016)

X-ray resonant scattering and chirality

Pioneer work on closure magnetic domains:

Science (1999)

Chiral Magnetic Domain Structures in Ultrathin FePd Films

H. A. Dürr,[1] E. Dudzik,[1,2] S. S. Dhesi,[1] J. B. Goedkoop,[3] G. van der Laan,[1*] M. Belakhovsky,[4] C. Mocuta,[4] A. Marty,[4] Y. Samson[4]

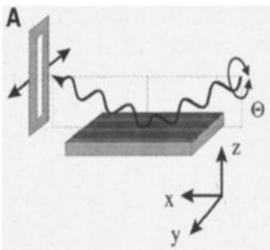

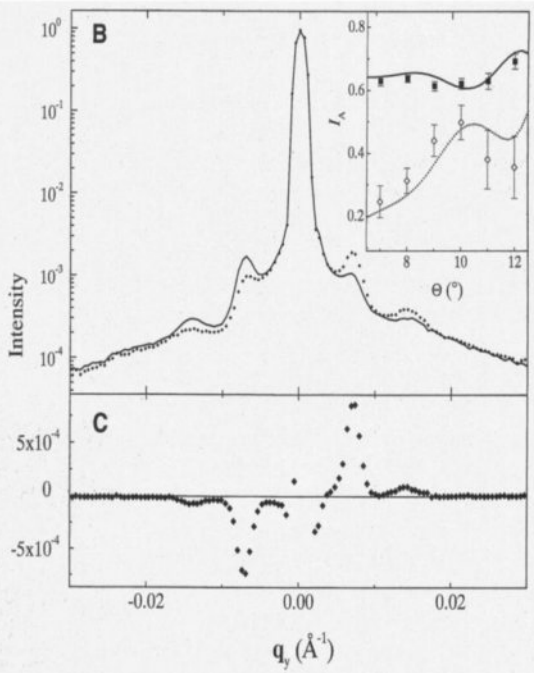

Fig. 2. (**A**) Experimental geometry with x-rays incident along the stripe direction at grazing angle Θ. (**B**) Diffraction scans with the wave vector, $\mathbf{q}_y$, transferred along the y axis perpendicular to the magnetic stripes. Left circularly polarized (dotted line, I^-) and right circularly polarized (solid line, I^+) x-rays with energy tuned to the Fe L_3 absorption edge (λ = 17.5 Å) impinge at an angle of Θ = 12° relative to the surface plane. The inset shows the values of $I_A = (I^+ - I^-)/(I^+ + I^-)$ versus Θ for the first-order (■) and second-order (◇) magnetic satellite peaks. The lines are a fit to the data as described in the text. (**C**) Difference signal, $I^+ - I^-$, of the diffraction scans in (B).

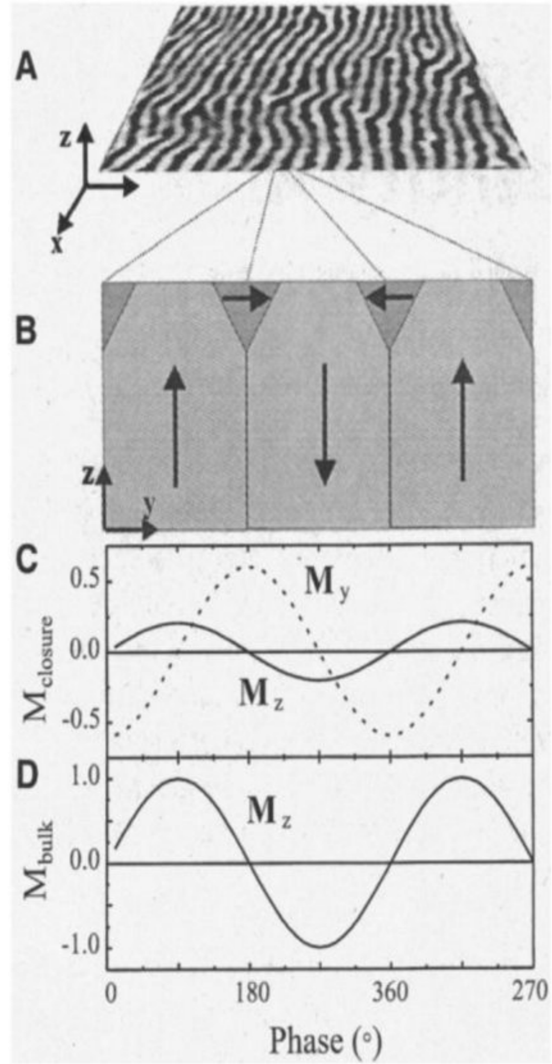

[Pt/Co/Ir] multilayers

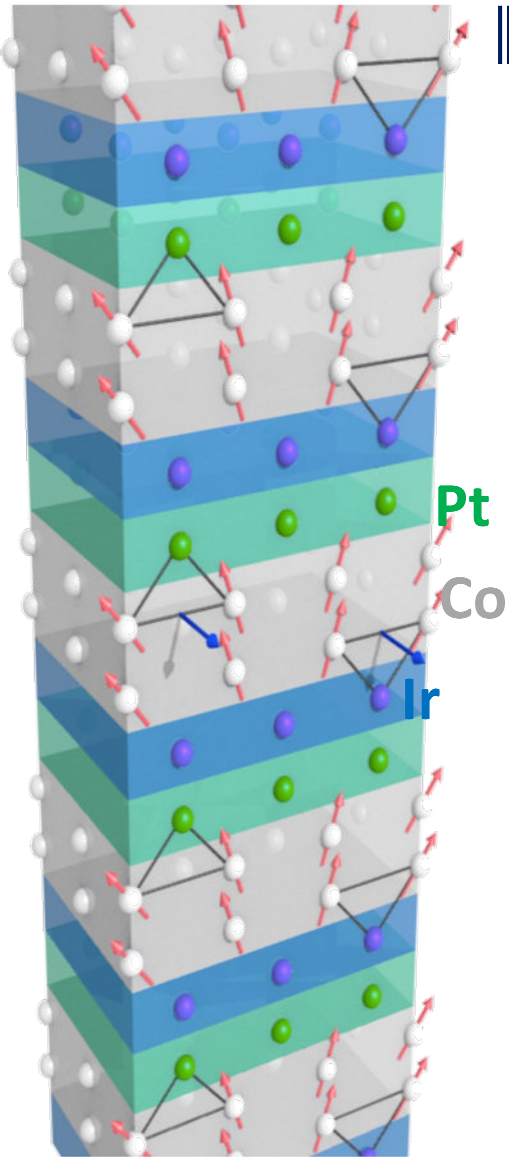

$\|$ Pt 10 | (**Ir** 1| Co 0.8 |**Pt** 1)$_n$ | Pt 3

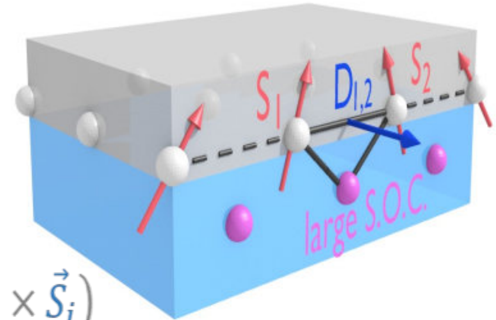

$$H_{H+DM} = -J\sum(\vec{S}_i \cdot \vec{S}_j) - \sum \vec{d}_{ij} \cdot (\vec{S}_i \times \vec{S}_j)$$

A. Fert *et al*, *Nature Nanotechnol.* **8**, 152 (2013)
A. Fert *Materials Science Forum* **59**, 439 (1990)

Some examples (6x6µm² MFM images):

$\|$ Pt 10 | (**Ir** 1| Co 0.6 |**Pt** 1)$_5$ | Pt 3

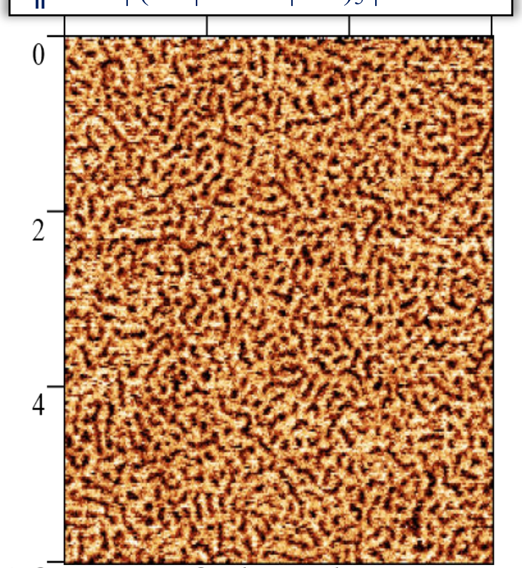

After out-of-plane demag.

$\|$ Pt 10 | (**Ir** 1| Co 0.8 |**Pt** 1)$_{20}$ | Pt 3

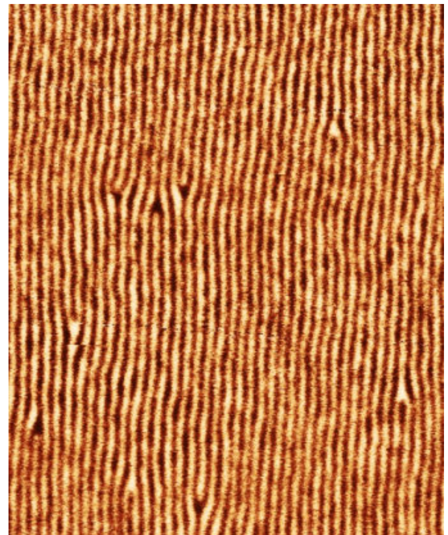

After in-plane demag.

[Pt/Co/Ir] multilayers

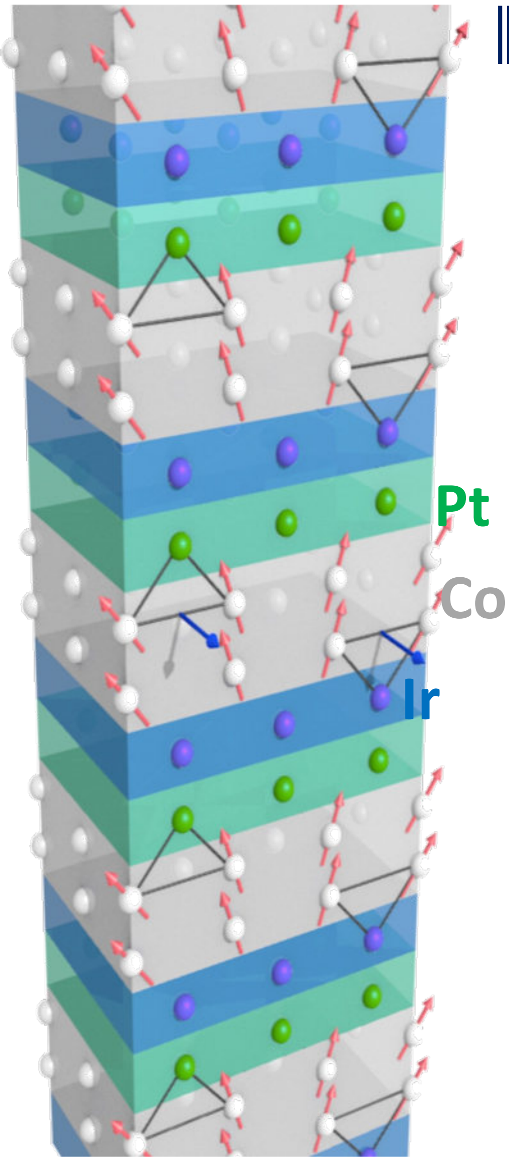

‖ Pt $_{10}$ | (**Ir** $_{1}$| Co $_{0.8}$ |**Pt** $_{1}$)$_{n}$ | Pt $_{3}$

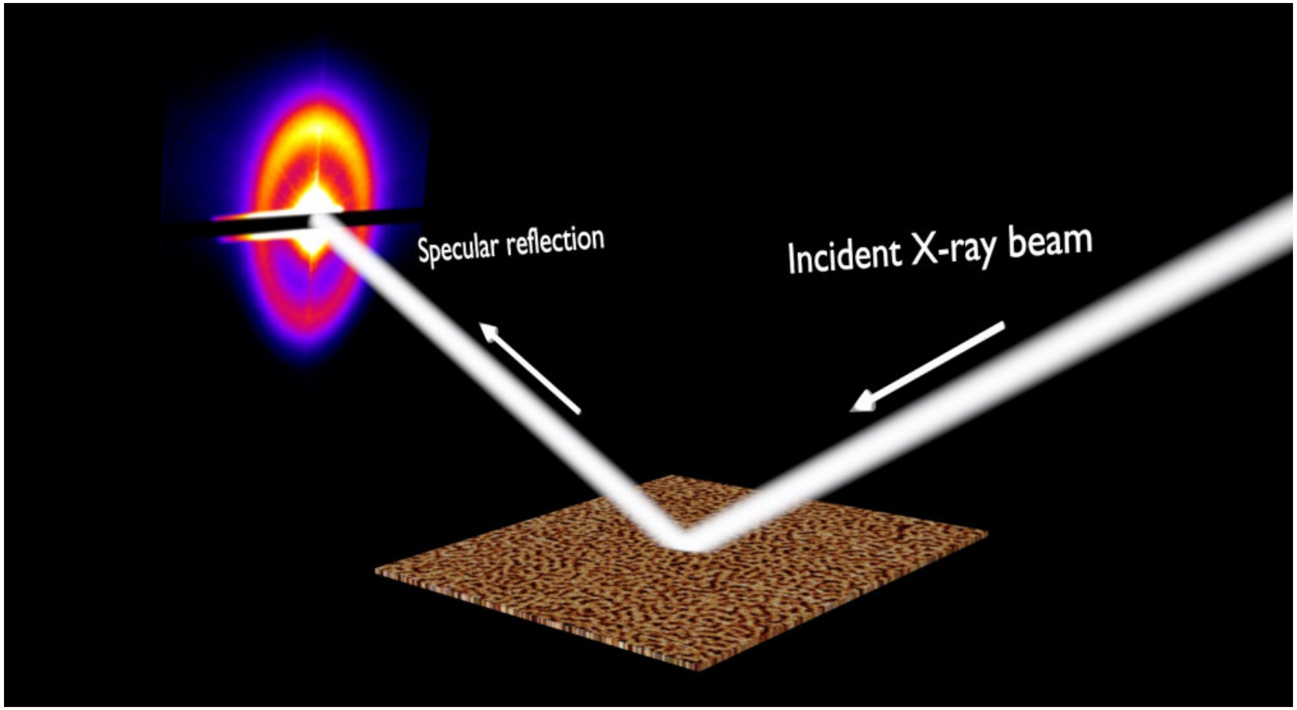

[Pt/Co/Ir] multilayers

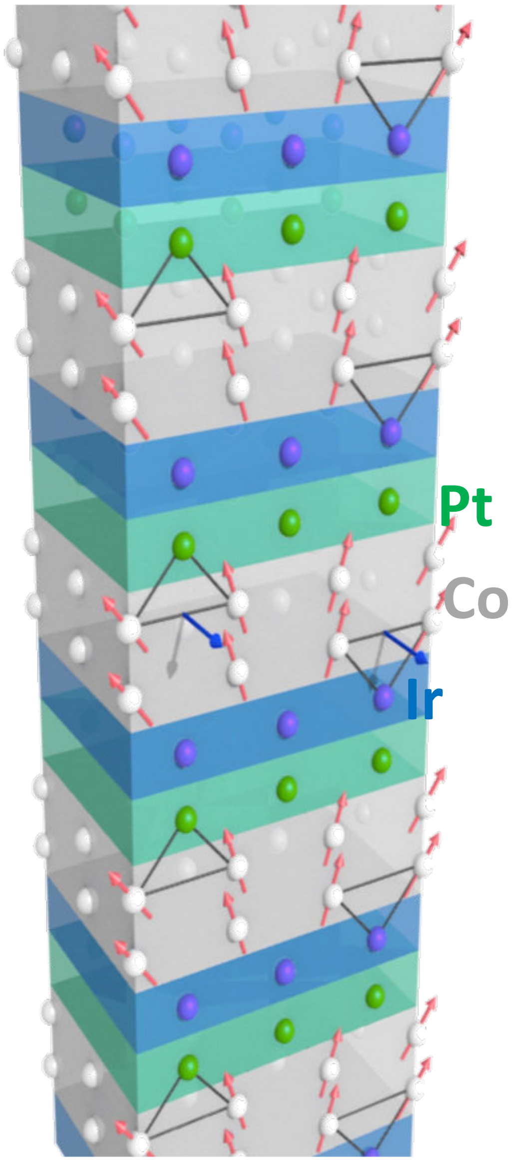

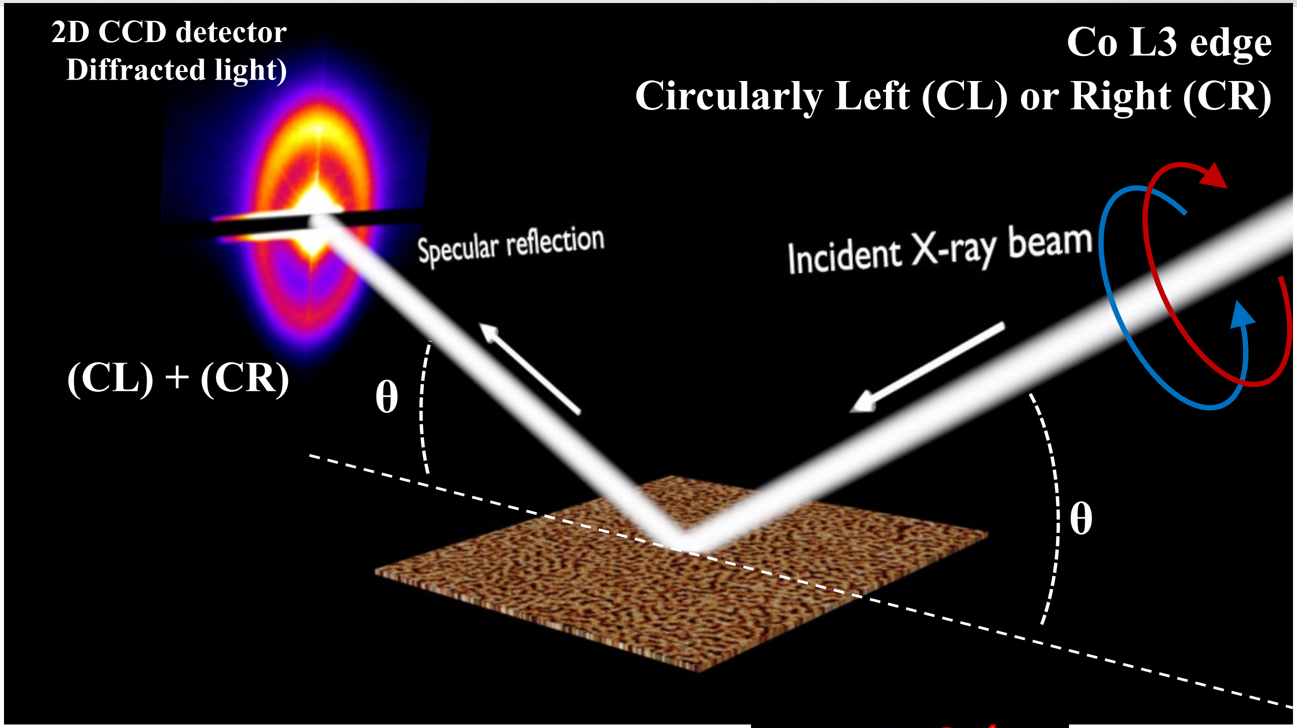

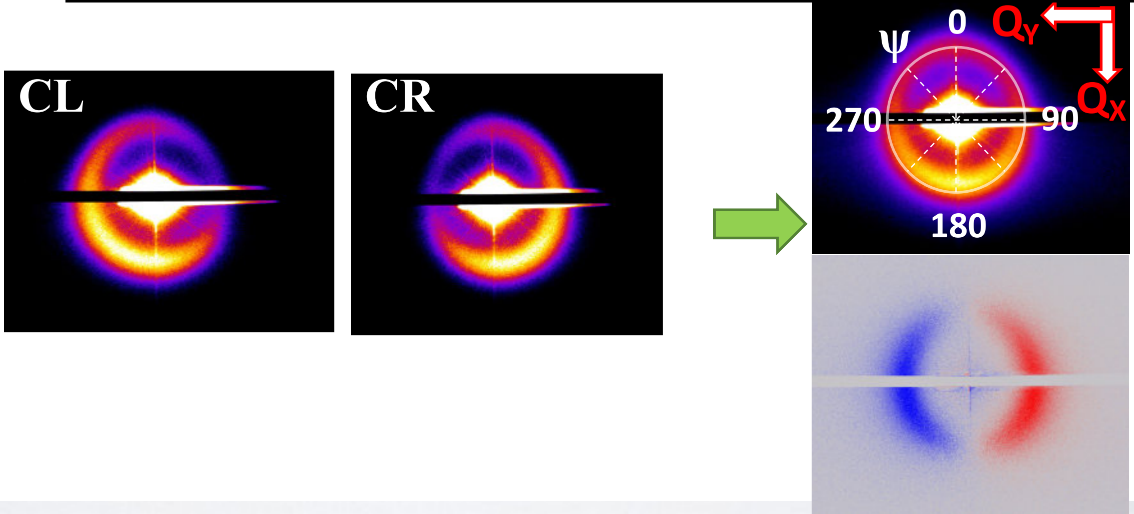

[Pt/Co/Ir] multilayers

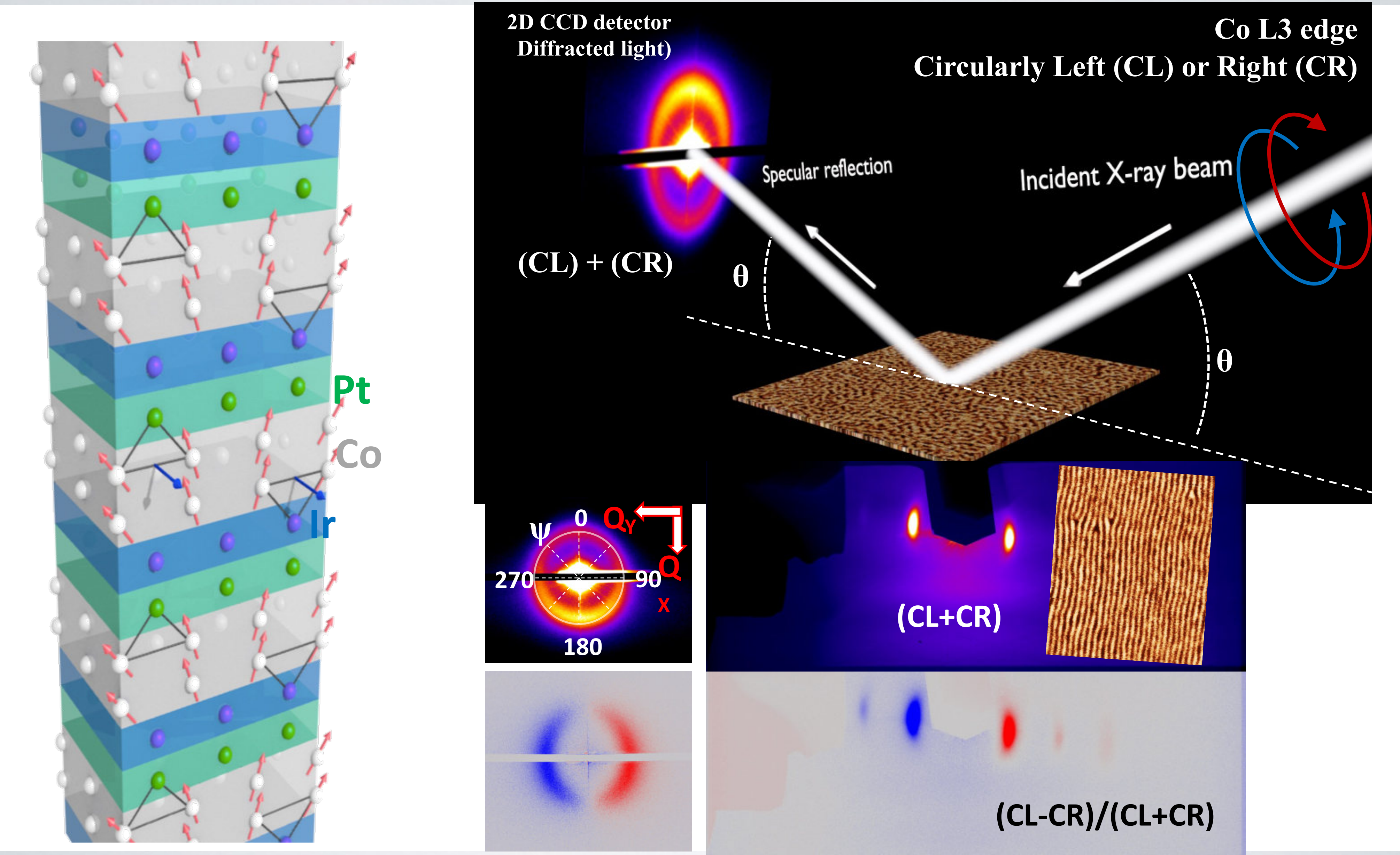

[Pt/Co/Ir] multilayers

Circular dichroism *orthoradial* profile:

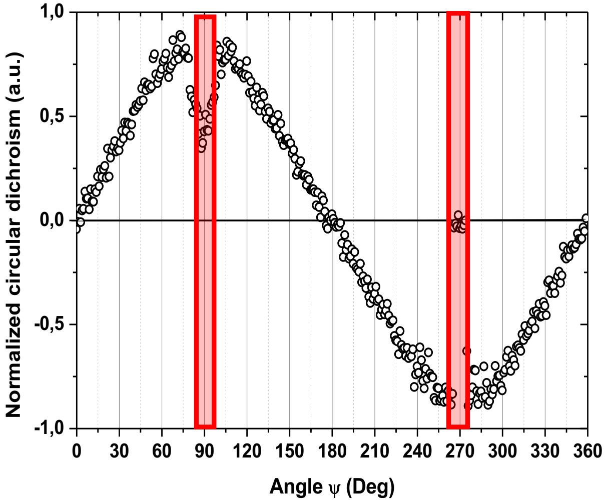

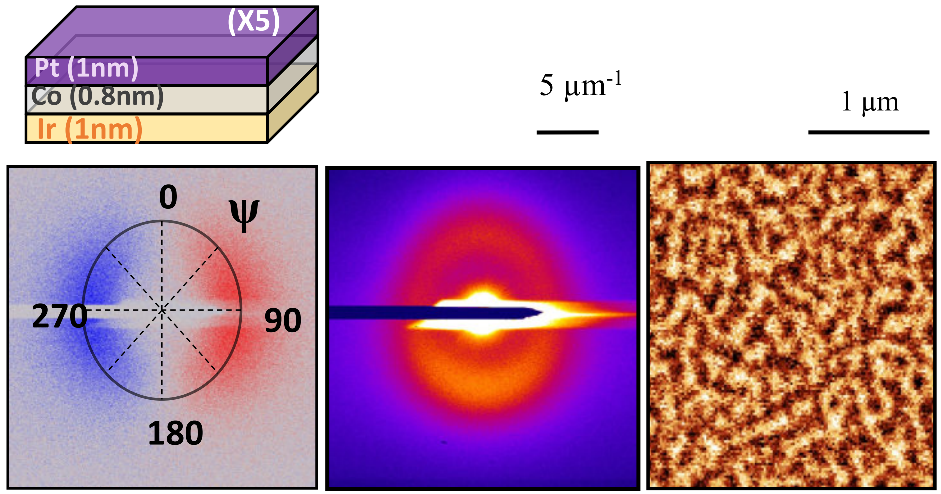

CL-CR/CL+CR

CL+CR

MFM

[Pt/Co/Ir] multilayers

Circular dichroism *orthoradial* profile:

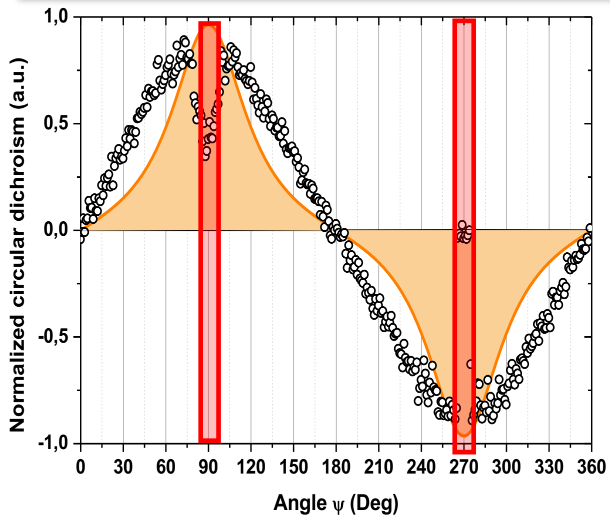

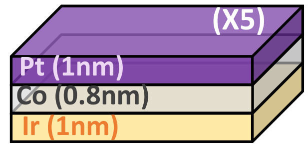

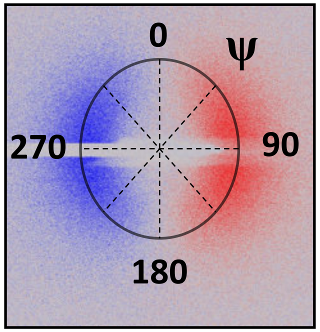

Approximated calculation of the circular dichroism profile:

In the Born approximation :

$$I(\boldsymbol{Q}) \propto \left| \sum_n f_n \cdot exp(i\boldsymbol{Q} \cdot \boldsymbol{r}_n) \right|^2$$

with:

$$f_n = f_{\text{off resonance}} + f_{\text{charge}}$$
$$-i\ \underbrace{(\hat{\epsilon} \times \hat{\epsilon}') \cdot \boldsymbol{m}_n + (\hat{\epsilon}' \cdot \boldsymbol{m}_n)(\hat{\epsilon} \cdot \boldsymbol{m}_n)}$$

Magnetic terms of the scattering amplitude for the magnetic ion carrying a magnetic moment $\mathbf{m_n}$ at the position $\mathbf{r_n}$

$\hat{\epsilon}$; $\hat{\epsilon}'$: polarization states of the incident and diffracted beam

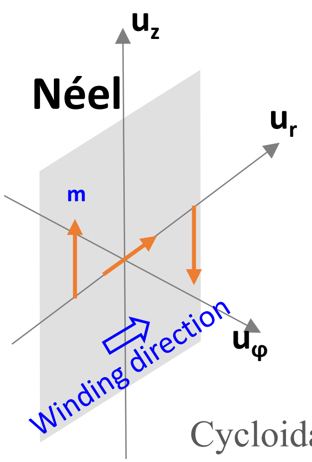

Cycloidal winding:

$$\boldsymbol{m} = \begin{pmatrix} m_r = \cos(\boldsymbol{q}_r \cdot \boldsymbol{r}) \\ m_\varphi = 0 \\ m_r = \cos\left(\boldsymbol{q}_r \cdot \boldsymbol{r} - \frac{\pi}{2}\right) \end{pmatrix}$$

<u>Calculation of diffracted intensity for incident polarization states:</u>

$$I(\boldsymbol{Q}) = Tr\left[\tilde{f}_n\, \rho\, \tilde{f}_n^{\dagger}\right]$$

In the Poincaré-Stokes representation:

$$\rho_{CL} = \begin{pmatrix} 1 & -i \\ +i & 1 \end{pmatrix} \text{ and } \rho_{CR} = \begin{pmatrix} 1 & +i \\ -i & 1 \end{pmatrix}$$

$$CD = \frac{I_{CL} - I_{CR}}{I_{CL} + I_{CR}}$$

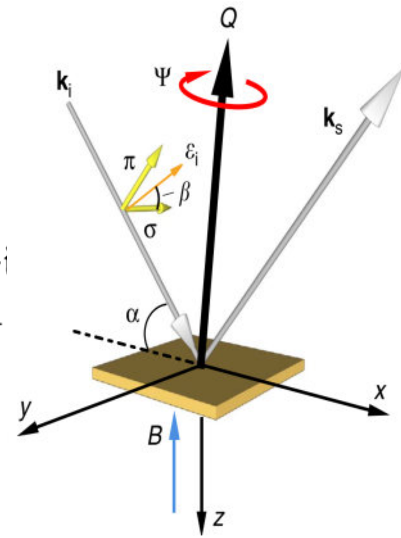

Hannon et al. *PRL (1988)*
Blume et al. *PRB (1988)*
Hill et al. *Acta Cryst A (1996)*
Van der Laan *C.R. Phys. (2008)*

[Pt/Co/Ir] multilayers

Circular dichroism *orthoradial* profile:

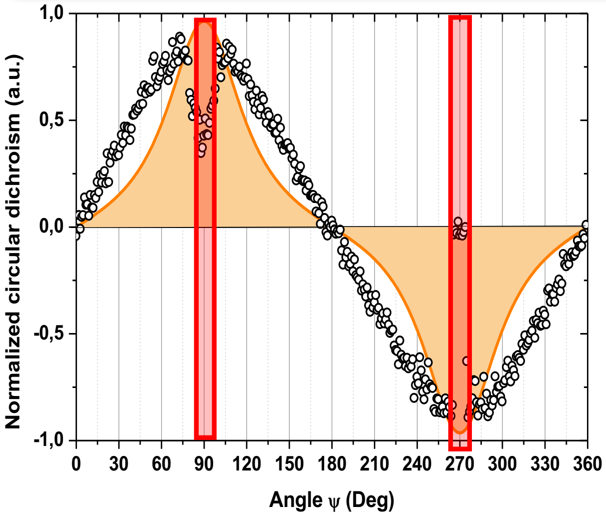

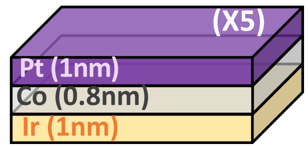

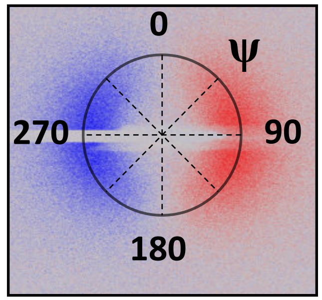

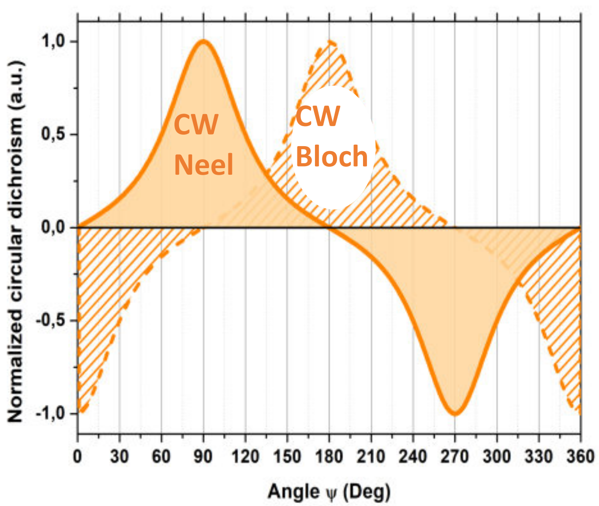

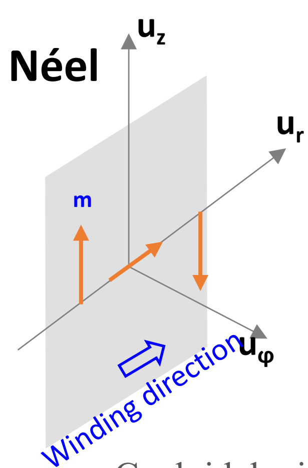

Cycloidal winding:

$$\boldsymbol{m} = \begin{pmatrix} m_r = \cos(\boldsymbol{q}_r \cdot \boldsymbol{r}) \\ m_\varphi = 0 \\ m_r = \cos\left(\boldsymbol{q}_r \cdot \boldsymbol{r} - \frac{\pi}{2}\right) \end{pmatrix}$$

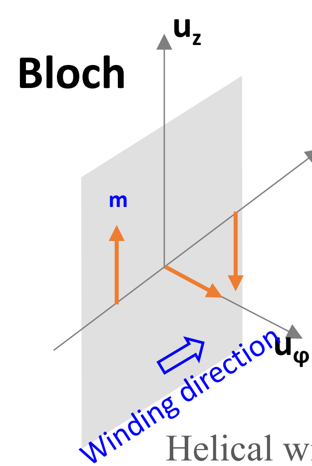

Helical winding:

$$\boldsymbol{m} = \begin{pmatrix} m_r = 0 \\ m_\varphi = \cos(\boldsymbol{q}_r \cdot \boldsymbol{r}) \\ m_r = \cos\left(\boldsymbol{q}_r \cdot \boldsymbol{r} - \frac{\pi}{2}\right) \end{pmatrix}$$

[Pt/Co/Ir] multilayers

Circular dichroism *orthoradial* profile:

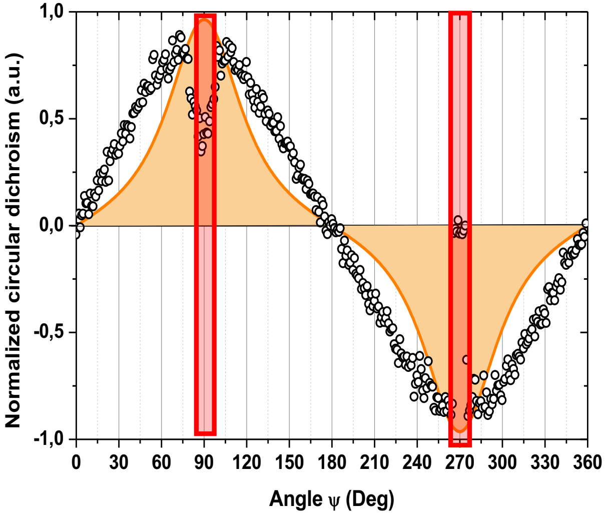

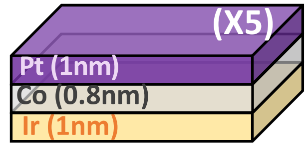

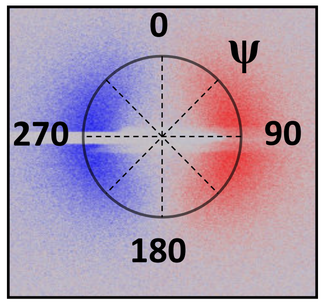

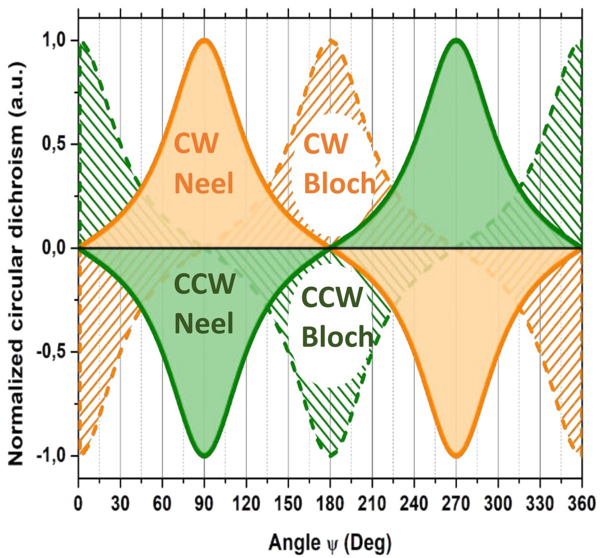

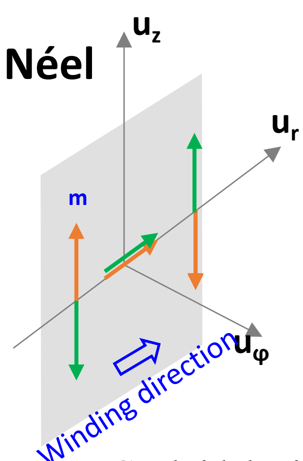

Cycloidal winding:

$$\boldsymbol{m} = \begin{pmatrix} m_r = \cos(\boldsymbol{q}_r \cdot \boldsymbol{r}) \\ m_\varphi = 0 \\ m_r = \cos\left(\boldsymbol{q}_r \cdot \boldsymbol{r} - \frac{\pi}{2}\right) \end{pmatrix}$$

+

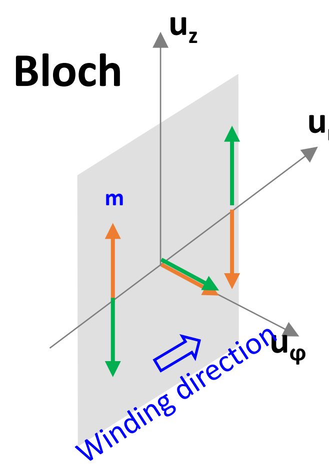

Helical winding:

$$\boldsymbol{m} = \begin{pmatrix} m_r = 0 \\ m_\varphi = \cos(\boldsymbol{q}_r \cdot \boldsymbol{r}) \\ m_r = \cos\left(\boldsymbol{q}_r \cdot \boldsymbol{r} - \frac{\pi}{2}\right) \end{pmatrix}$$

+

[Pt/Co/Ir] multilayers

Circular dichroism *orthoradial* profile:

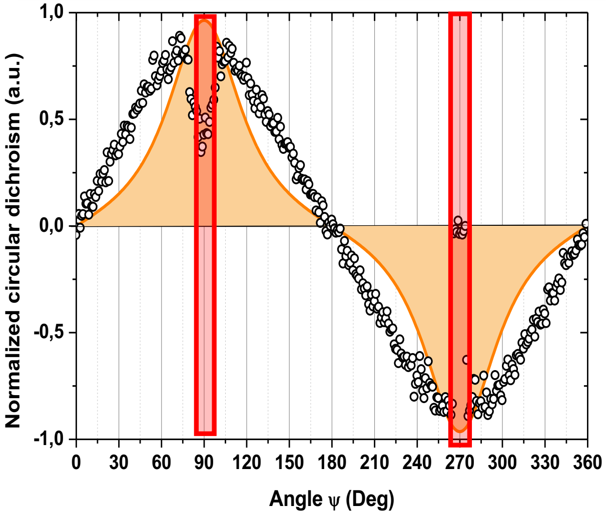

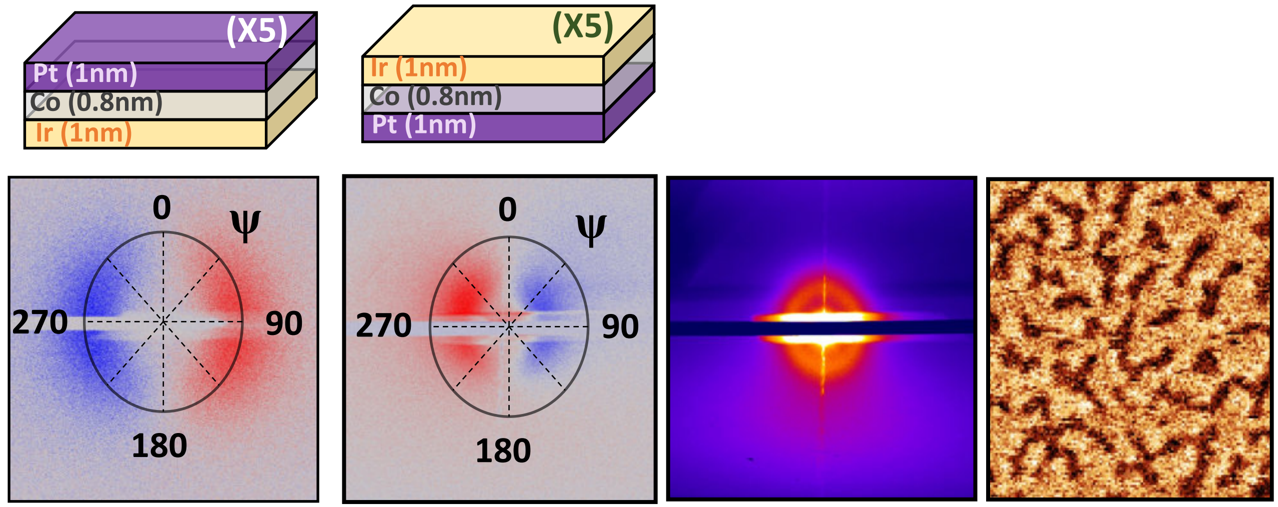

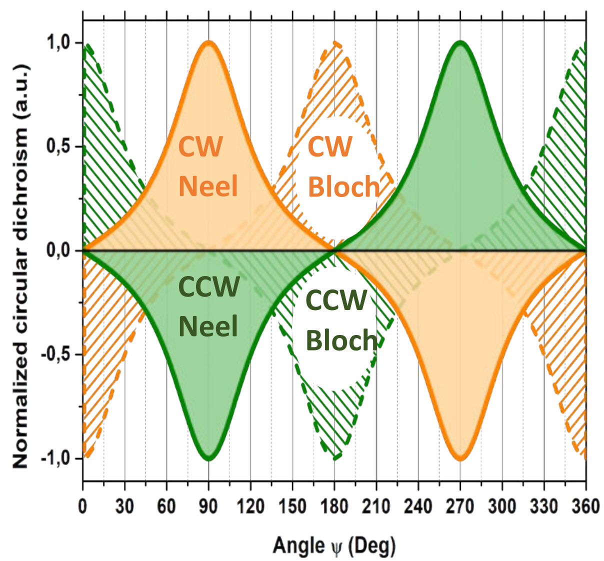

Néel

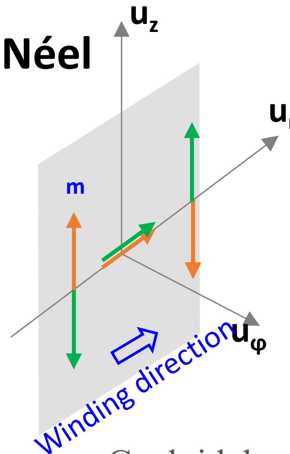

Cycloidal winding:

$$\boldsymbol{m} = \begin{pmatrix} m_r = \cos(\boldsymbol{q}_r \cdot \boldsymbol{r}) \\ m_\varphi = 0 \\ m_r = \cos\left(\boldsymbol{q}_r \cdot \boldsymbol{r} \mp \frac{\pi}{2}\right) \end{pmatrix}$$

Bloch

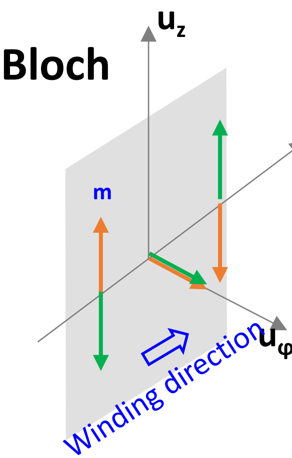

Helical winding:

$$\boldsymbol{m} = \begin{pmatrix} m_r = 0 \\ m_\varphi = \cos(\boldsymbol{q}_r \cdot \boldsymbol{r}) \\ m_r = \cos\left(\boldsymbol{q}_r \cdot \boldsymbol{r} \mp \frac{\pi}{2}\right) \end{pmatrix}$$

[Pt/Co/Ir] multilayers

Circular dichroism *orthoradial* profile:

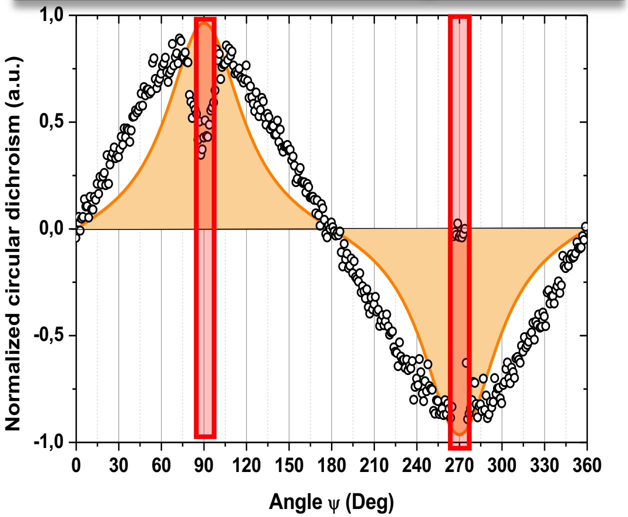

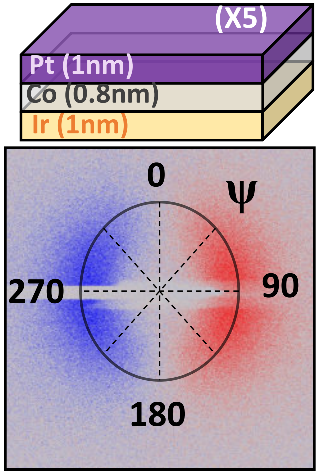

Micromagnetic simulations:

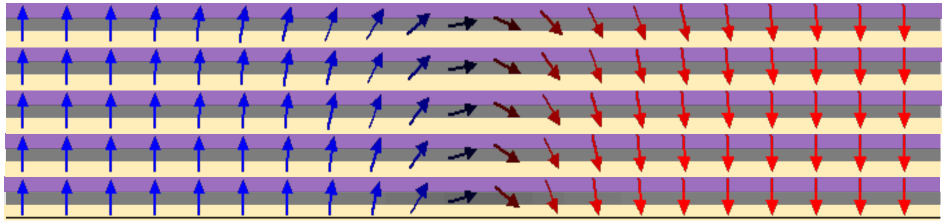

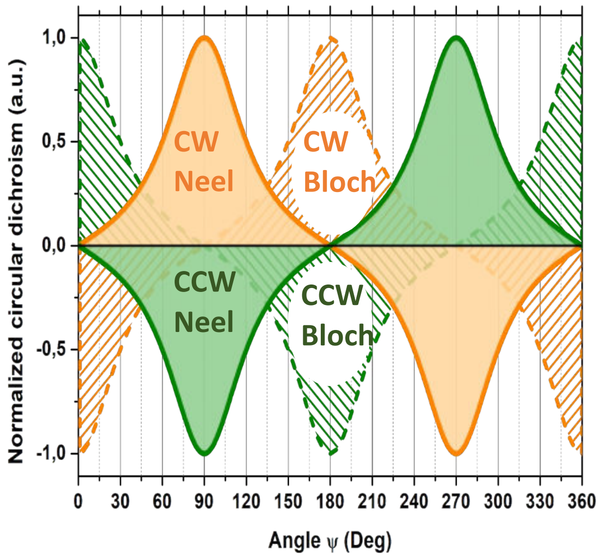

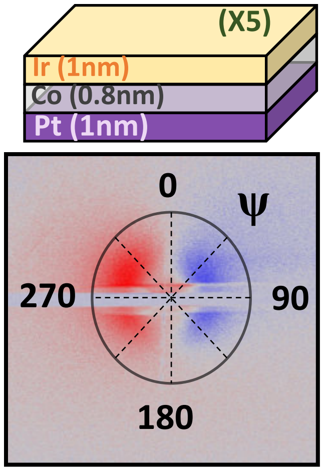

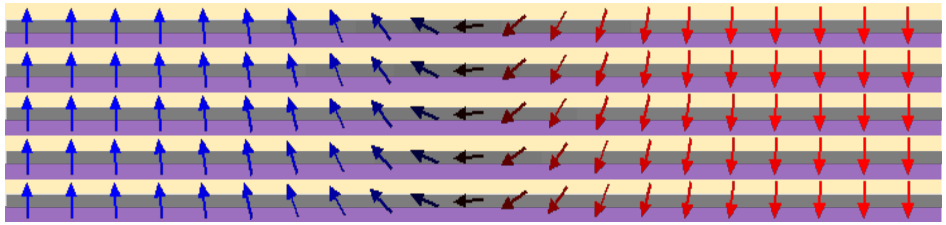

VALID for X5 but for larger number of period .....

Chauleau, ...NJ, ... et al, PRL 120, 037202 (2018)

For a large number of repetitions ....

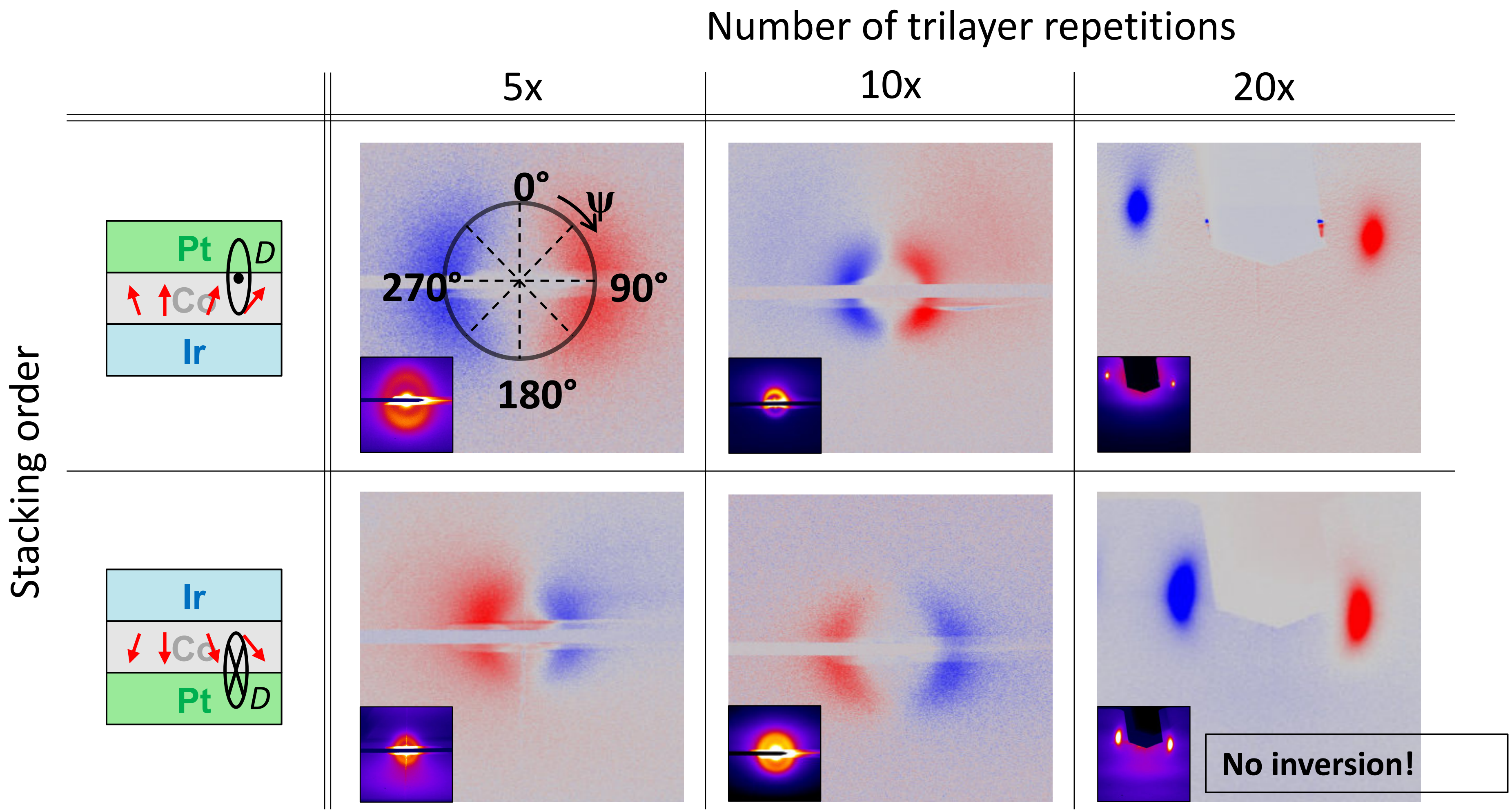

WHY ???

Chirality depends on position in the stack and soft x-ray penetration depth is small => hybrid chirality

=> Inverted chirality at the top and the bottom

=> SOT must be adapted for more efficient motion

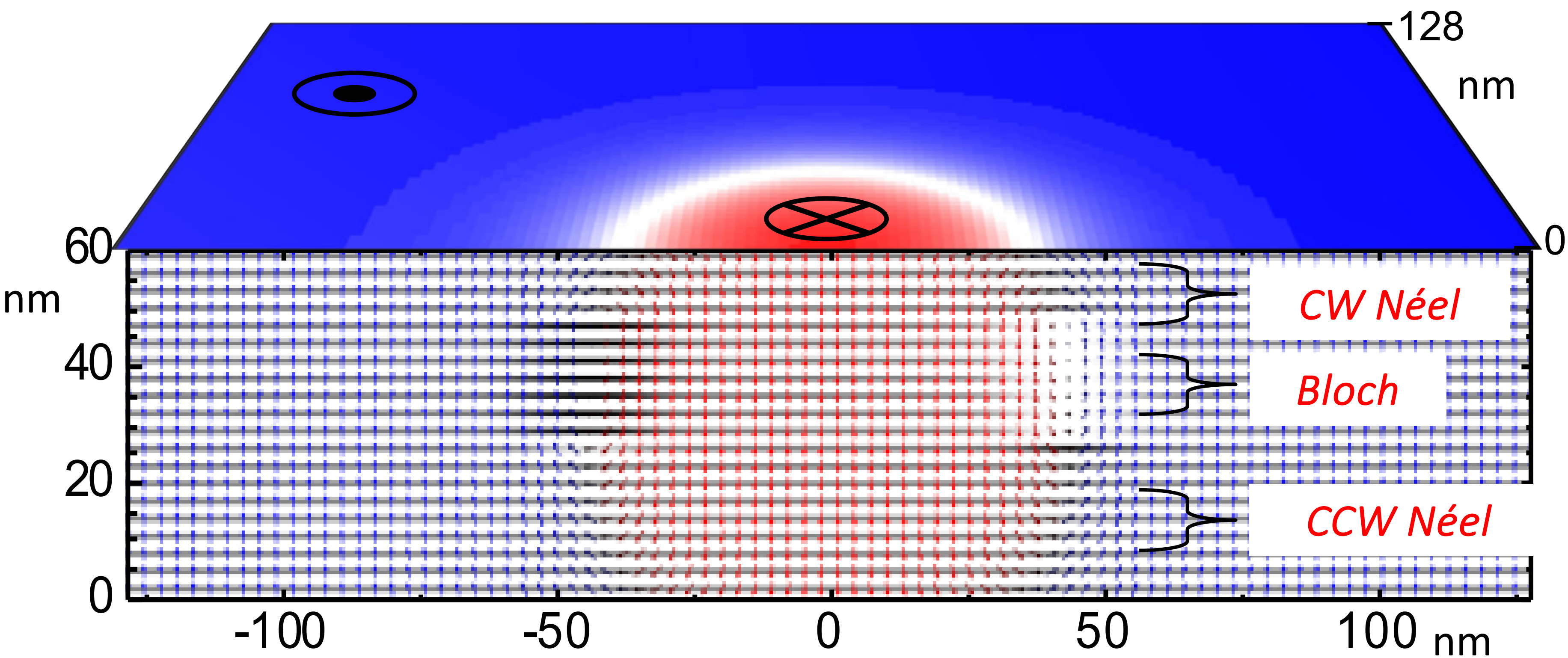

W. Legrand, … NJ, …*et al*, Science Advances, 4, eaat0415 *(2018)*

AFM coupled multilayers

$(Co\backslash Ru\backslash Pt)_{4\text{-}AFM}$

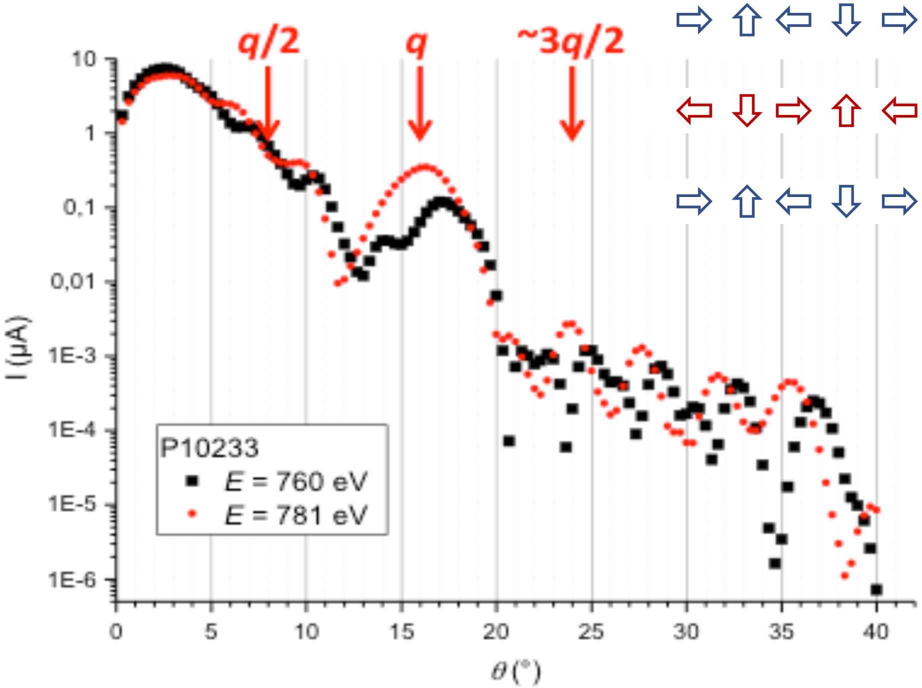

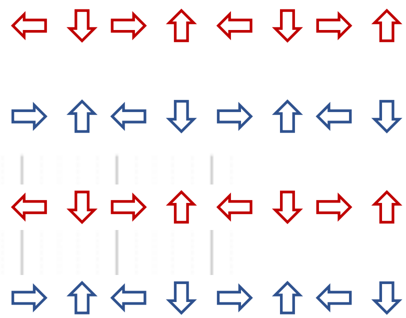

CCW-SS

Q_{Bragg}

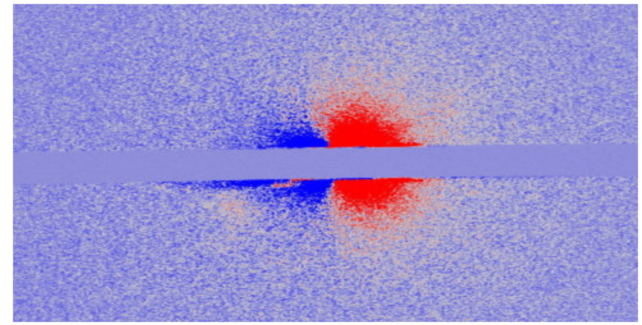

$Q_{bragg}/2_= Q_{AF}$

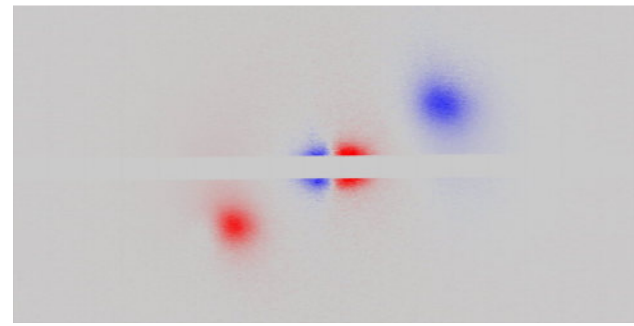

$3Q_{bragg}/2_= Q_{AF}$

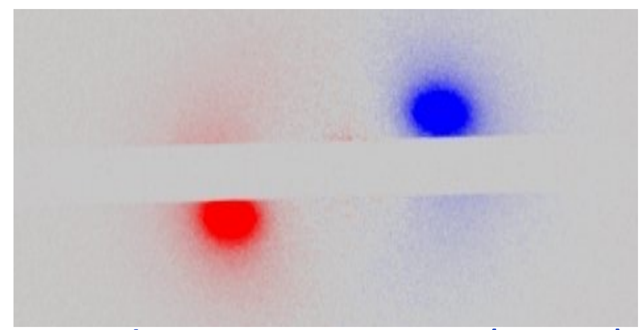

CCW Neel type but AFM coupled

E Burgos-Parra, ...NJ, .. *et al*, In preparation (2019)

Ultra fast time resolved chirality

Perform time resolved pump probe @ FERMI free electron laser (raw data)

=>100fs IR laser pump (800nm)

=> 60fs x-ray pump

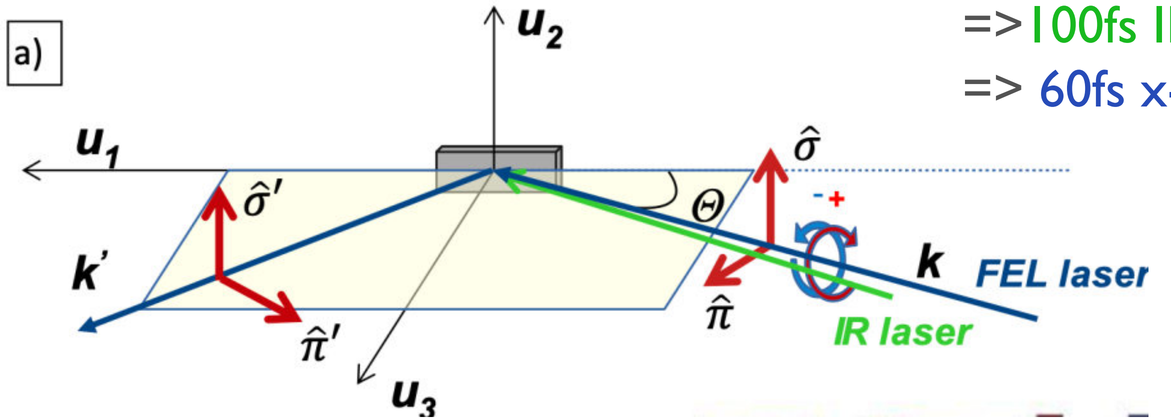

Typical result @ Co $M_{2,3}$ edge (60eV)

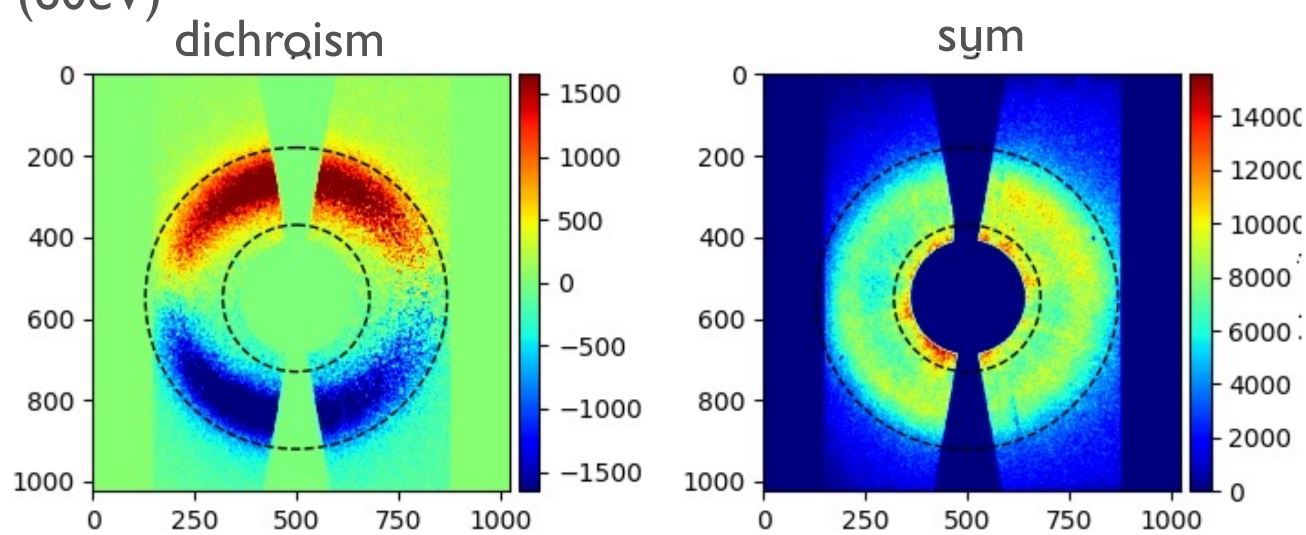

Ultra fast time resolved chirality

Ultrafast time scale:

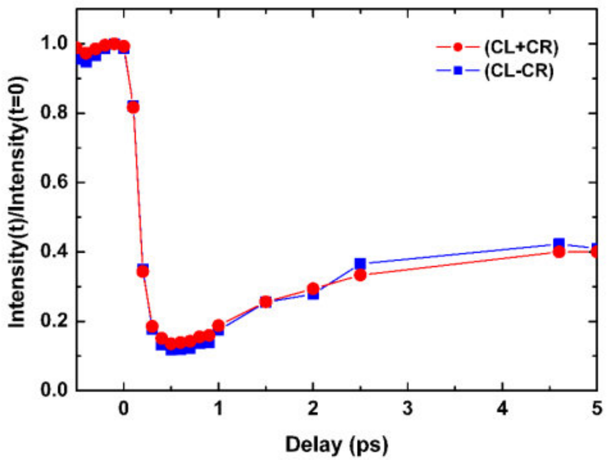

Léveillé *et al.* Nat. Commun 13, 1412 (2022)

Hundreds of ps time scale:

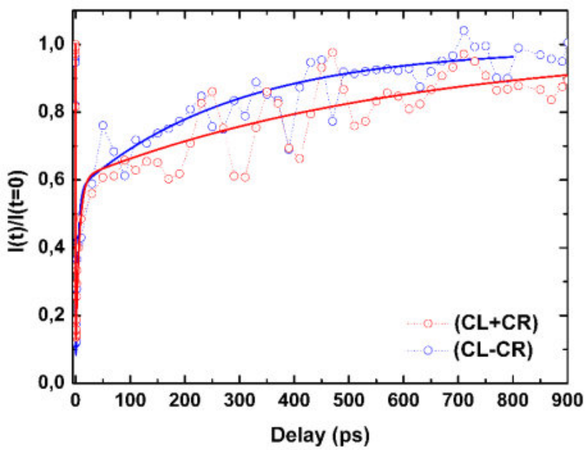

Signals normalized by the mean value before t_0

Chiral signal (CL-CR) recovers faster than the sum (CL+CR) !
Oscillations in the sum signal at longer time (magnetization precession)

$\Rightarrow$ Domain walls demagnetized faster than domains.
$\Rightarrow$ Domain walls magnetization recovers faster than domains.

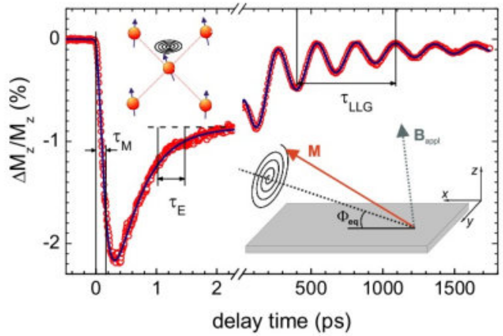

Koopmans *et al.*, PRL 95 (2005)

C. Léveillé,… NJ, Nature Comm 13, 1412 *(2022)*

Ultra fast time resolved chirality

@ FERMI free electron laser

Asymmetry ratio deviate from unity during the first 2ps

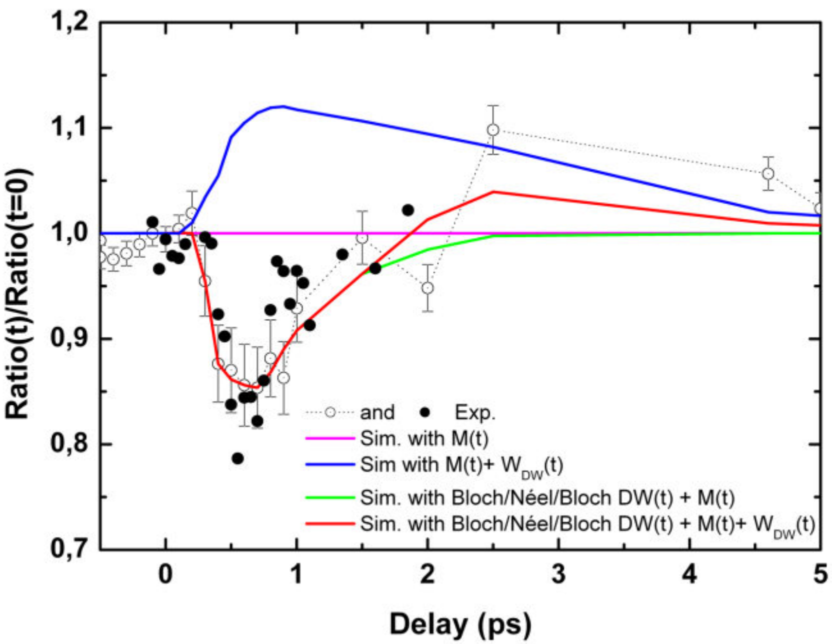

Simulation of the Asymmetry ratio

Demagnetization in Domain and DW are the same

Demagnetization in Domain and DW are the same AND we account for DW expansion (B. Pfau et Al, Nat. Comm 2012) as seen by peak position

Demagnetization in Domain and DW are the same AND we include spin torque in DW Induced by hot electrons (Viret al al PRB 53, 8464 (1996))

Demagnetization in Domain and DW are the same AND we include spin torque in DW Induced by hot electrons AND DW expansion.

C. Léveillé,… NJ, Nature Comm 13, 1412 *(2022)*

Ultra fast time resolved chirality

$\tau \propto \vec{m} \times \vec{\mu}$ with $\vec{m}$ the magnetic moment inside the DW
$\vec{\mu}$ the hot electron magnetic moment

« Coherent » process

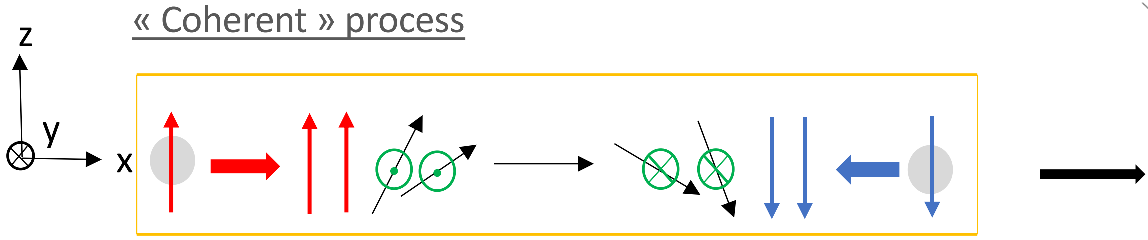

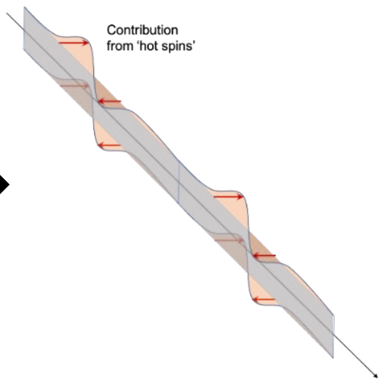

« incoherent » process

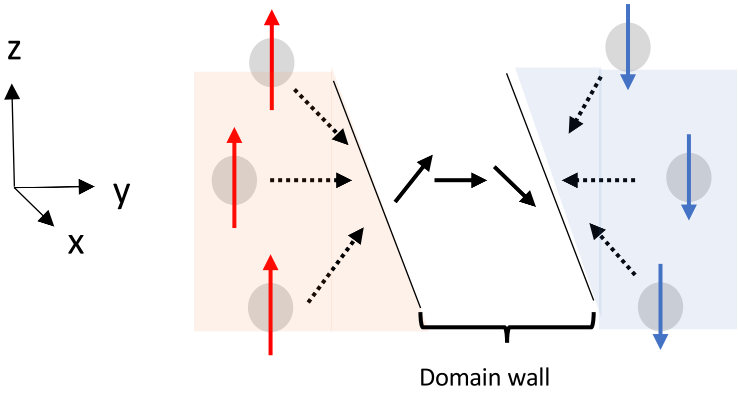

- Disorder in the magnetic moment induced by hot electrons coming from all directions
- Electrons from the DW ejected by scattering with hot electrons

Ultra fast time resolved chirality

Perform time resolved pump probe @ FERMI free electron laser

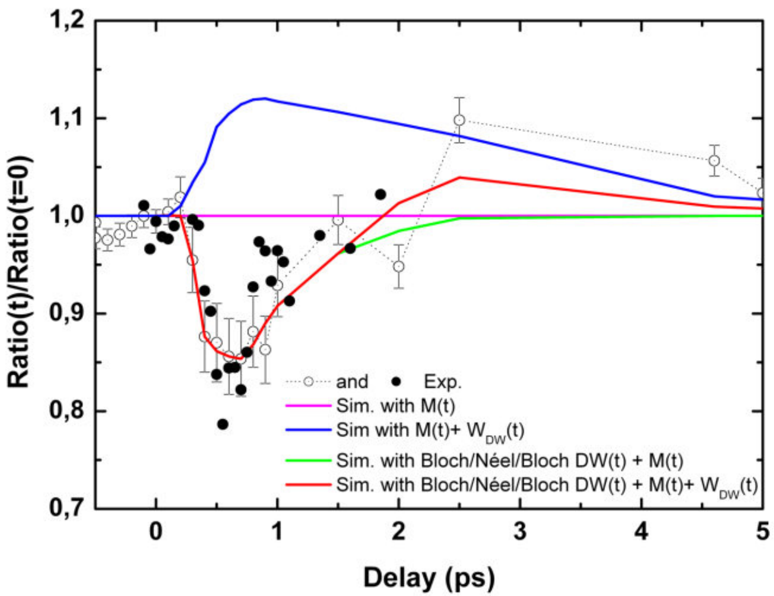

Asymmetry ratio deviate from unity during the first 2ps

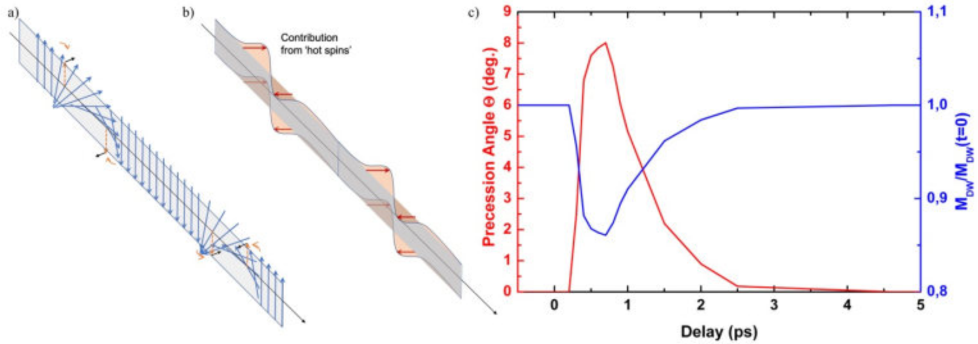

During the first 2ps after optical pump, spin torque from hot electron (coming from the domains) induce the DW chirality change from a pure Néel to a transient Bloch-Néel-Bloch

C. Léveillé,… NJ, Nature Comm 13, 1412 *(2022)*

Take Home message

- Direct determination of chirality by CD-XRMS in FM multilayers
  * Determination of the type (Neel versus Bloch)
  * Determination of the widing sens (CW or CCW)
  * New method to measure *D* (not detailed)
  * Element selectivity
  * x-ray wavelength resolution
  * Applicable to any material (amorphous, …)

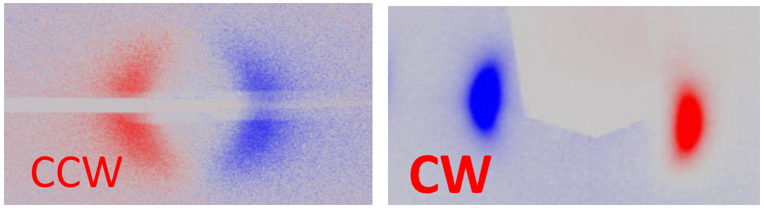

Chauleau, … NJ, et al, PRL 120, 037202 (2018)

- Hybrid chiral structure by CD-XRMS: competition between DMI and dipolar interaction
  - Predicted to occurs for many repetitions *N*, high M_s and *t*
  - Similar for DWs and skyrmions
  - Strong impact on velocity

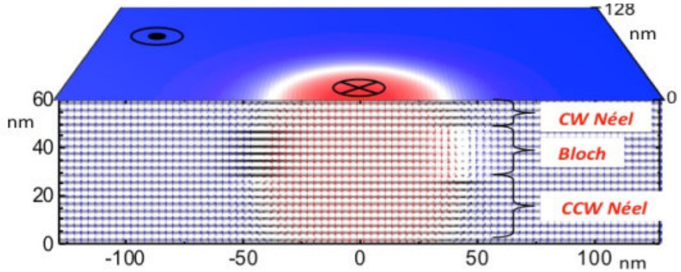

W. Legrand,… NJ.. *et al*, Science Advances, 4, eaat0415 *(2018)*

- Direct determination of chirality by CD-XRMS in AFM multilayers
  * For x-ray the contrast is the same for AFM and FM multilayers
  * Element selectivity, spatial resolution, …

E. Burgos-Parra, C. Leveillé, W. Legrand …NJ *et al*, in preparation

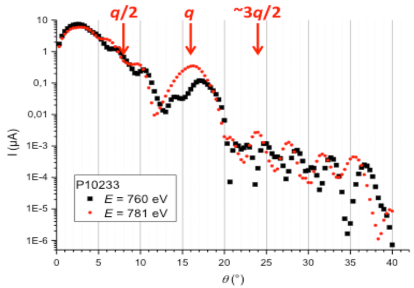

•AND NATURAL 10-50ps time resolution @ synchrotron
• 100fs at X-ray FEL

X-ray resonant scattering : revealing chirality in thin films

2 magnetic systems

Pt/Co multilayers :

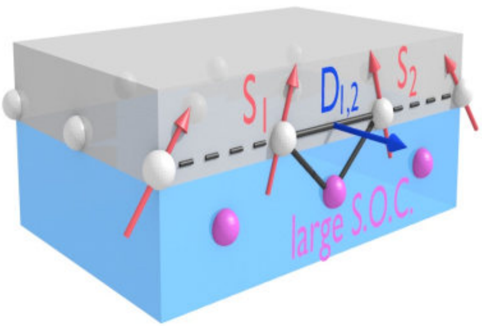

From A. Fert *et al*, *Nature Nanotechnol.* **8**, 152 (2013)

Multiferroic $BiFeO_3$:

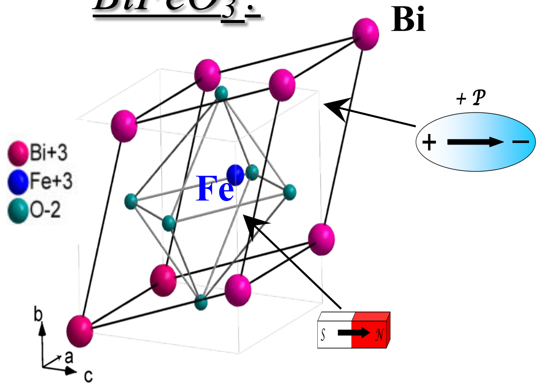

From Kubel *et al*, Acta Cryst. B. **46**, 698 (1990)

$BiFeO_3$: the archetypical of multiferroics

Ferroelectricity

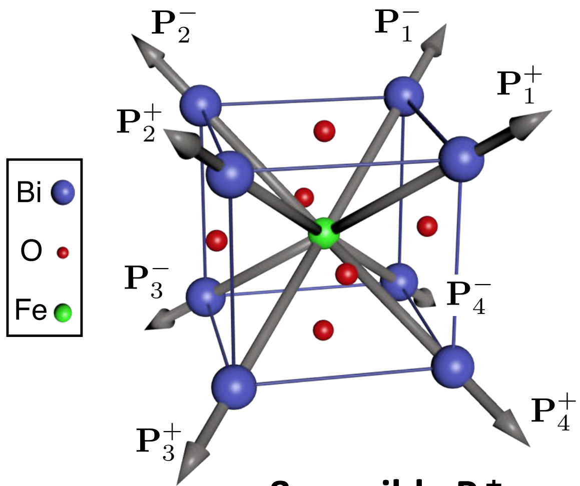

8 possible $P_i^{\pm}$

- Rhombohedral R_{3C}
- Large P (100 µC/cm²) [111]
- T_C = 1100 K

Wang *et al.*, Science 299, 1719 (2003)
Lebeugle *et al.*, Appl. Phys. Lett. 91, 022907 (2007)

Magnetism

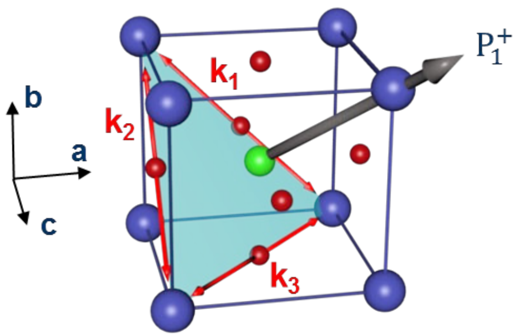

Each Pi±:
3 propagation directions (k1,k2,k3)

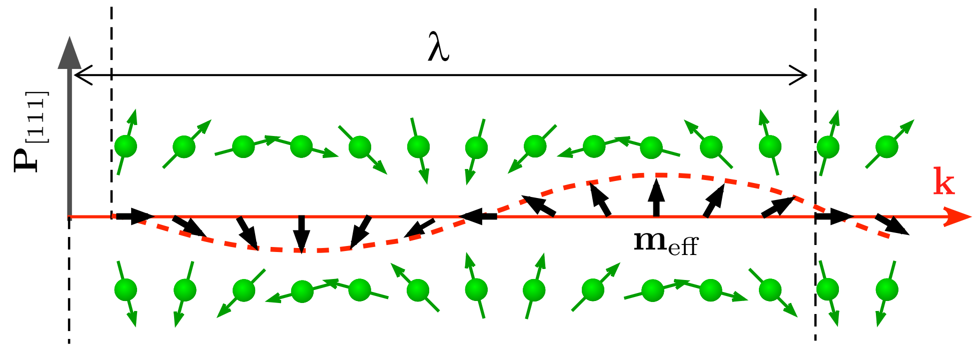

- G-type antiferromagnet (T_N = 640 K)
- Additional cycloidal modulation along k_i
- Cycloidal period of λ ~ 62-64 nm

Sosnowska *et al.*, J. Phys. C: Solid State Phys. 15, 4835 (1982)
Lebeugle *et al.*, Phys. Rev. Lett. 100, 227602 (2008)

Cycloidal ANTIFERROMAGNET

Neutron diffraction

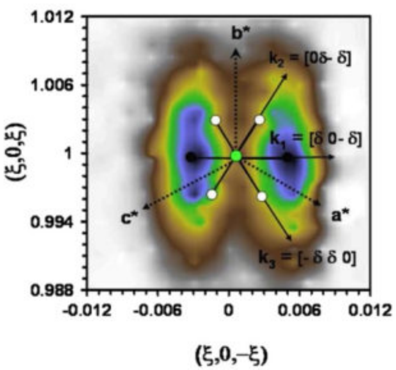

Lebeugle et al., Phys. Rev. Lett. 100, 227602 (2008)

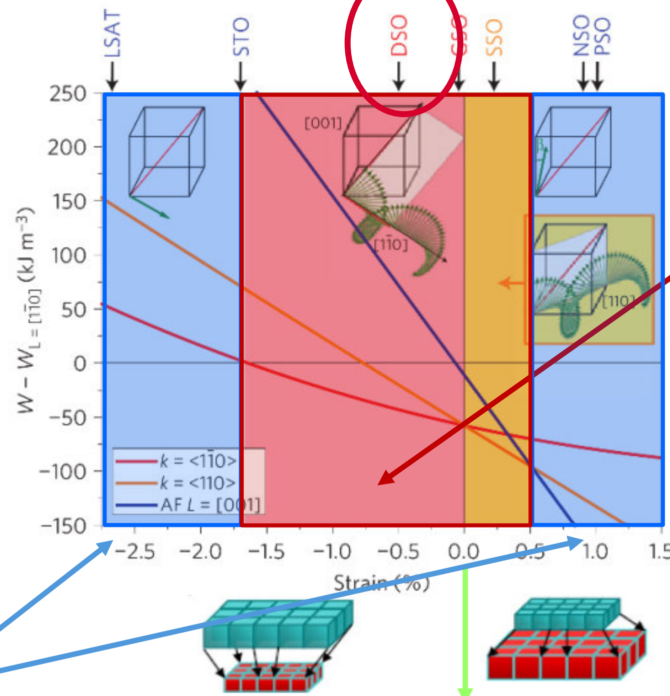

Low strain

Cycloid

High strain

no cycloid

Mössbauer spectroscopy

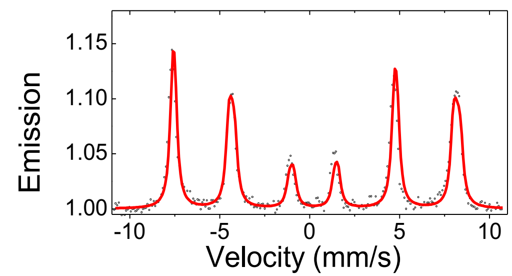

Sando et al., Nature Mater. 12, 641 (2013)

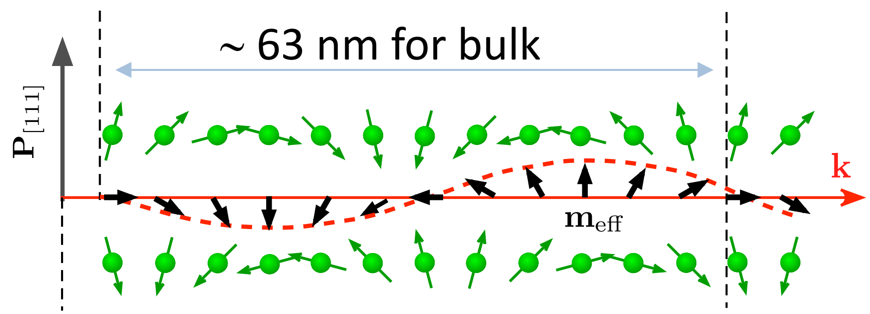

Sosnowska et al., J. Phys. C: Solid State Phys. 15, 4835 (1982)

Lebeugle et al., Phys. Rev. Lett. 100, 227602 (2008)

$BiFeO_3$: Ferroelectric properties

Real space : PFM

Sample: DSO(110)/SRO/$BiFeO_3$ (001) (≈ 35 nm)

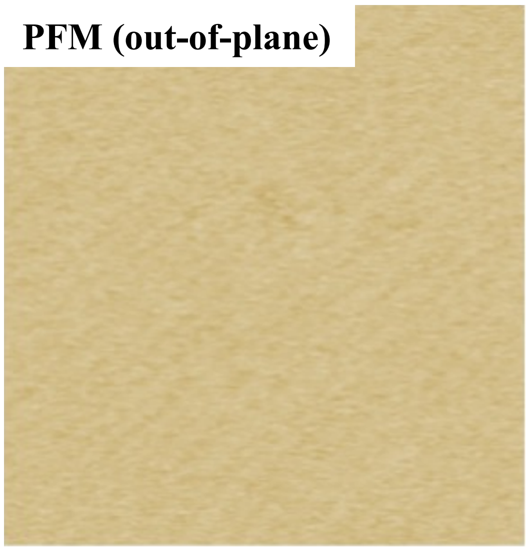

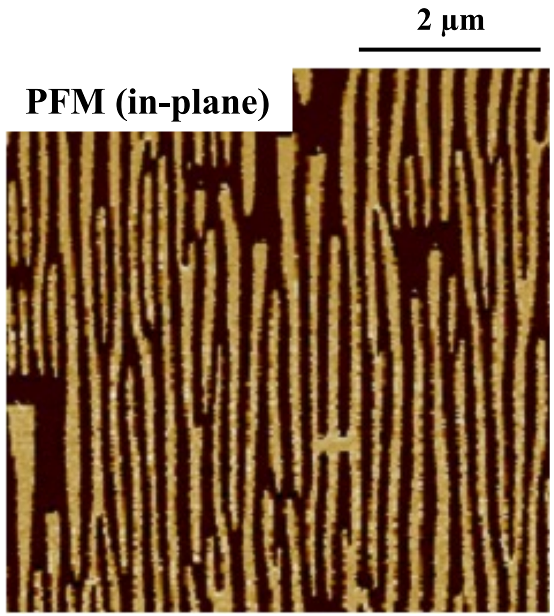

Stripe FE domain configuration

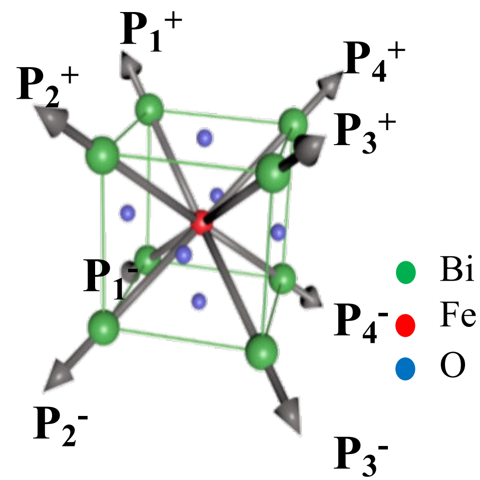

Piezoresponse force microscopy:

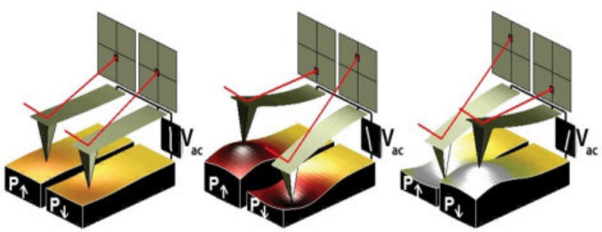

From: www.asylumresearch.com

Properties of these DWs

For example: conductive properties in insulating oxides

Seidel et al. *Nat. Materials* (2009)

Rojac et al. *Nat. Materials* (2016)

Magnetic properties: uncompensated magentic moment?
Matching of the AF cycloids with different Q vector?...

$BiFeO_3$: Ferroelectric properties

Real space : PFM

Sample: DSO(110)/SRO/$BiFeO_3$ (001) (≈ 35 nm)

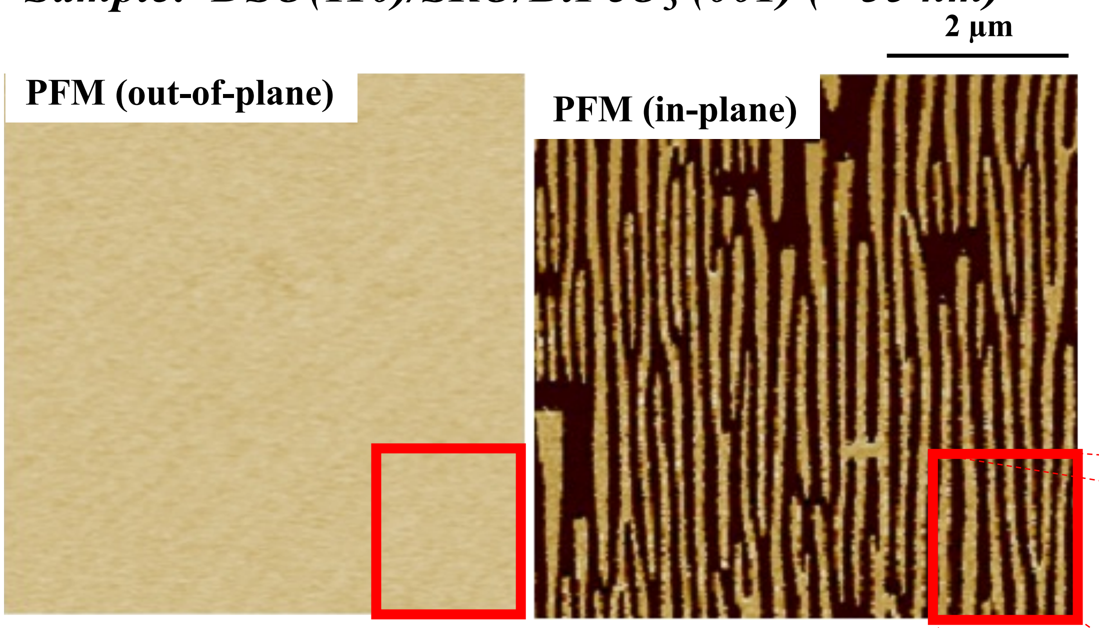

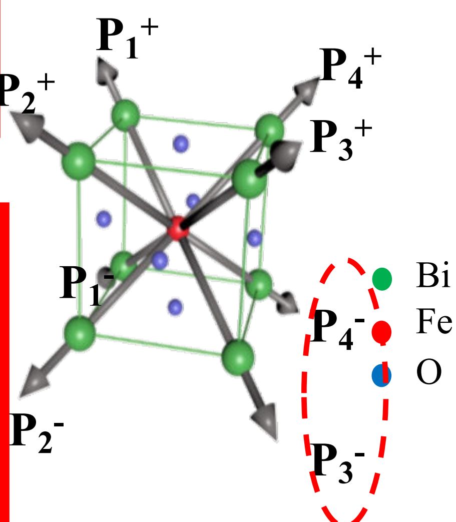

Piezoresponse force microscopy:

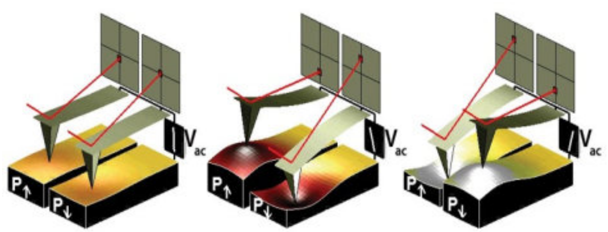

From: www.asylumresearch.com

71° Ferroelectric domain walls

$BiFeO_3$: Magnetic properties

Real space : Scanning NV magnetometry

P. Maletinsky, *Nature Nanotech.* **7**, 320–324 (2012)

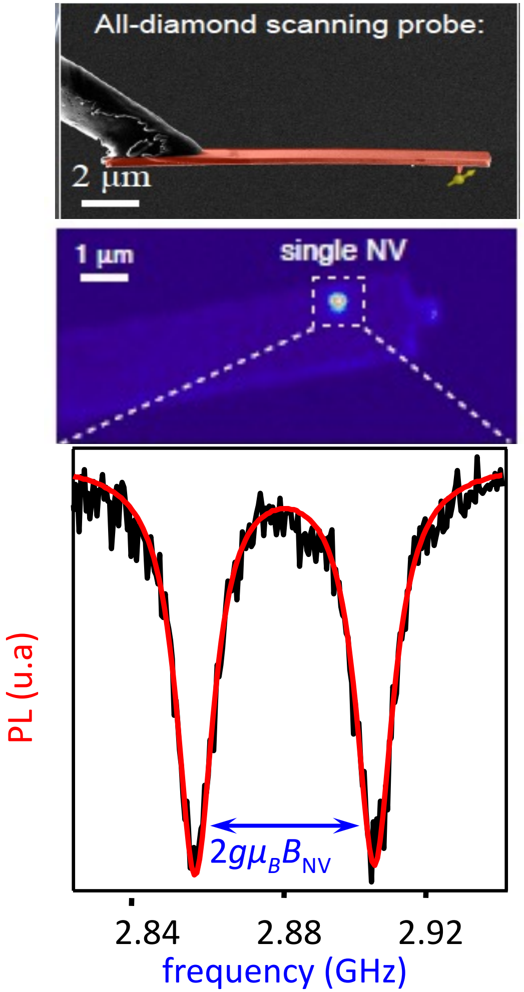

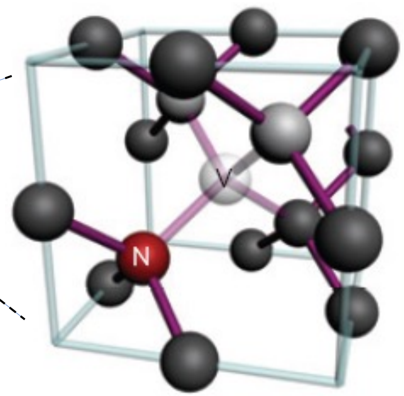

"Hortensia" diamond
(Louvre, Paris)

Single NV defect in diamond tip: magnetic sensor with an atomic size

$BiFeO_3$: Magnetic properties

Real space : Scanning NV magnetometry

P. Maletinsky, *Nature Nanotech.* **7**, 320–324 (2012)

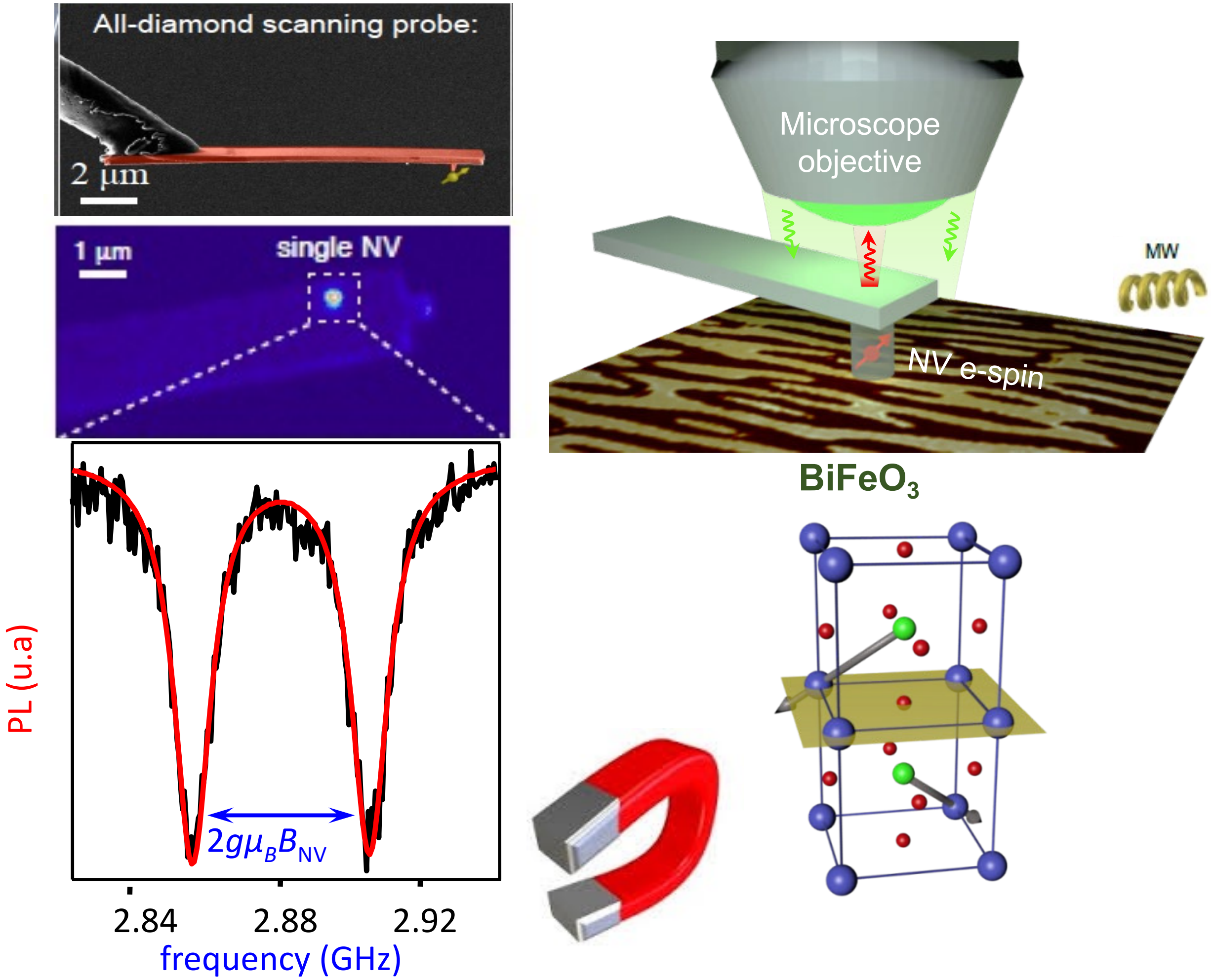

BiFeO$_3$: Magnetic properties

Real space : Scanning NV magnetometry

P. Maletinsky, *Nature Nanotech*.**7**, 320–324 (2012)

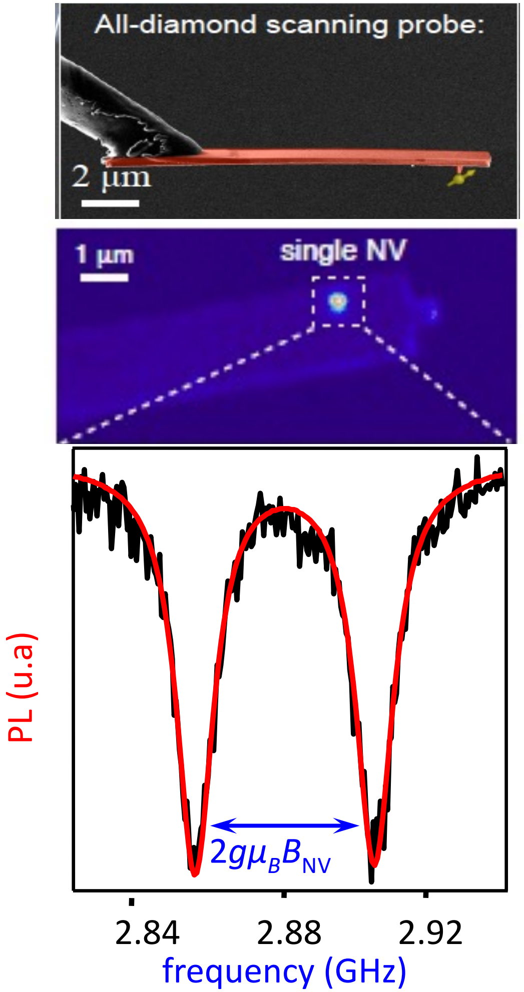

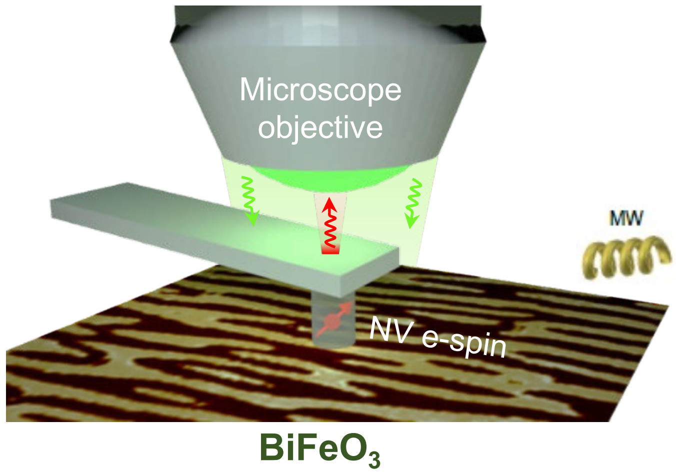

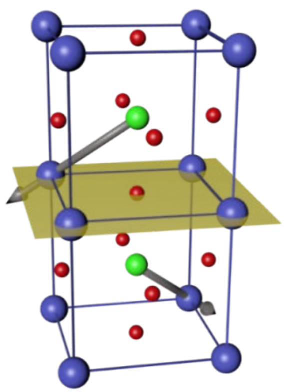

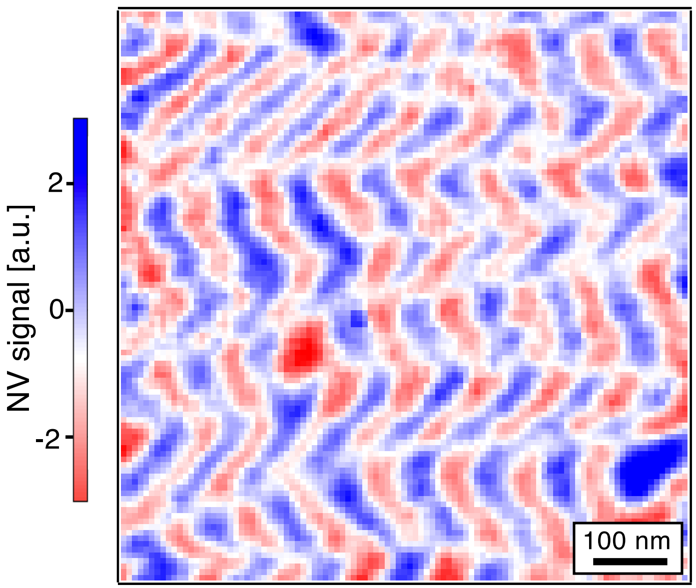

BiFeO$_3$: Magnetic properties

Real space : Scanning NV magnetometry

P. Maletinsky, *Nature Nanotech.***7**, 320–324 (2012)

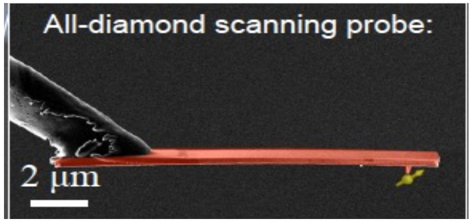

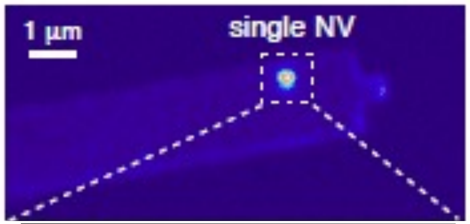

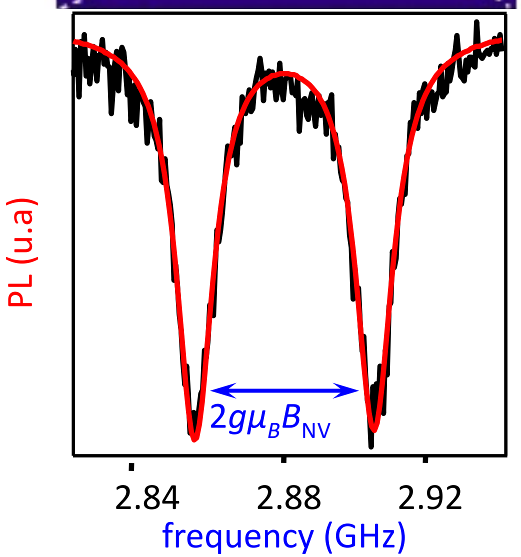

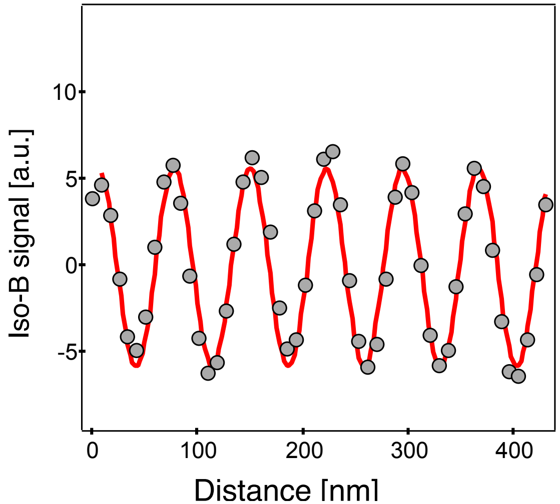

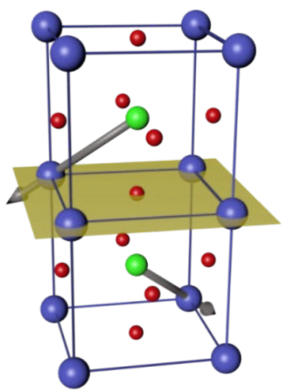

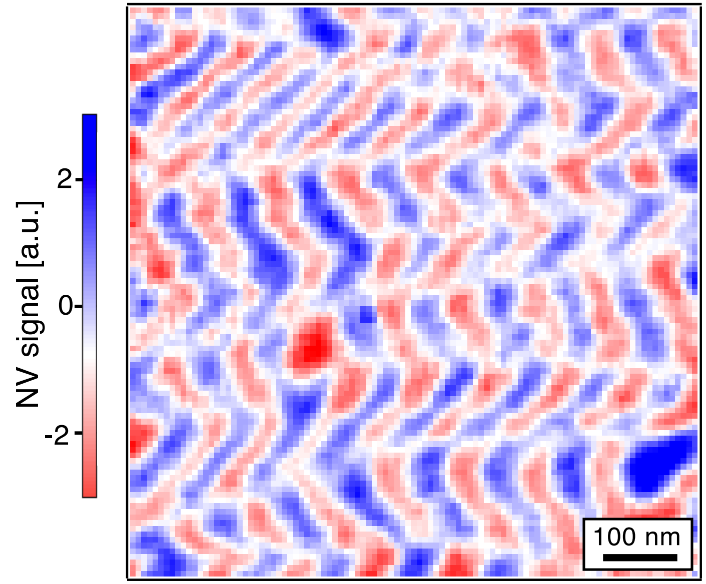

BiFeO$_3$: Magnetic properties

Real space : Scanning NV magnetometry

P. Maletinsky, *Nature Nanotech.* **7**, 320–324 (2012)

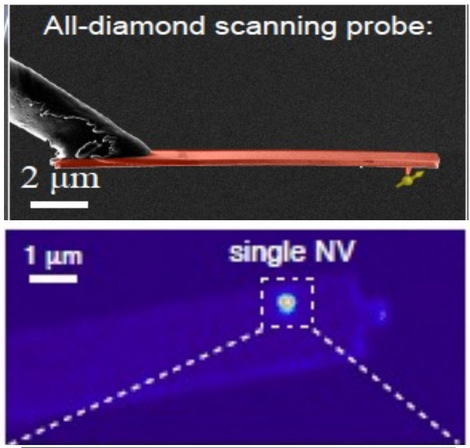

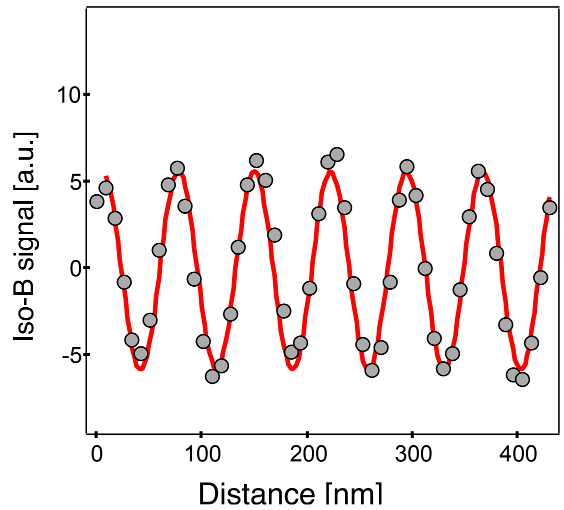

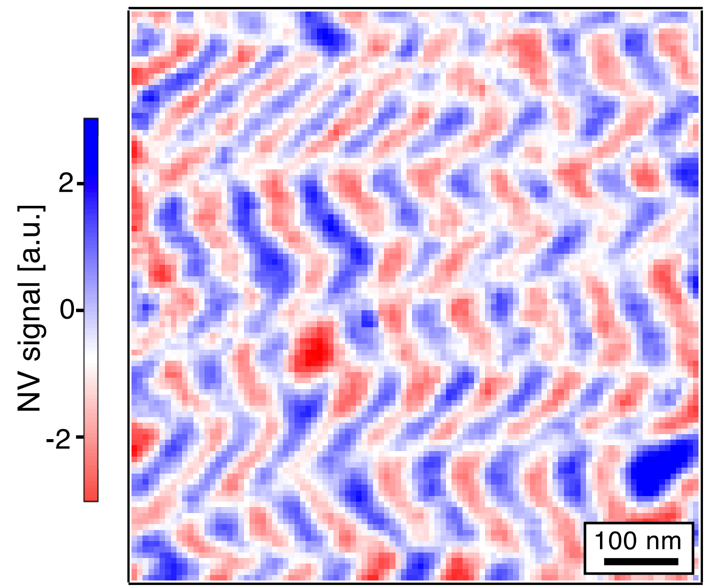

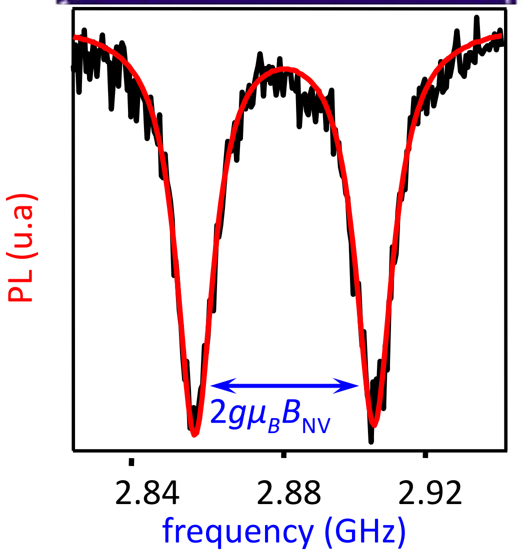

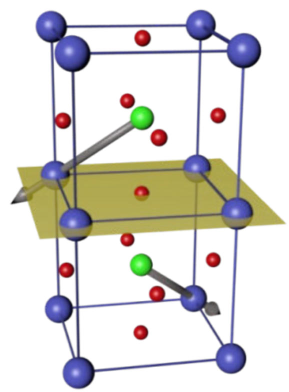

=> In plane spin cycloid propagation

=> Imprint from FE domains

Gross, ..NJ .. et al, Nature 549, 252 (2017)

$BiFeO_3$: Ferroelectric properties

Reciprocal space: soft x-ray resonant scattering

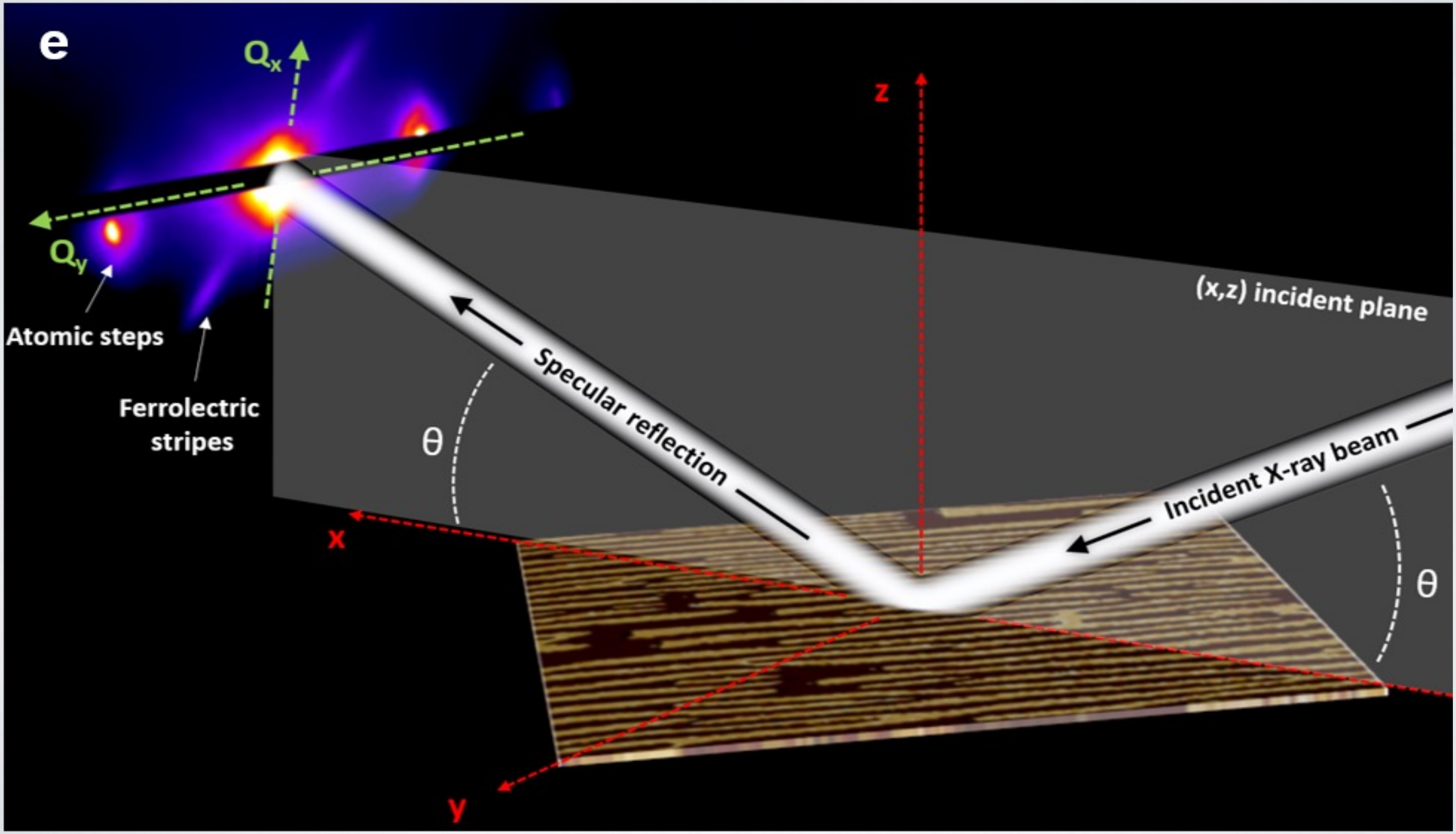

$BiFeO_3$: Ferroelectric properties

Reciprocal space: soft x-ray resonant scattering

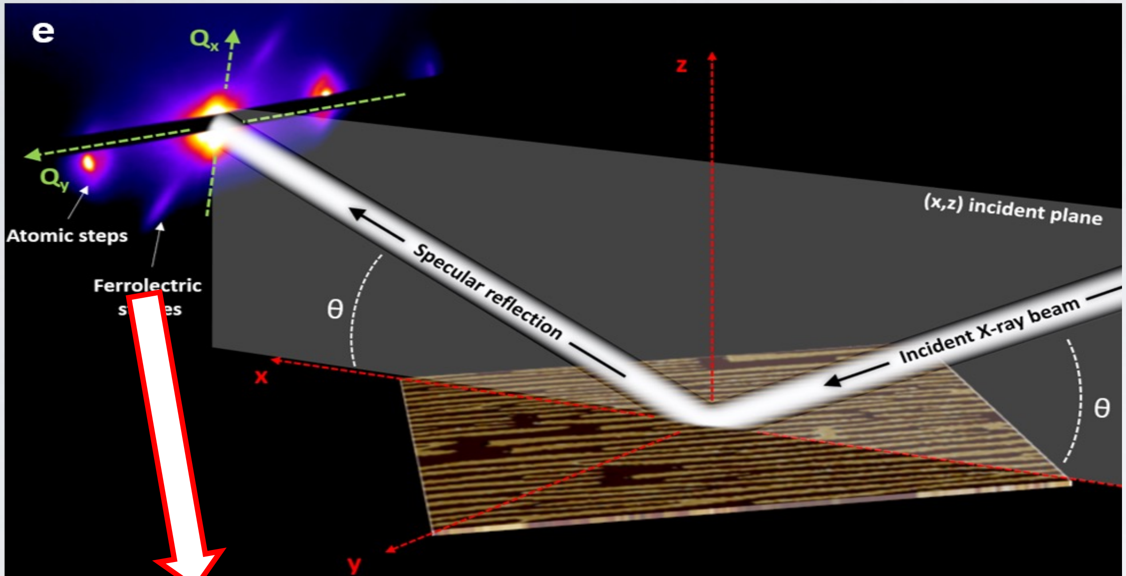

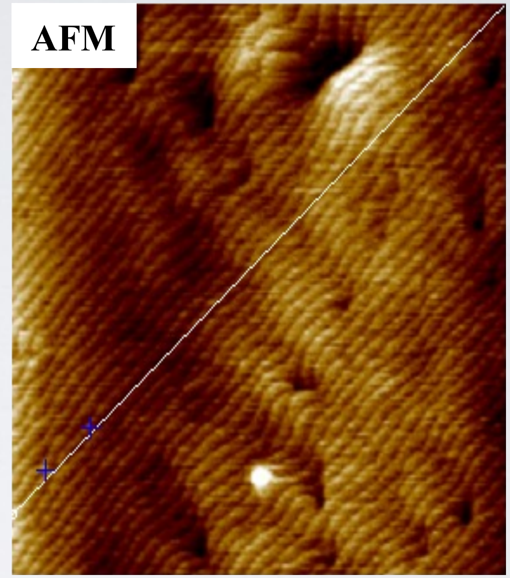

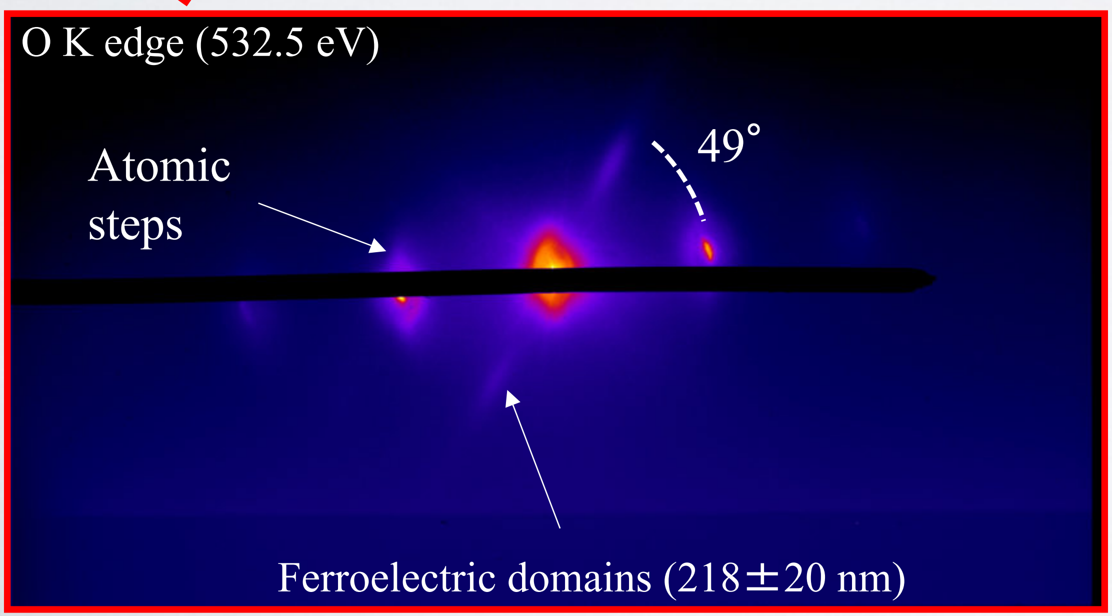

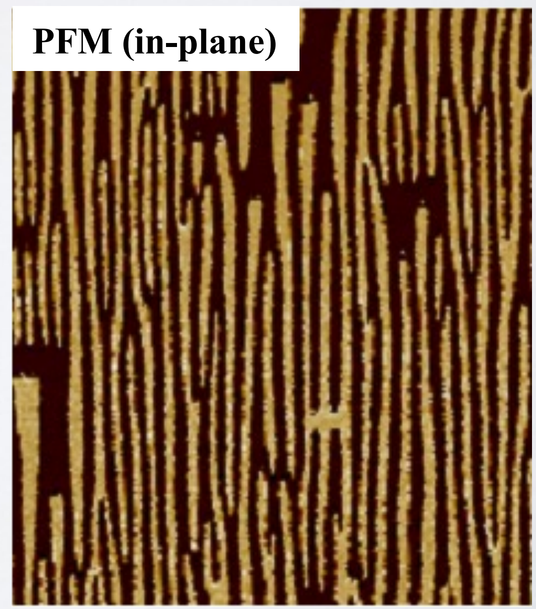

BiFeO$_3$: Ferroelectric properties

Reciprocal space: soft x-ray resonant scattering

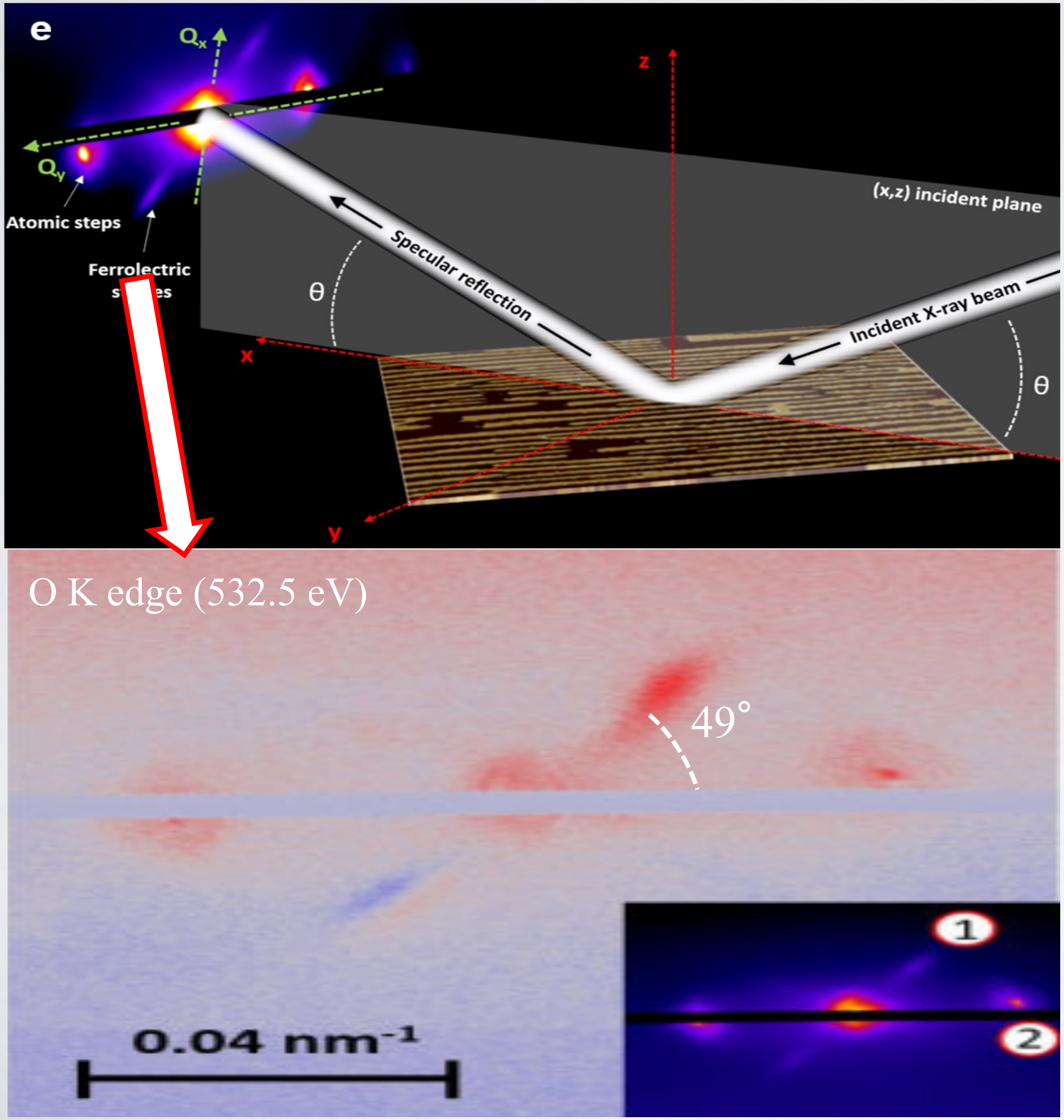

⇒ Dichroism at the O K edge

⇒ Indirect* access to Chiral Ferroelectric order at the Domain Wall

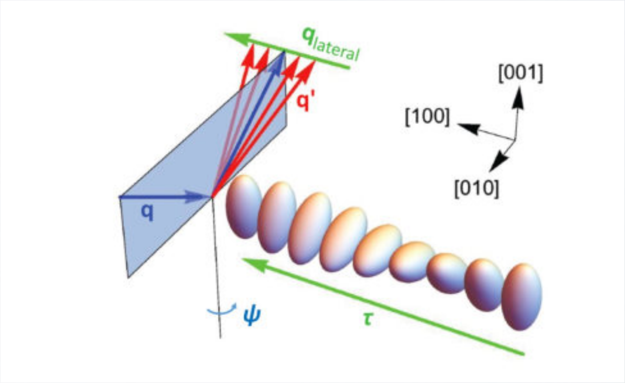

*Lovesey and Van der Laan, Phys. Rev. B 98, 155410 (2018)

$BiFeO_3$: Ferroelectric properties

reciprocal space: soft x-ray resonant scattering
71° versus 109° ferroelectric domain walls

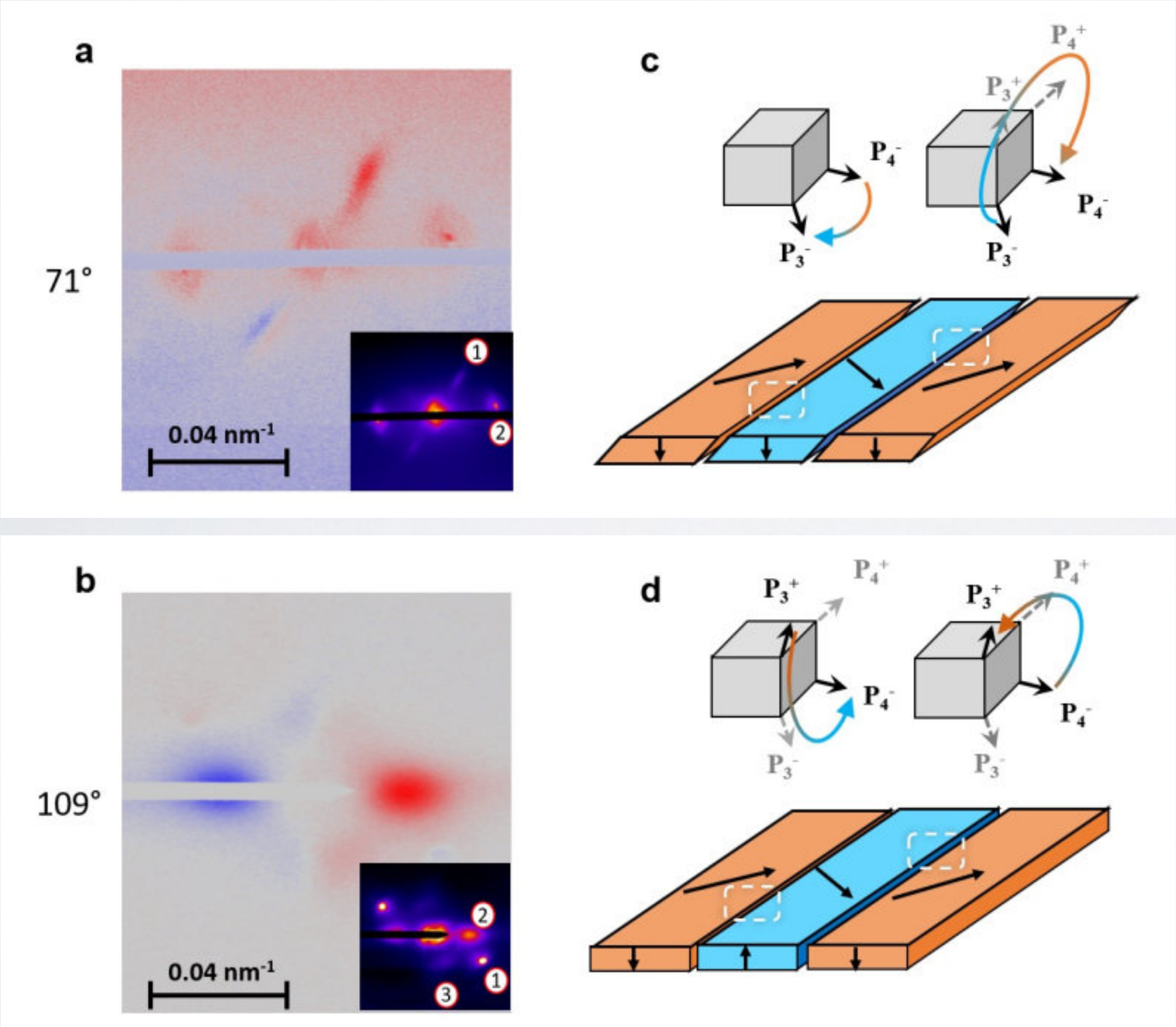

⇒ Dichroism at the O K edge

⇒ Indirect* access to Chiral Ferroelectric order at the Domain Wall

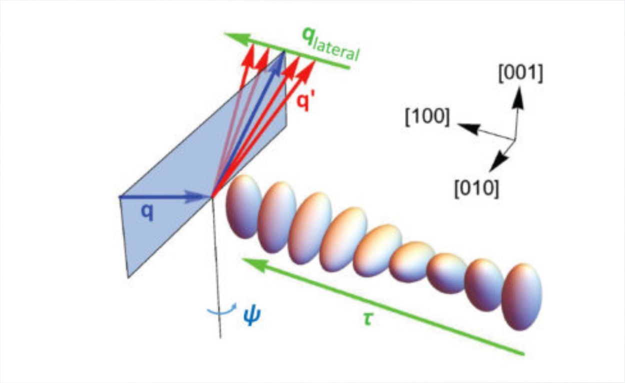

*Lovesey and Van der Laan, Phys. Rev. B 98, 155410 (2018)

$BiFeO_3$: Magnetic properties

Reciprocal space: soft x-ray resonant scattering

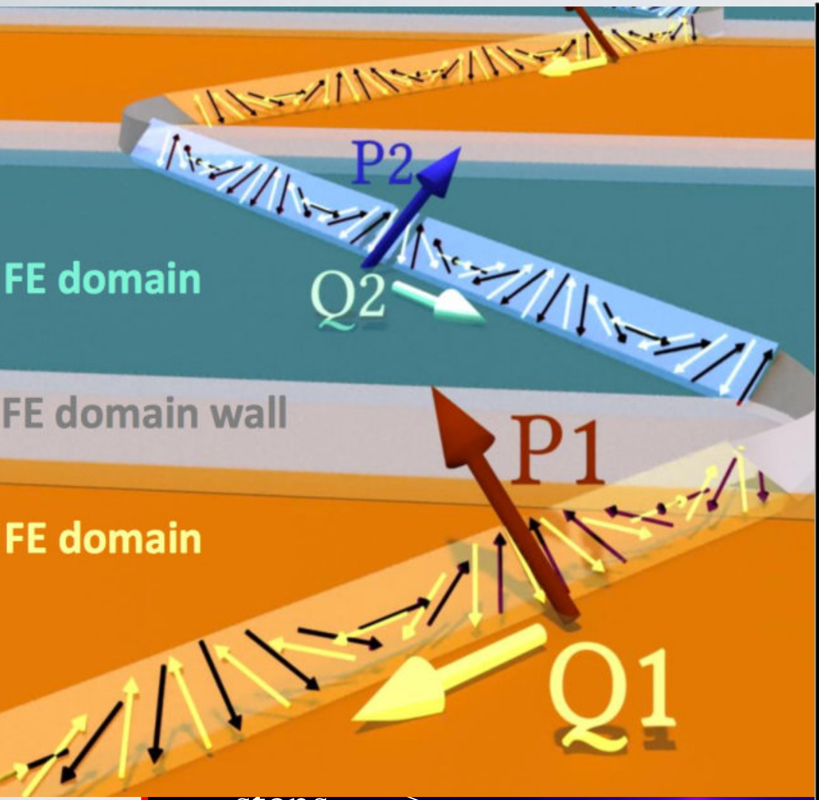

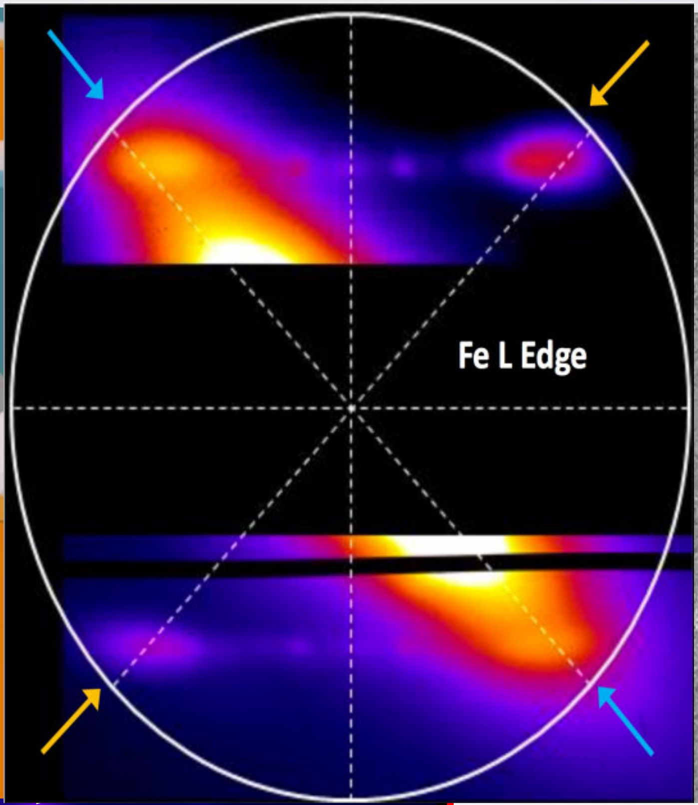

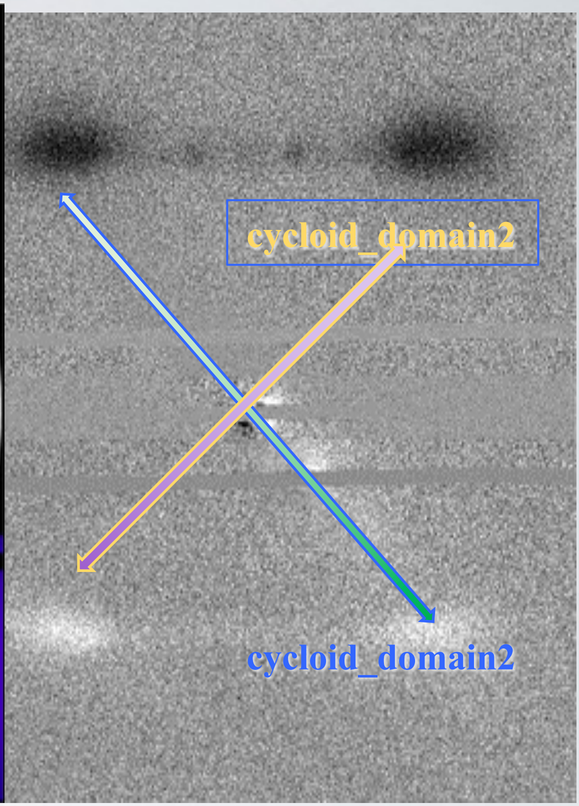

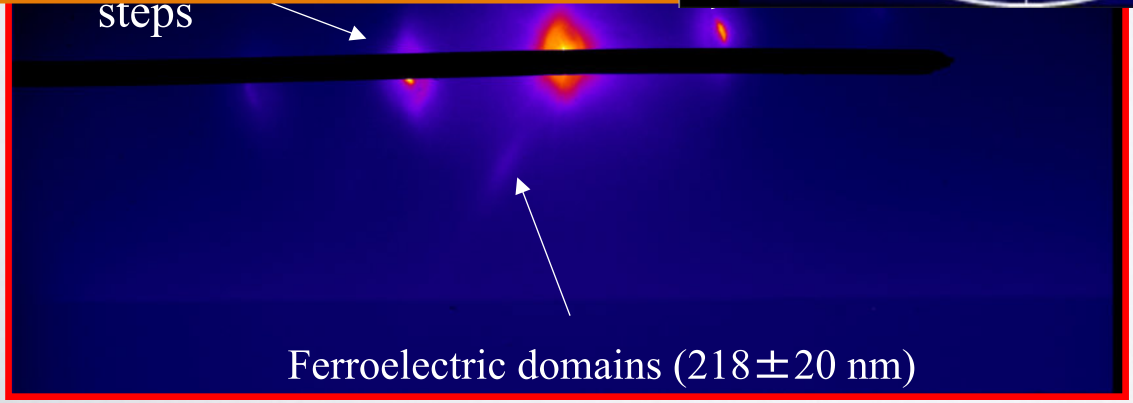

Cycloids 80 ± 8 nm

>> of Bulk period

$BiFeO_3$: Magnetic properties

Reciprocal space: soft x-ray resonant scattering

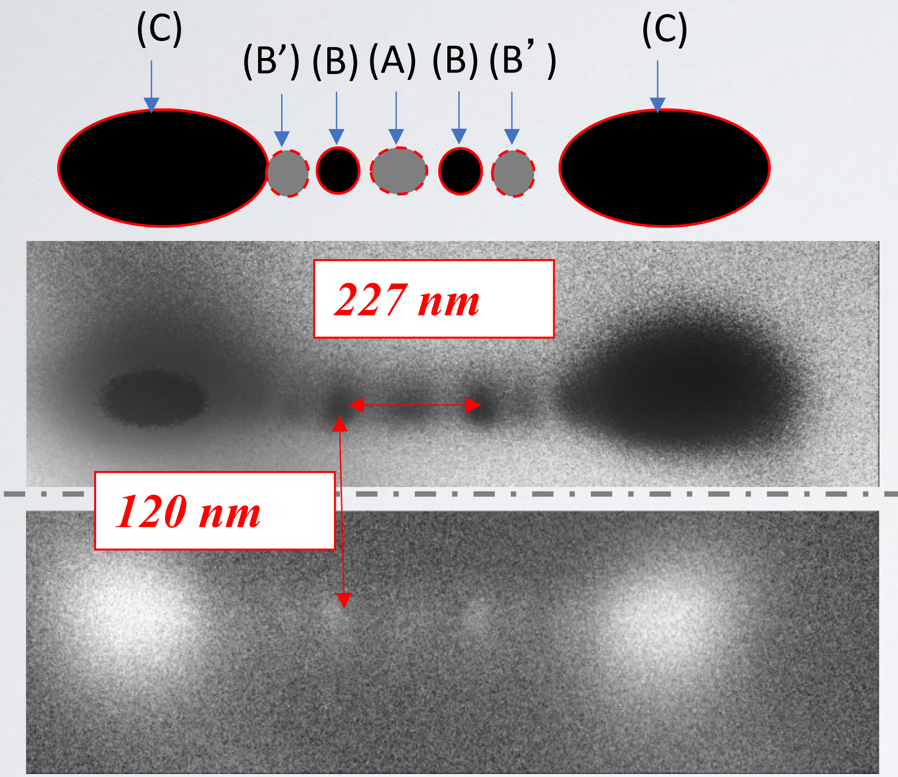

What does it means in real space ?

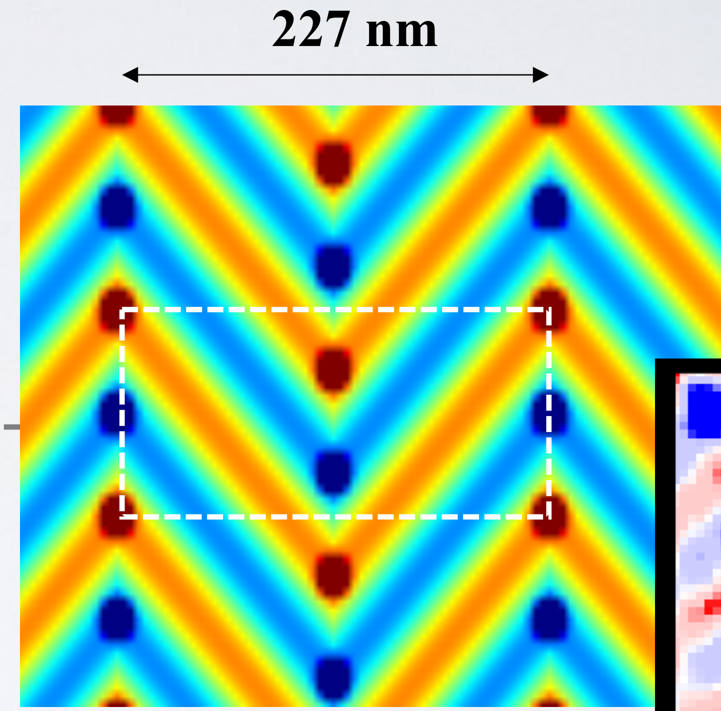

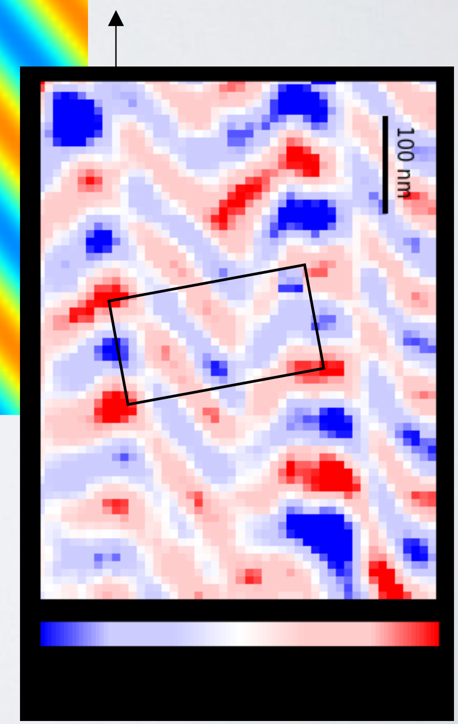

Image in real space
NV Center image

$BiFeO_3$: Micromagnetic simulation

Magnetic energies involved in the problem:

Exchange: $E_{ex} = J\sum \vec{S}_i \cdot \vec{S}_j$ with J the NN exchange energy

Anisotropy: $E_{anis} = K\sum (\vec{u}_P.\vec{S}_i)^2$ with K the anisotropy constant (along P)

Zeeman: $E_Z = \sum \mu_B \vec{S}_i \cdot \vec{B}$ with B the applied field

Magneto-electric: $E_{ME} = \gamma_{ME}\sum \vec{P}\cdot\left(\vec{R}_{ij}\times(\vec{S}_i\times\vec{S}_j)\right)$ with γ_{ME} the inhomogeneous ME coupling constant

Dzyaloshinskii-Moryia: $E_{DMI} = \sum \vec{D}_{ij}\cdot(\vec{S}_i\times\vec{S}_j)$ with D_{ij} the Dzyaloshinskii-Moryia constant //P + staggered

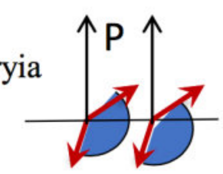

→ Analytical minimization not possible in the general case

$BiFeO_3$: Micromagnetic simulation

Chain of (AF) spins: $\vec{S}_i$ + use of effective 1D energies

Energies:

Low field: $E_{ex} >> E_{EM} > E_{DM} >> E_{anis} > E_z$ → ME effect dominates → cycloidal state

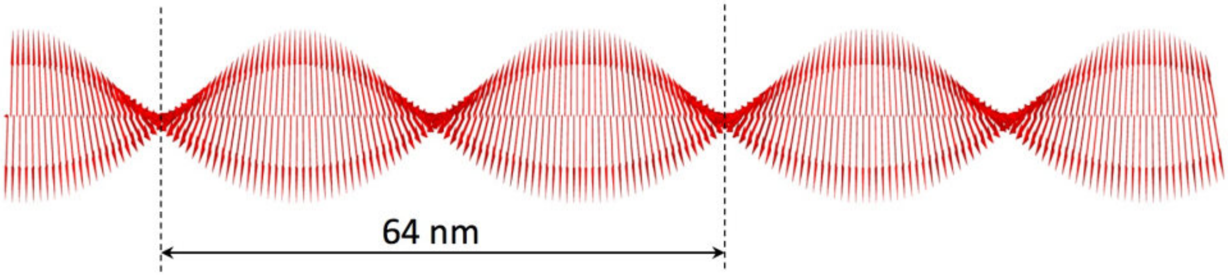

$$q = \frac{\gamma_{ME} P}{4J} a$$ (a = cell parameter)

Parameters for BFO:

$A = 3\ 10^{-12}$ J/m $A/a^2 = 2\ 10^7$ J/m^3

$K_{eff} = 6.6\ 10^4$ J/m^3 (includes anisotropy + DM)

$\gamma_{ME} P = 6\ 10^{-4}$ J/m^2 $\gamma P/a = 1.5\ 10^6$ J/m^3

$M = 8\ 10^5$ A/m

$a = 3.9$Å

BiFeO$_3$: Micromagnetic simulation

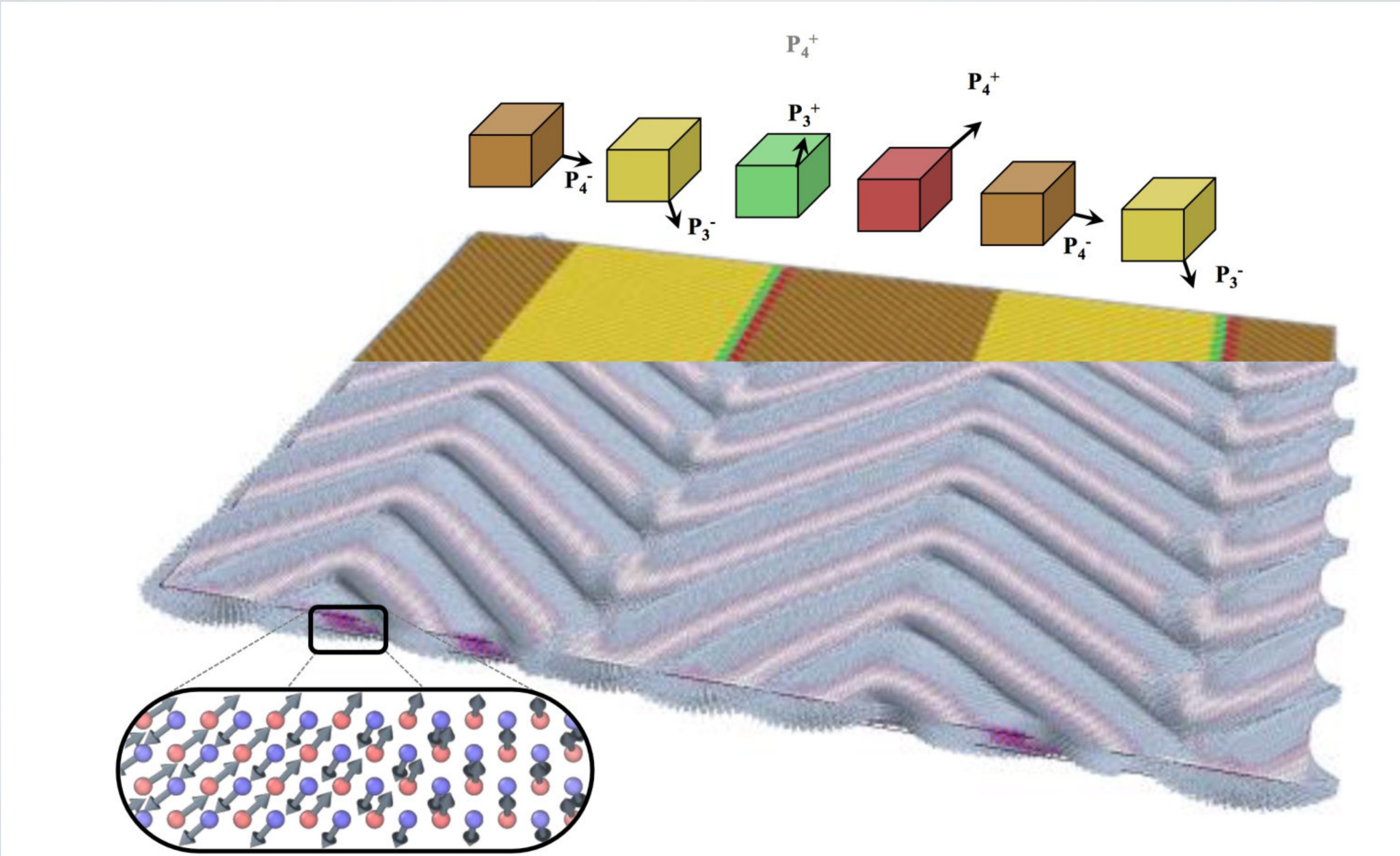

BiFeO$_3$: CONCLUSION

Soft X-ray Scattering

NV Center magnetometry

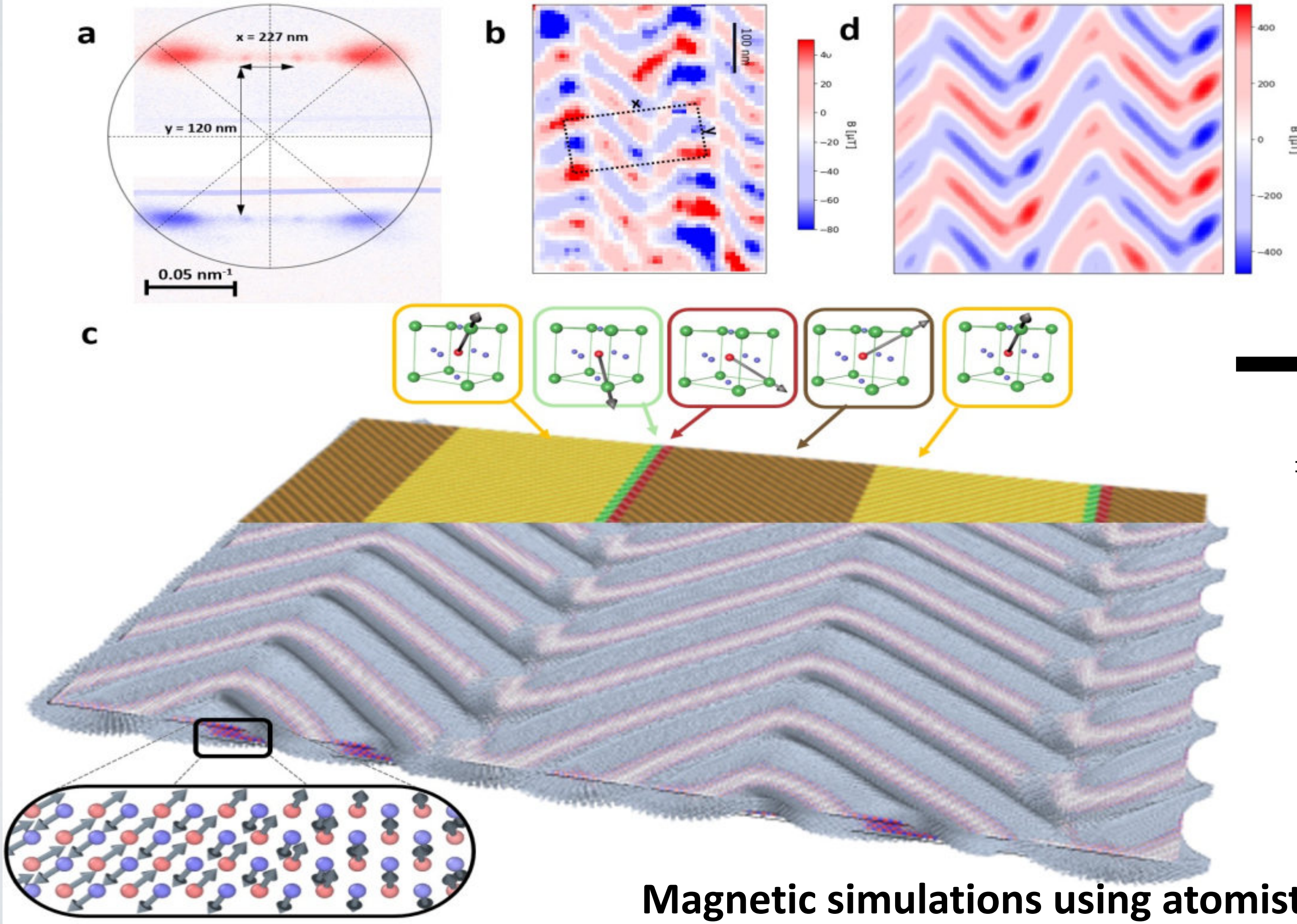

P rotate along the long winding
⇒ chirality of FE
⇒ as seen at O K edge

Magnetic simulations using atomistic code

Chauleau et al, Nat. Materials, Nov 2019

$BiFeO_3$: Strain effects… Perspectives

Stabilization of a cycloid of type 2 in thin film using strain

Soft X-ray Scattering **NV Center magnetometry**

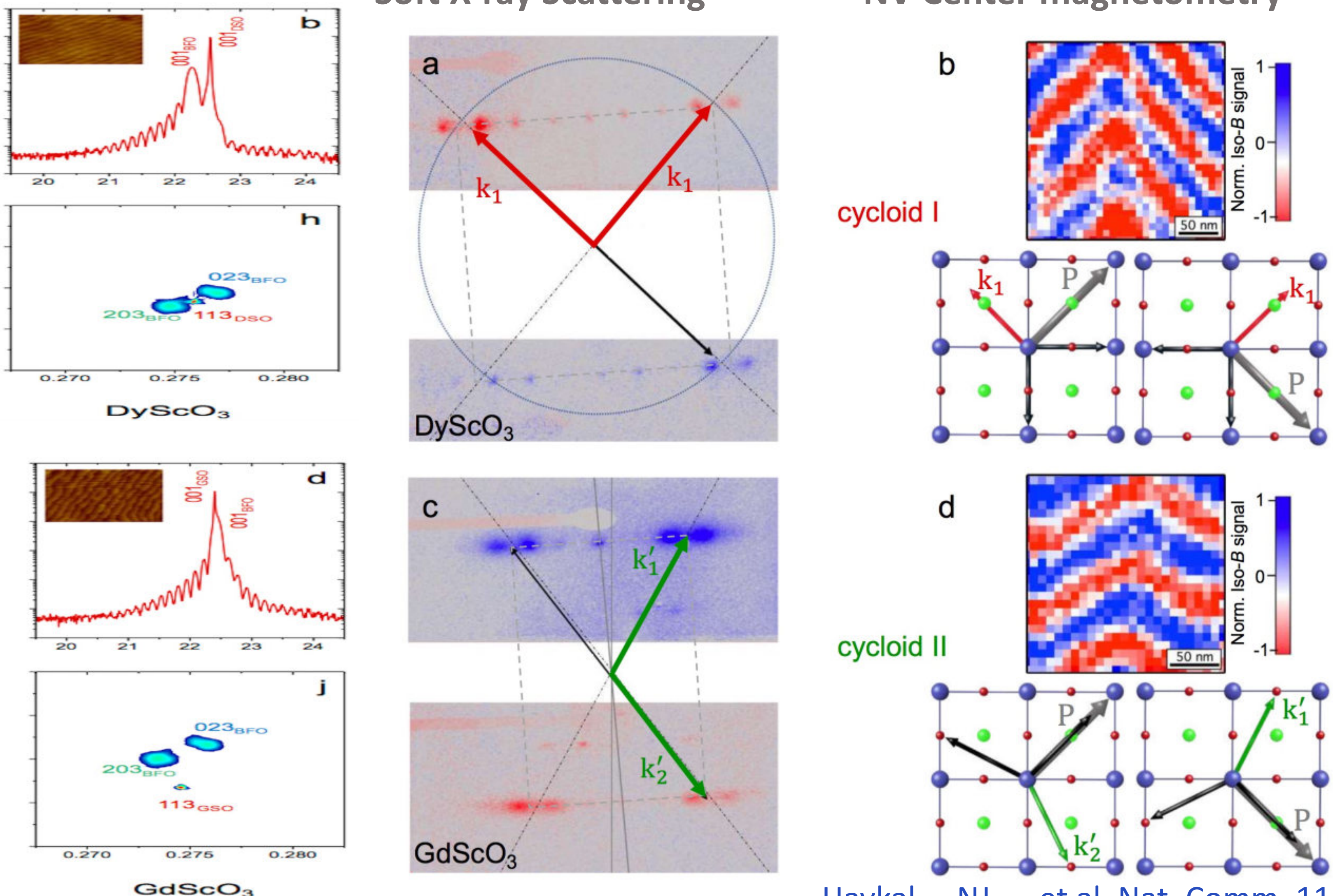

Haykal, …NJ, … et al, Nat. Comm. 11, 1704 (2020).

$BiFeO_3$: Take Home message

- Existence of cycloids of Larger period in each FE domain

I Gross, …, NJ, … et al., Nature 2017
JY Chauleau, … NJ, … et al, Nature Mat (2019)

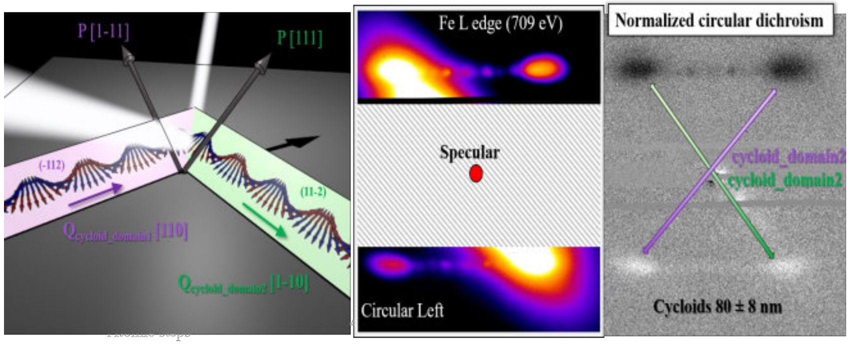

- Existence of chiral circular object at the ‘nodes’ of cycloid at the FE Domain Wall
- Chirality of FE at DW

JY Chauleau, … NJ, … et al, Nature Mat (2019).

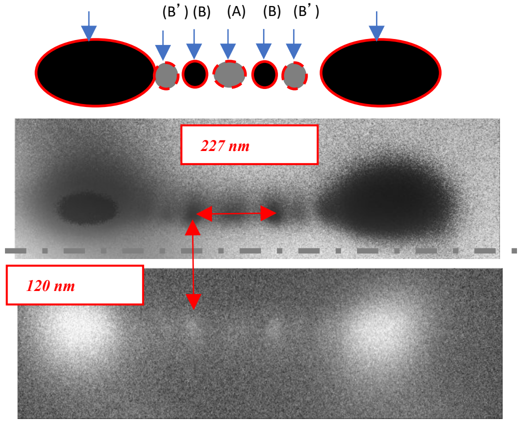

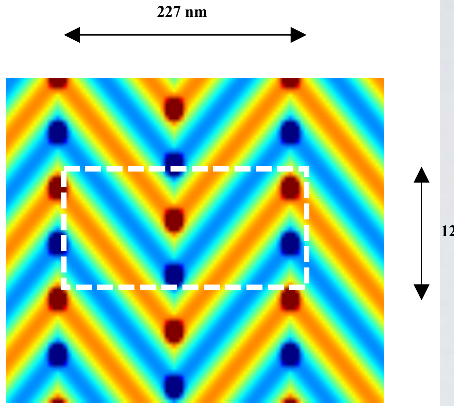

- In thin film with FE domain => cycloid plane from 35° to > 10° at surface
- Effect of strain

JY Chauleau, ….NJ, …. et al, in preparation
A Haykal, …NJ, … et al, Nature Comm. 2020

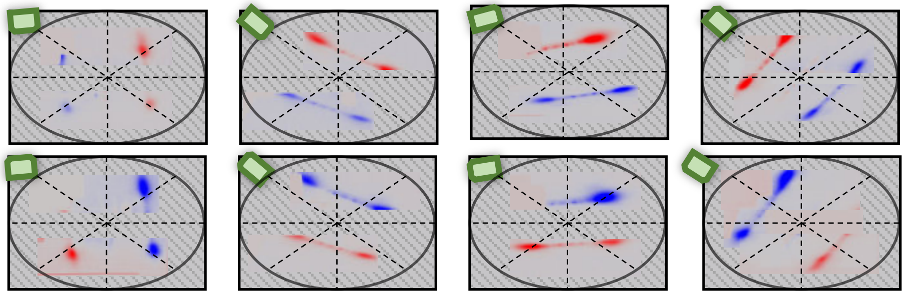

Conclusions

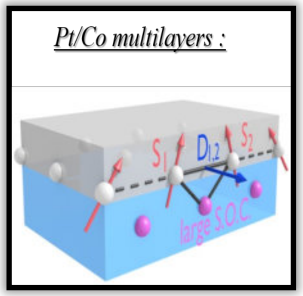

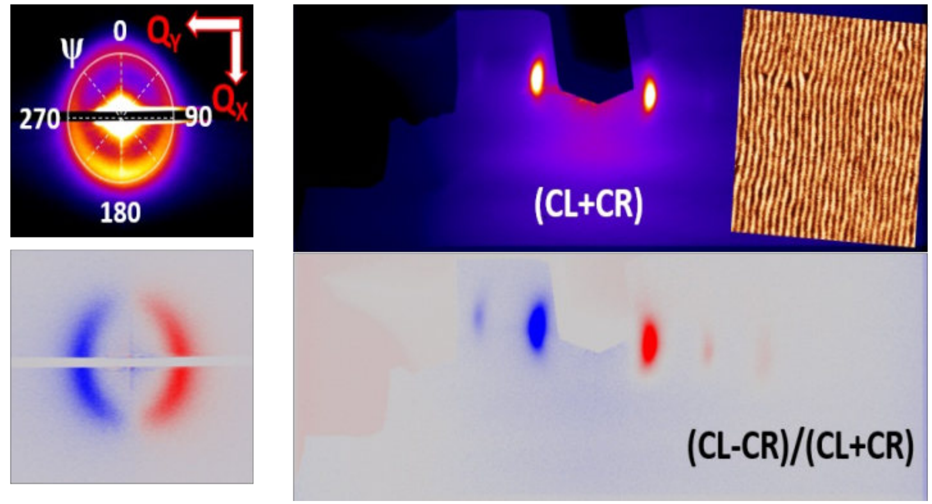

Determination of Neel vs Bloch
CW vs CCW chirality

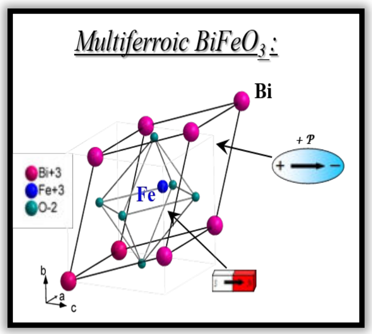

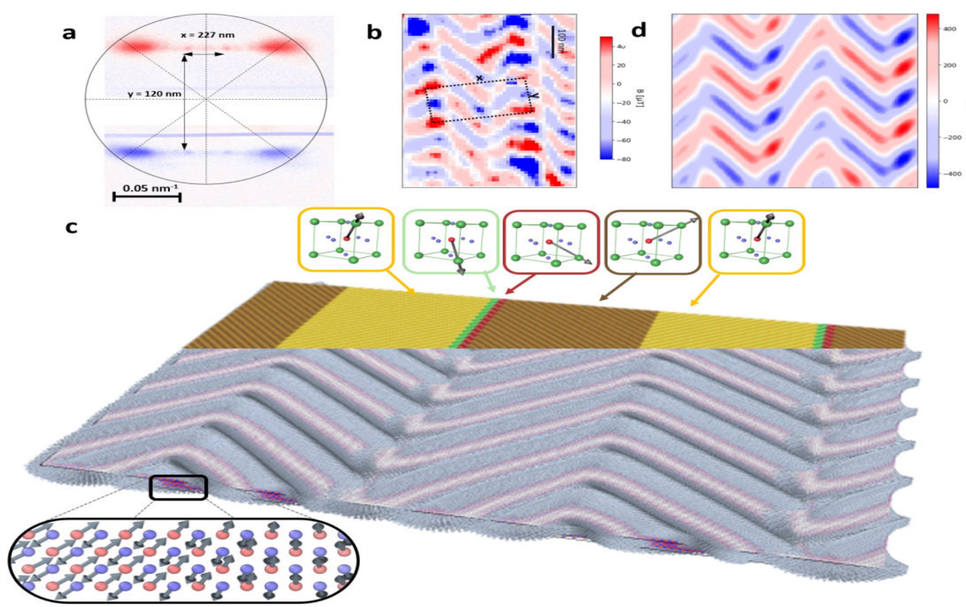

Access to the complex FE-AF texture in $BiFeO_3$ epitaxial layers

Outline

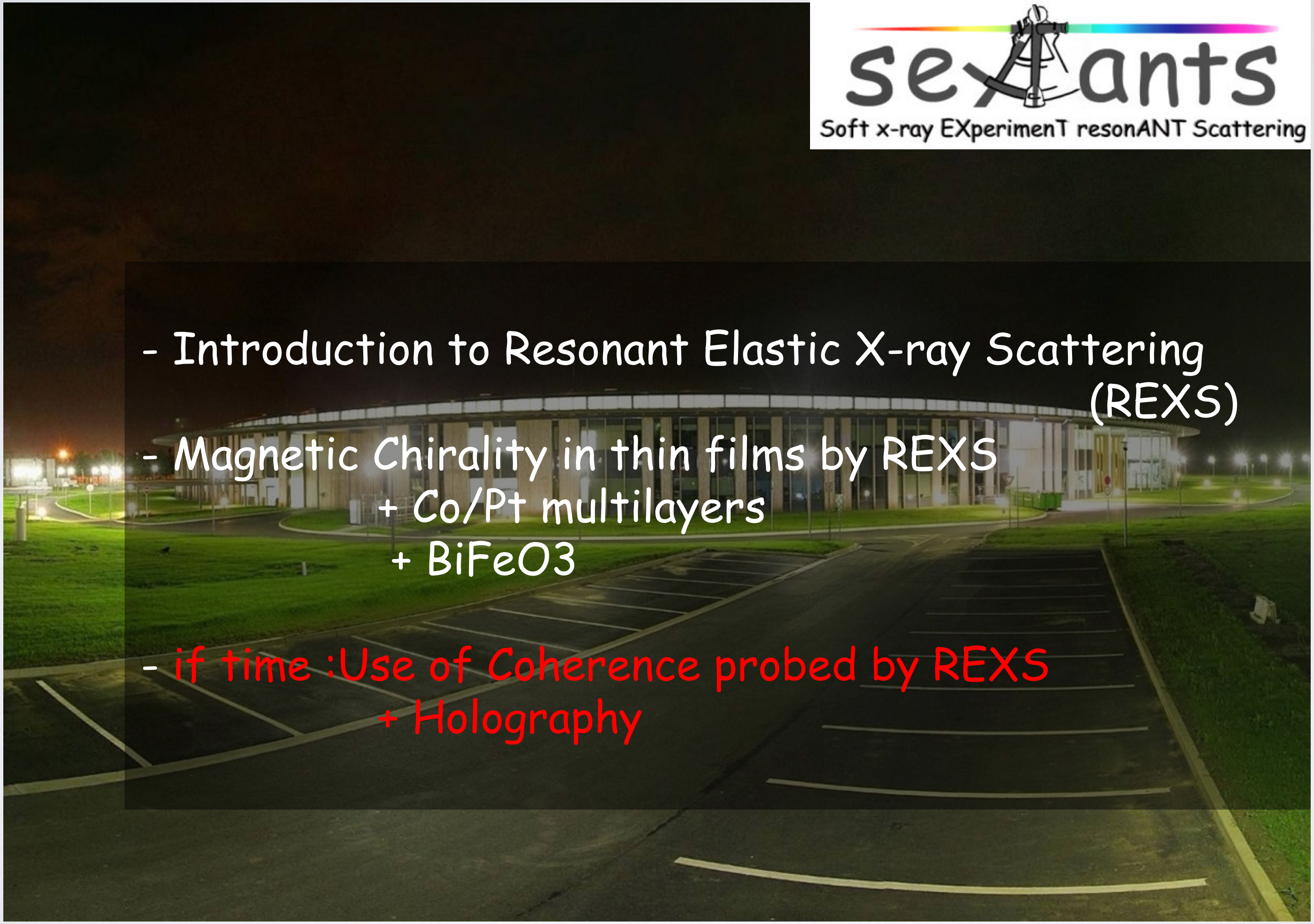

- Introduction to Resonant Elastic X-ray Scattering (REXS)
- Magnetic Chirality in thin films by REXS
  + Co/Pt multilayers
  + BiFeO3
- if time :Use of Coherence probed by REXS
  + Holography

CXS an introduction - Holography

Fourier Transform Holography (FTH) imaging technique

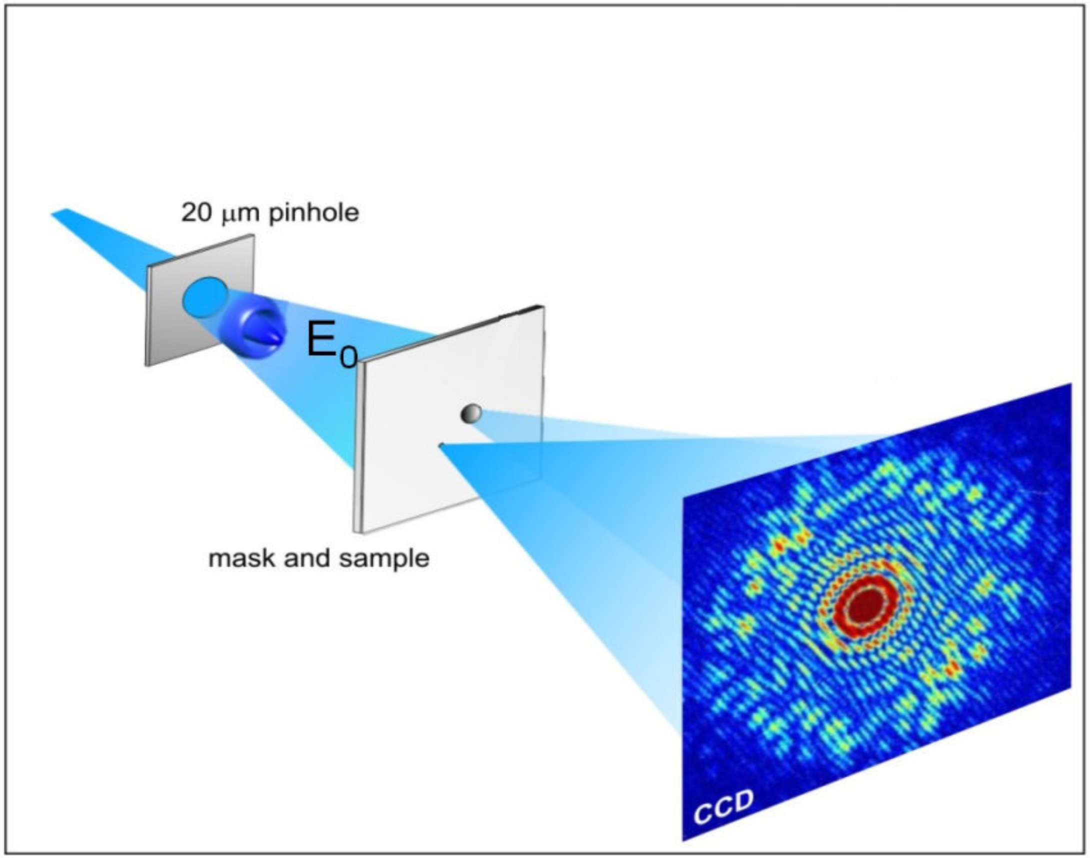

S. Eisebitt et al., Vol 432, 2004, Nature

object: $o(x,y) = E_0\, t_o(x,y)$

reference: $r(x,y) = E_0\, t_r(x,y)$

Hologram intensity:

$$= |\,\mathbf{F}\{r + o\}|^2$$
$$= |R + O|^2$$
$$= |R|^2 + |O|^2 + OR^* + RO^*$$

Reconstructed real space images:

$\mathbf{F}$\{Hologram intensity\}

$$= r \star r + o \star o + o \star r + r \star o$$

CXS an introduction - Holography

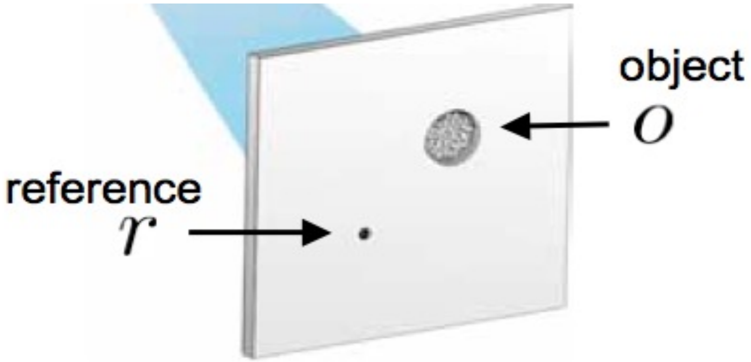

$$= \quad |\mathcal{F}\{r+o\}|^2$$

$$= \quad |R+O|^2$$

$$= \quad |R|^2 + |O|^2 + OR^* + RO^*$$

$$\mathcal{F}\{\text{Hologram Intensity}\}$$

$$r \star r + o \star o + o \star r + r \star o$$

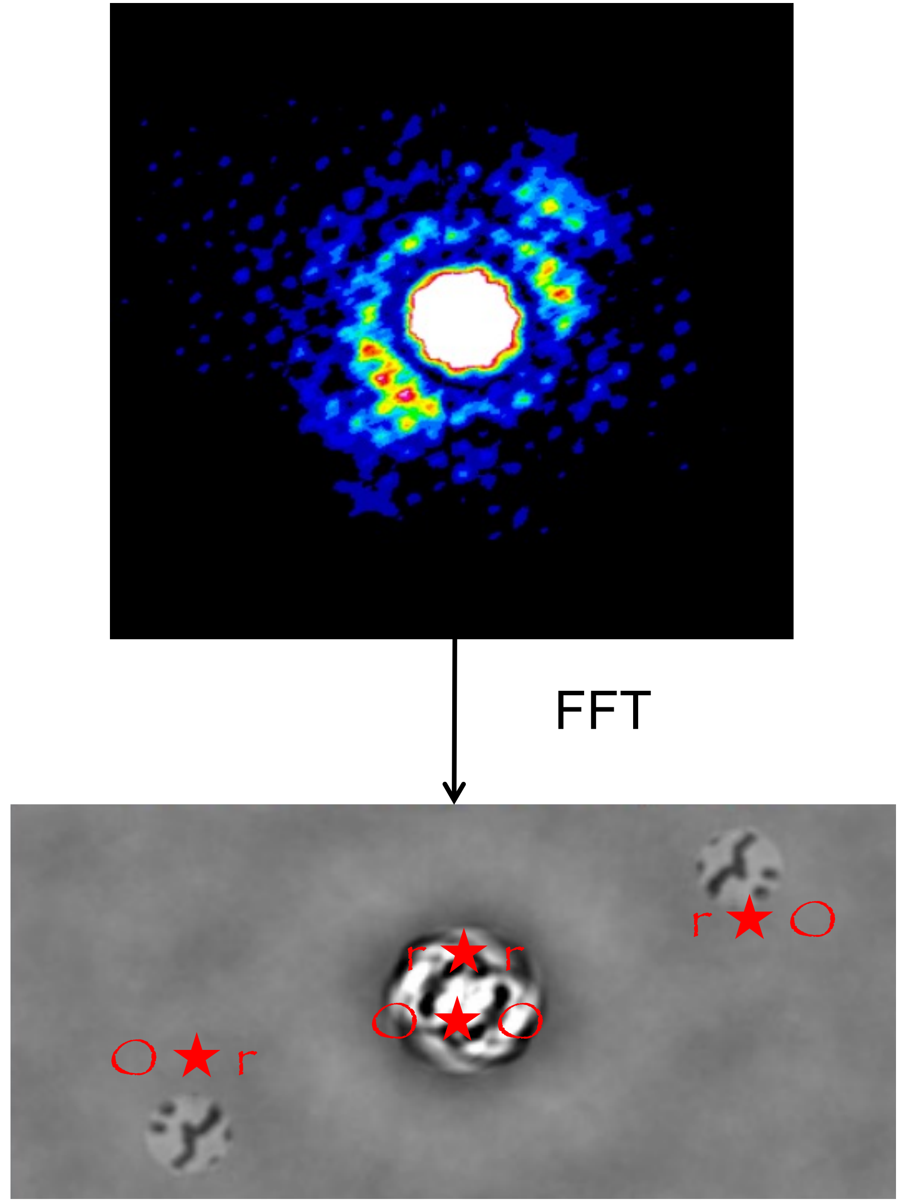

COMET: New station for Coherent Magnetic scattering Experiments in Transmission

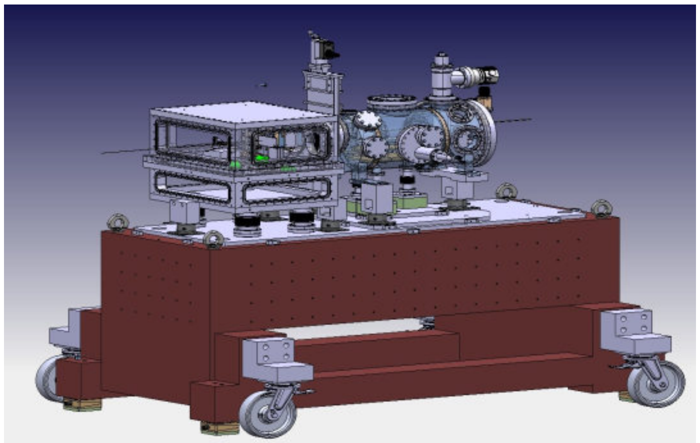

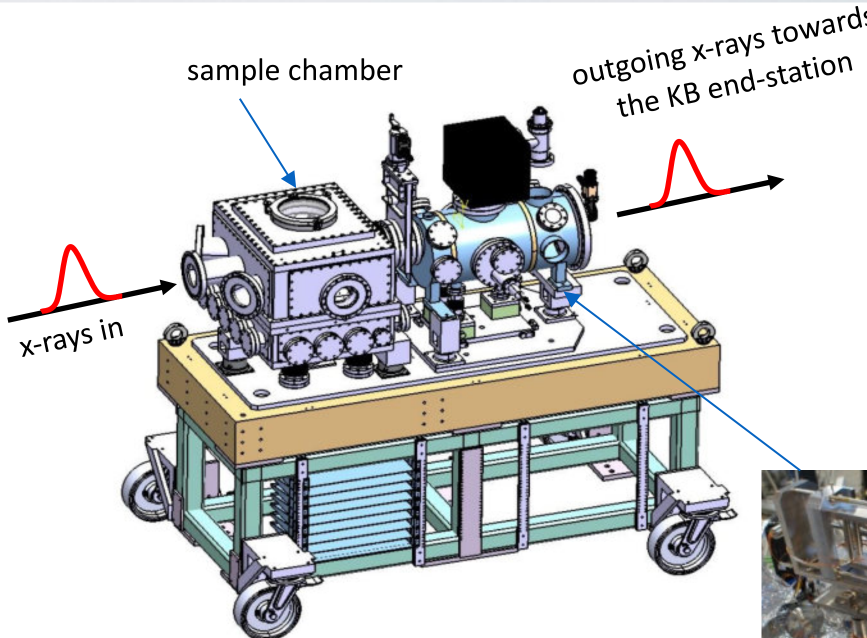

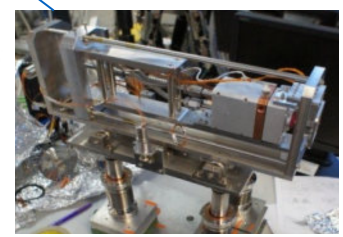

removable 2D detector

- Imaging by Fourier Transform Holography (FTH)
- Integrated or separated mask/sample approach
- extendable field of view
- Normal or tilted transmission geometry for imaging in-plane or out-of-plane magnetic domains
- 2D Magnetic field: 0.9 Tesla
- Temperature: 25 K / 400K
- regular spatial resolution: ~ 40 nm /15nm best (with standard reference holes)

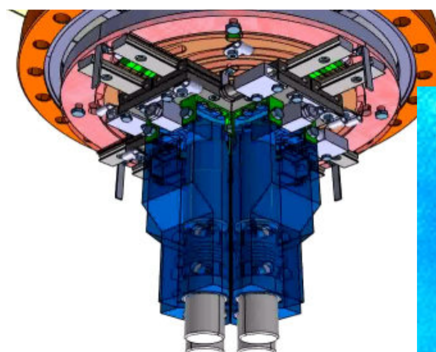

Domains

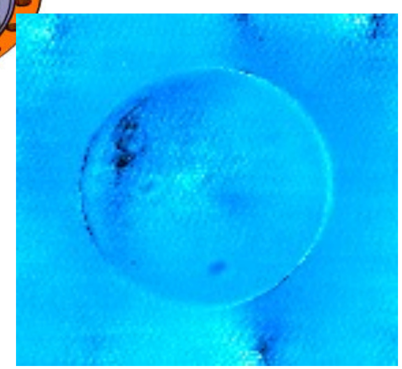

Skyrmions

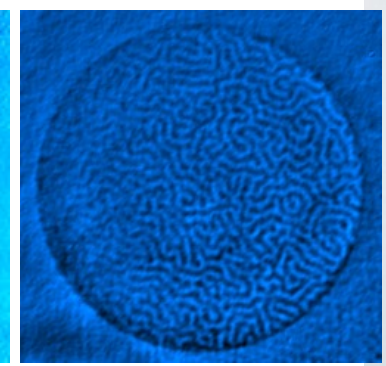

H. Popescu, … NJ, *J. Synchrotron Rad. 26(1), 280- 290 (2019)*

Imaging of phase transition: field/temperature 20nm spatial resolution

In bulk materials : MnNiGa

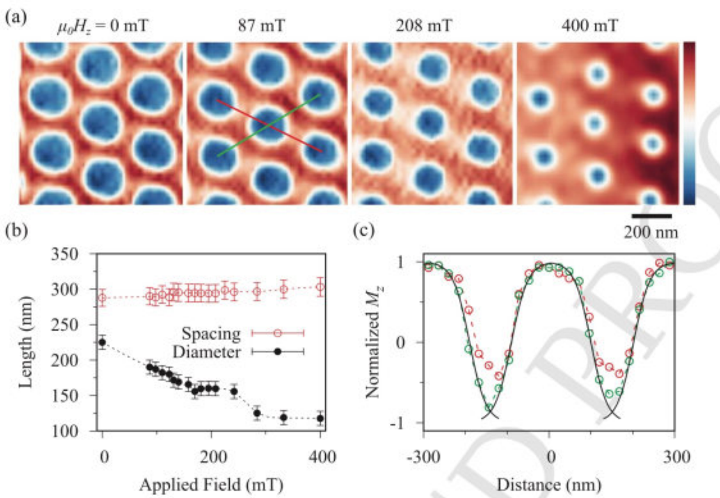

JC Loudon et al, Adv. Materials 1806598 (2019)

In Pt/Co/Ir multilayers (UMPhy-thales/SEXTANTS)

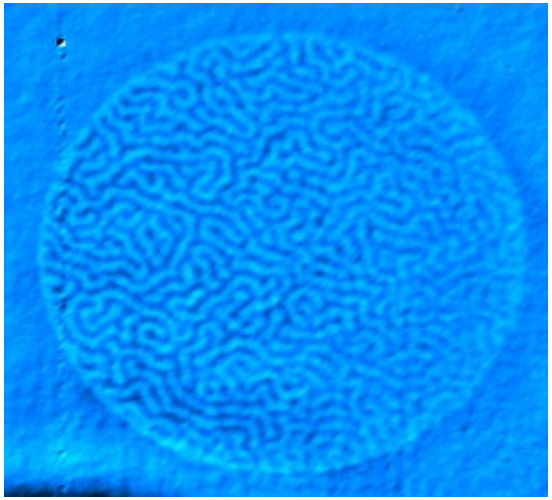

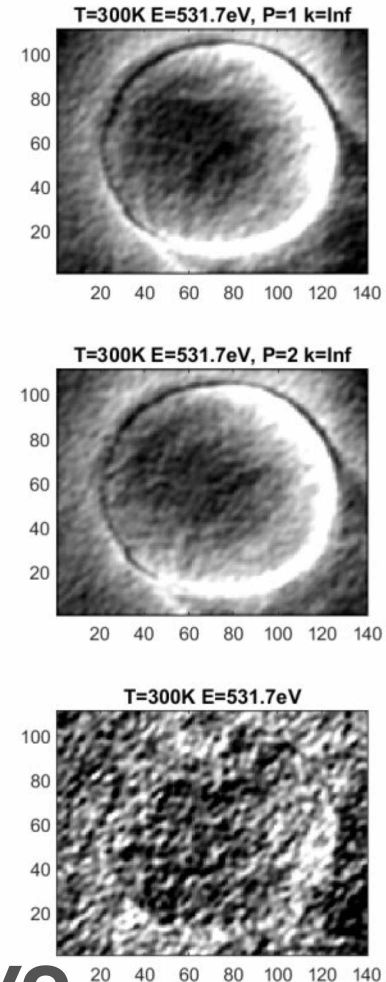

FeGe (Hatton et al., Durham, UK) :

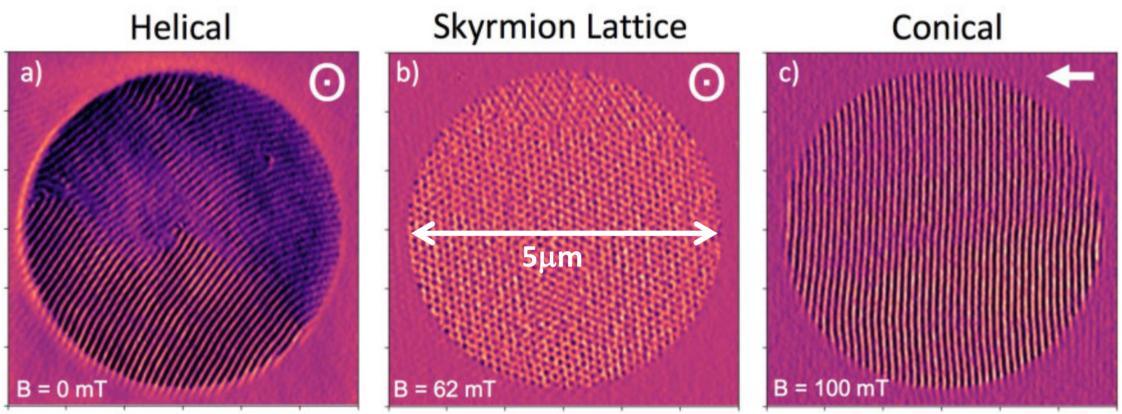

MIT in VO_2 (M. Golden et al. Amsterdam Univ)

P.T.P Le et al, Adv. Functional Materials in print

imaging of vortex : time dependance

In plane: Vortex

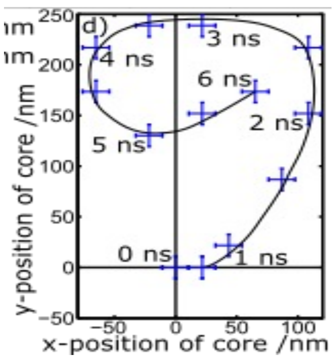

⇒ In plane component already studied in PEEM/STXM

but 25nm spatial resolution full field with acquisition time same as static

Out of plane : vortex core + DW

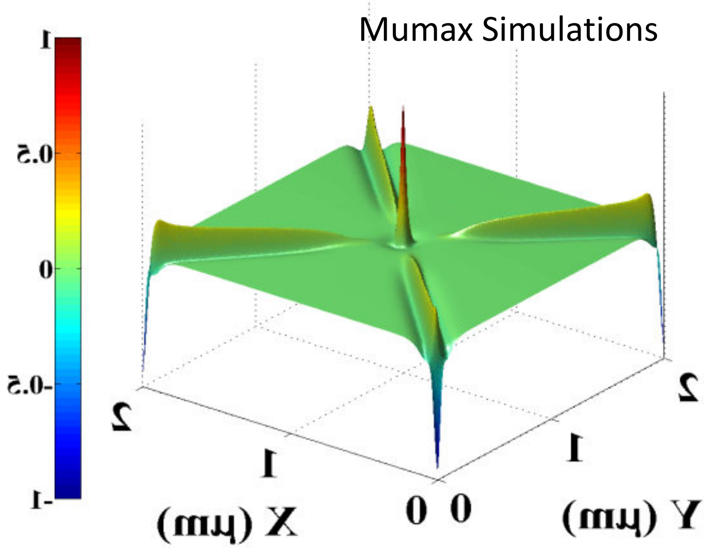

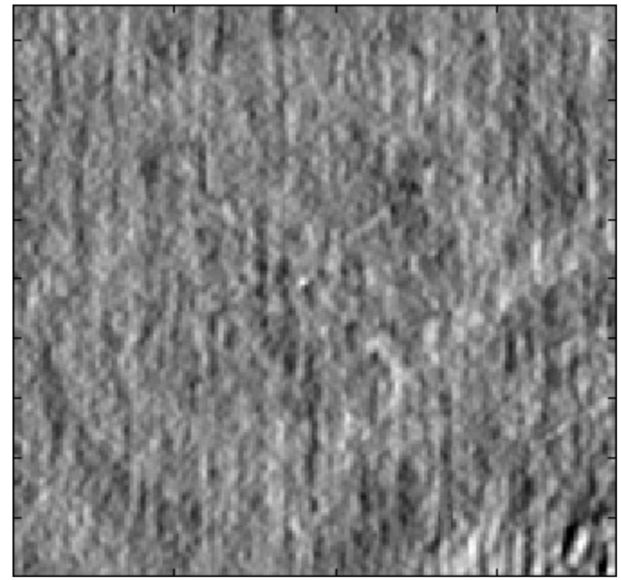

- ⇒ First observation of Out of plane component in DW
- ⇒ wave bullet–like excitation propagate inside the DW
- ⇒ Beside the core we show existence of 4 singularities
- ⇒ Polarization of the 4 singularities ⇔ vortex core
- ⇒ Can be controlled by specific magnetic pulse

N bukin et al, *Scientific Reports, 2016*

F Ogrin (Exter, UK)
G van der Laan (DLS, UK)
G Beutier (Grenoble, France)

Moving to 3D images => FTH-tomography

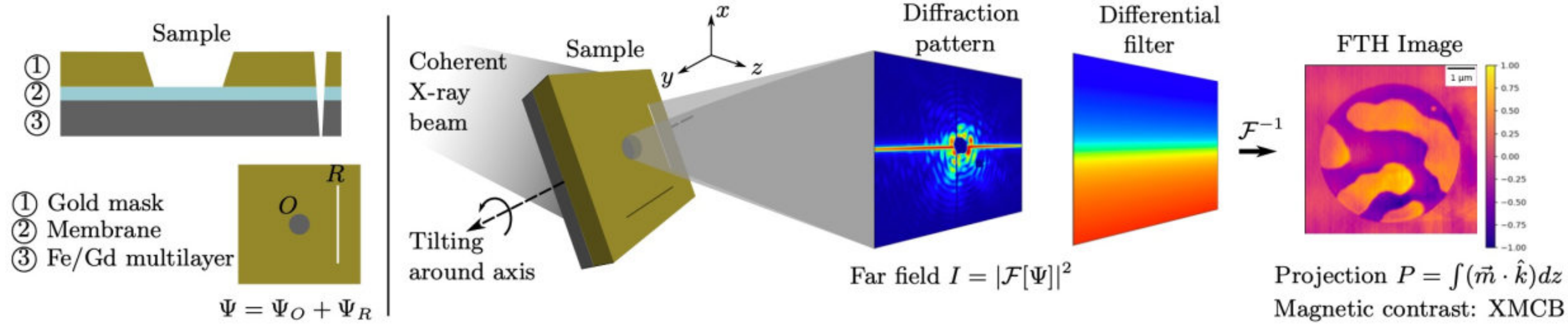

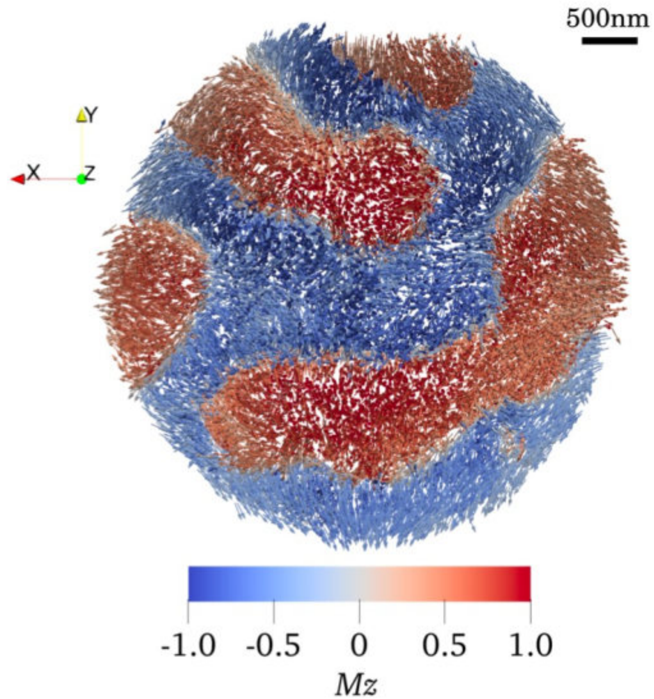

(a) Complete reconstructed disk.

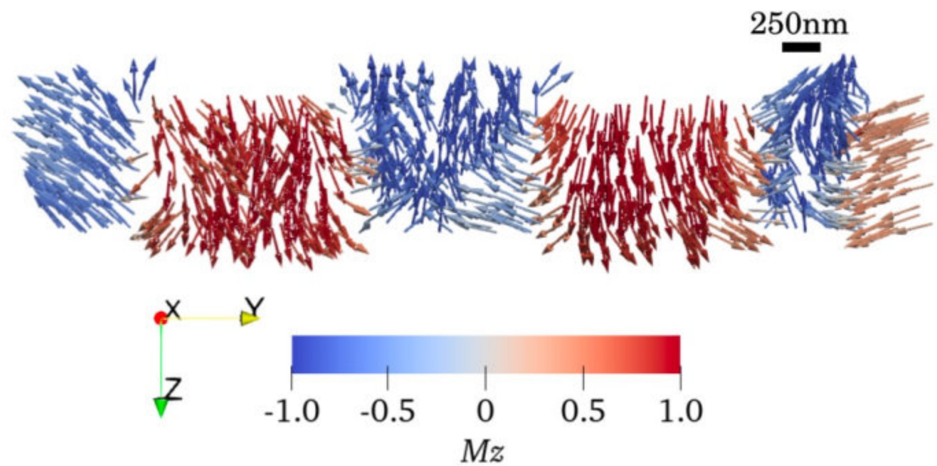

M. Pietro Martinel et al, In preparation

REXS based imaging in soft x-rays

SOLEIL actual: only in transmission !

Ptychography (≈50nm resolution):
Limited by motors
⇒ 1nm stage should be available in the next 6 months

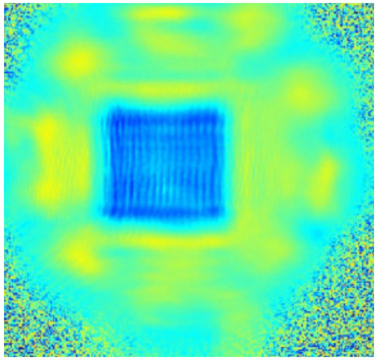

2x2μm rectangle of $(Co_{0.4}Pd_{0.8})$x100

SOLEIL upgrade (with new 2.5m in vacuum HU + new optics)
=> opening reflection geometry !

⇒ **coherent flux at 800eV** **=> x100**
⇒ **Beamzize from 10 to 1 microns** **=> x100 in useful flux**
⇒ **Undulator peak narrow**
+ Low dispersive monochromator for 3d TM **=> x10**

x10^5 more useful photons flux !!!!

REXS Ptychography

. Resolution is wavelength limited
. Bulk/surface sensitivity => 3D images
. Access to the relevant parameters for condensed matter physic
(structural, magnetic, electrical, orbital, …)
. No experimental constraint around the sample !!!!!
(magnetic field, Electric field, IR or THz pump, …)

Acknowledgment

J.Y Chauleau, E. Burgos Parra, C. Leveillé, H. Popescu, N. Jaouen *(Co/Pt & BiFeO_3)*

J.Y. Chauleau, C. Blouzon, J. Tranchida, P. Thibaudeau, M. Viret *(BiFeO_3)*

J.Y. Chauleau, W. Legrand, E. Burgos Parra, C Leveillé, N. Reyren,
K. Bouzehouane, A. Fert, V. Cros *(Pt/Co)*
S. Fusil, C. Carretero, V. Garcia, M. Bibes, A. Barthelemy *(BiFeO_3)*

I. Gross, A. Aykal, A. Finco, W. Akthar, V. Jacques *(BiFeO_3)*

J.-V. Kim *(BiFeO_3)*

Sando *(BiFeO_3)*

SoGraph
Multidolls
Wavenext
Santa

Programme transversal DRF-DAM: *ACOSpin*
Labex NanoSaclay: *Axion*